π^+ PHOTOPRODUCTION AT ANGLES FROM 50° TO 165° C.M. AND ENERGIES FROM 500 TO 1350 MEV

Thesis by

Henry A. Thiessen

In Partial Fulfillment of the Requirements

for the Degree of

Doctor of Philosophy

California Institute of Technology

Pasadena, California

1967

(Submitted September 27, 1966)

ACKNOWLEDGMENTS

This experiment was supervised by Professor R. L. Walker. His interest, encouragement, and willingness to talk over problems have made a great contribution to the success of the experiment.

I am indebted to Dr. J. Owen Maloy for many helpful discussions during the design and construction of the electronics. Joe Laurinovics and Ray Green did most of the construction of the electronics. Professor A. V. Tollestrup suggested the use of integrated circuits.

Mr. Mike Hauser joined the experiment at the time when the fast electronics was being set up. Since then, he has played a major role in planning and carrying out the experiment. I gratefully acknowledge the large number of helpful comments and the many hours of data taking which Mike has contributed.

The data analysis of this experiment was done in close collaboration with Mr. Stan Ecklund. Since his experiment was very similar to this one, it was possible to use several computer programs for both experiments. I am indebted to Stan for his contribution to the programming as well as for his many helpful discussions.

No synchrotron experiment can succeed without the competent help of the synchrotron technical staff. In particular, I would like to thank Larry Loucks, Al Neubeiser, and Earl Emery for their contributions to the maintenance of the synchrotron and the liquid hydrogen target.

For financial support, I am indebted to the National Science Foundation, the Atomic Energy Commission, the California Institute of Technology, my parents, and my wife's parents.

ABSTRACT

The cross section for the reaction $\gamma + p \rightarrow \pi^+ + n$ was measured at the Caltech synchrotron. The π^+ was detected in a multi-channel magnetic spectrometer, and the data were recorded in the memory of a pulse height analyzer. The results are presented in the form of energy distributions at 12 fixed laboratory angles from 34° to 155°. 378 cross section measurements are reported with photon energies between 500 MeV and 1350 MeV. No detailed fitting of the entire angular range was attempted; however, a narrow bump in the cross section at 180° is explained as the effect of a cusp at the eta meson threshold.

To Challis

TABLE OF CONTENTS

LIST OF TABLES

LIST OF FIGURES

I. INTRODUCTION

There is presently a considerable theoretical interest in photoproduction data. Several authors have used the data for evaluating sum rules.[1, 2, 3] For these purposes, a multipole and isotopic spin decomposition of the photoproduction amplitudes is desired. Similar decompositions are already available for the pion scattering data.[4, 5, 6, 7, 8] This experiment was designed to collect a large number of points of the cross section for $\gamma + p \rightarrow \pi^+ + n$ with sufficient resolution to extract the energy dependence of the cross section. When the data of this experiment are combined with the data of Ecklund and Walker,[9] a consistent set of cross sections is available for angles between 6° and 165° c. m. and photon energies between 589 MeV and 1269 MeV, with some additional data available between 500 and 1350 MeV. In particular, this experiment covered the angular range from 50° to 165° c. m. for the entire range of energies (see Section V-C for further details). These data are being combined with data from the other single pion photoproduction reactions and an attempt is being made to determine the decomposition of the photoproduction amplitudes.[10] However, it appears likely that much more data will be required on the polarization and the cross section in the other channels before a unique decomposition can be made for energies greater than 800 MeV.

A second important consideration in the design of this experiment was to set up a spectrometer which can be used simultaneously with the already existing High Energy Magnet. A 600 MeV/c spectrometer was constructed by modifying the former Low Energy Magnet, then the spectrometer was carefully calibrated and instrumented with several general purpose counters. This spectrometer is available as a laboratory instrument, and an experiment is now in progress which uses both magnets simultaneously.[11]

Since this experiment and the experiment of Ecklund and Walker were done at approximately the same time, a considerable amount of work was saved by avoiding a duplication of effort. Thus the same computer programs were used in the data reduction of both experiments. In general, this author did most of the programming for magnet resolution, etc., while Stan Ecklund did the evaluation of the cross section integrals and a large amount of data fitting. In practice, a strict division of the work was not always possible, and many parts of this thesis are very similar to his thesis.

II. EXPERIMENTAL METHOD, GENERAL

The reaction $\gamma + p \rightarrow \pi^+ + n$ was studied at the Caltech 1.5 GeV Electron Synchrotron. The experimental method was very similar to that which was used in several past experiments(12, 13, 14, 15, 16, 17), namely, the photon beam irradiated a liquid hydrogen target and the positive pions produced were detected and momentum analyzed in a magnetic spectrometer.

The kinematics of the reaction relate the observed quantities, $P_{\pi lab}$, $\theta_{\pi lab}$, to desired quantities, k, $\theta_{\pi CM}$ (where k is the photon lab energy) under the assumption that only one pion was produced. If two or more pions are produced, as in the reactions,

$$\begin{aligned} \gamma + p \rightarrow\ & \pi^+ + n + \pi^0 \\ \rightarrow\ & \pi^+ + p + \pi^- \\ \rightarrow\ & \pi^+ + N + (n\pi)\ \ldots \end{aligned}$$

then there will be a minimum photon energy, $k_{2\pi}$, required to produce a π^+ with the observed angle and momentum. In general, $k_{2\pi}$ will be greater than k. In the energy region of this experiment, it is possible to choose E_o, the maximum energy of the photon spectrum, to lie between k and $k_{2\pi}$ so that the multiple pion reaction will not be observed.

The background of particles incident on the spectrometer includes protons, electrons, and muons. Protons are eliminated by velocity selection in a lucite Cerenkov counter, crude time-of-flight requirements, and dE/dx selection in two scintillation counters.

Electrons and muons are indistinguishable from pions in the electronics. This experiment relies on the fact that previous experiments have shown that electron contamination at large angles from the photon beam is small; several checks with magnet field reversed have been made to look for this kind of contamination. The major source of muons is the decay of the π^+, $\pi^+ \rightarrow \mu^+ + \nu$, since typically 20% of the pions decay while passing through the spectrometer. Muon pair production, $\gamma + p \rightarrow \mu^+ + \mu^- + p$, is usually eliminated by the same kinematical requirement that eliminates pion pair production. In addition, the cross section for muon pair production should be down by a factor $e^4 = (\frac{1}{137})^2$ from pion pair production. Thus this source of events can be safely ignored.

The spectrometer, the 600 MeV/c Magnet, differs from those used in the earlier work in that it collects data in several momentum channels simultaneously. Because the kinematic transformation between lab and center-of-mass co-ordinate systems varies rapidly with p_π and $\theta_{\pi lab}$, it was not feasible to measure angular distributions at fixed values of k. Instead, the data were taken as energy scans at fixed lab angle. Several spectrometer momentum settings were required for each scan and an appropriate value of E_o was chosen for each spectrometer setting. Angular distributions were obtained by linear interpolation in the measured data.

The data were taken during two separate periods, May - August 1965, and December 1965 - March 1966. Each point was measured at least once during each period, and checks were made for consistency between runs.

III. APPARATUS

A. The Photon Beam, Liquid Hydrogen Target, and Beam Monitoring Equipment

The photon beam was generated by bremsstrahlung in a 0.2 radiation length tantalum radiator in the Caltech 1.5 GeV Electron Synchrotron. At energies greater than 0.91 GeV, the synchrotron produced a nearly uniform 100 msec. beam spill once per second. For energies less than 0.91 GeV, it was possible to run the synchrotron twice per second with a beam spill time of 50 msec. At the lowest energy used in this experiment, 0.66 GeV, it was extremely difficult to obtain a uniform beam spill. The cause of this difficulty was not fully understood, but it is believed that the radio frequency control system was sensitive to noise from many sources when operated at the very low power levels required to make a uniform dump at this energy. The result of this difficulty was a large spike superimposed upon the normal spill. This spike, which was of about 200 μsec duration, contained on the order of 5% of the total energy of the dump. During the first data-taking period, this problem was eliminated by careful tuning, but during the second period it was not possible to eliminate this effect. Since an accidentals monitoring system was used continuously during the experiment, the 660 MeV points were repeated with this poor spill.

The liquid hydrogen target is the same one that has been used by the magnet group for all experiments since that of J. Boyden.[18] The liquid hydrogen is contained in a long 3 inch diameter cylinder ("appendix") with 0.005 inch mylar walls. The axis of this cylinder is perpendicular to the beam line and is coincident with the axis of rotation of the spectrometer. The beam line was adjusted to intersect the axis of the cylinder and the beam was collimated to a rectangular cross section 1 1/2 inch horizontal by 1 3/4 inch vertical. Because it has been observed that after long use "ice" builds up on the walls of the appendix[19], the target was disassembled and cleaned at approximately monthly intervals. In addition, empty target runs were usually taken within a week of full target runs, so that a gradual accumulation of "ice" would be corrected by the empty target subtraction.

The beam area layout during the first data-taking period is shown in Figure 1. For the second data-taking period, the quantameter was relocated on the scraping wall immediately upstream of the hydrogen target. Otherwise, the setup was unchanged between the two data-taking periods.

Figure 1 shows the High Energy Magnet at an angle for which the beam line intercepted the magnet yoke. During the running period of this experiment, Mr. F. Wolverton was setting up another experiment to detect protons at small angles from the photon beam with the High Energy Magnet. Occasionally, Mr. Wolverton needed to make a test with the High Energy Magnet in the beam line. Under these circumstances, a careful check of the consistency of data taken with the High Energy Magnet in the beam line and data taken under normal circumstances showed no significant difference.

The beam monitoring equipment consisted of several different instruments which were used at various times during the run. The primary standard was a Wilson type quantameter.[20] An absolute calibration of this instrument against a Faraday Cup was made at the Stanford Mark III Linear Accelerator on 2 May, 1966.

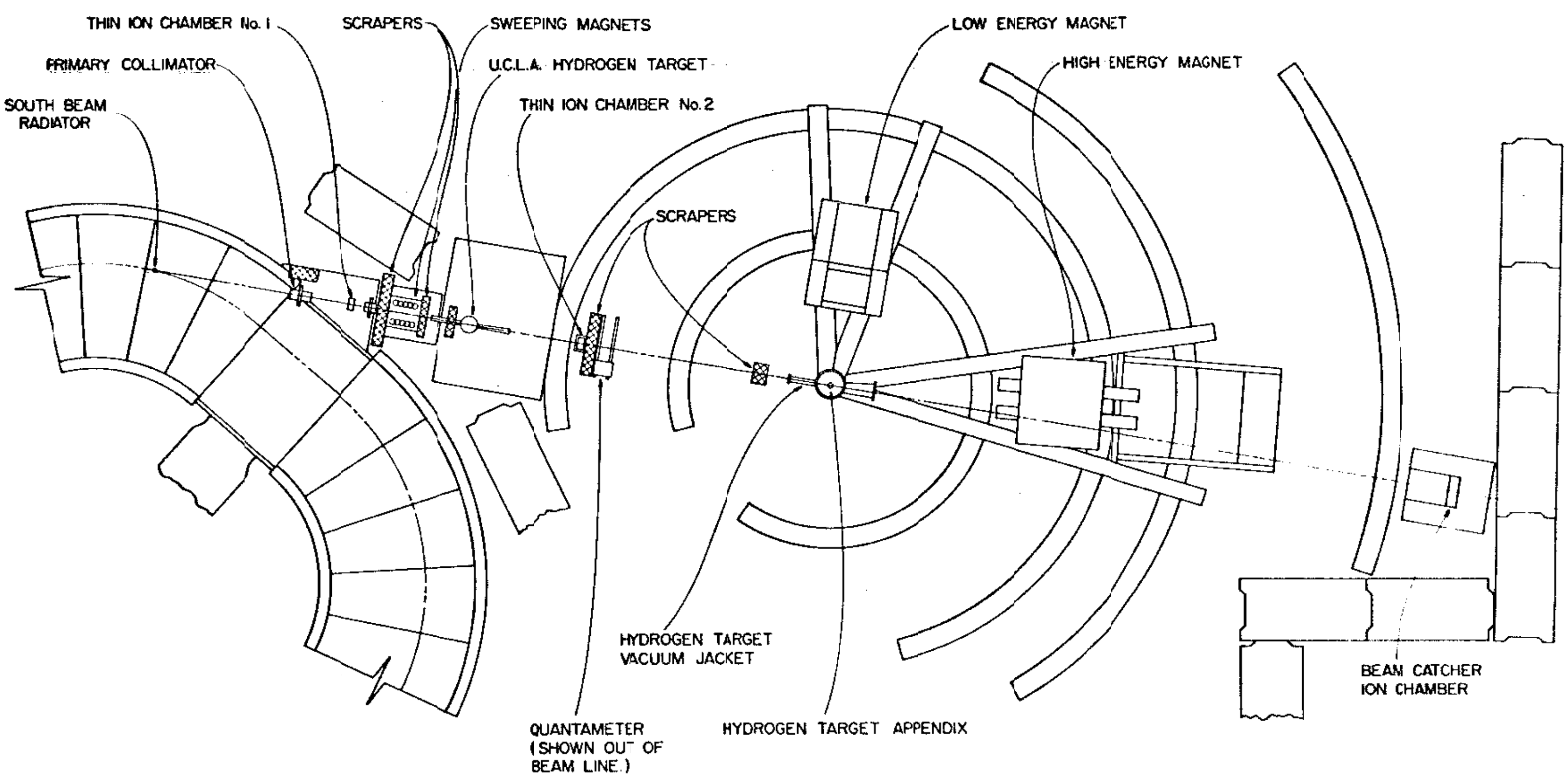

Figure 1. Beam Area Layout

This calibration differed from the previous absolute calibrations and the theoretical value by less than 1.5%.[21]

The secondary monitors consisted of two very thin ion chambers located upstream of the hydrogen target, a thick ion chamber located in the beam catcher, a 2-counter telescope which monitored particles produced at 90° from the hydrogen target, and a radio frequency monitor of the circulating beam which is commonly called the "40 mc. probe". The uses of these secondary monitors are described in Appendix I.

B. Magnetic Spectrometer and Counters

The magnetic spectrometer used for this experiment, designated the 600 MeV/c Magnet, was constructed by modifying the former Low Energy Magnet. The magnet is of the wedge-shaped, uniform field type and is very similar in design to the magnets which have been used by Professor R. L. Walker and his students for many years. An elevation view of the spectrometer is shown in Figure 2.

The calibration of the spectrometer is the subject of a separate report[22], and only a few important results will be summarized here. The solid angle of the spectrometer is 3.3×10^{-3} sr. and the total momentum acceptance is 10.3%. The momentum interval is divided into seven smaller channels. With the beam size typically used in this experiment (1.5 inch horizontal by 1.8 inch vertical) the r.m.s. momentum resolution obtained is 1.10%, when no scattering or other similar resolution degrading effects are included. (Note that the full width at half maximum is 2.2 times the r.m.s. width for a Gaussian resolution function). A graph of these basic resolution functions is presented as Figure 3.

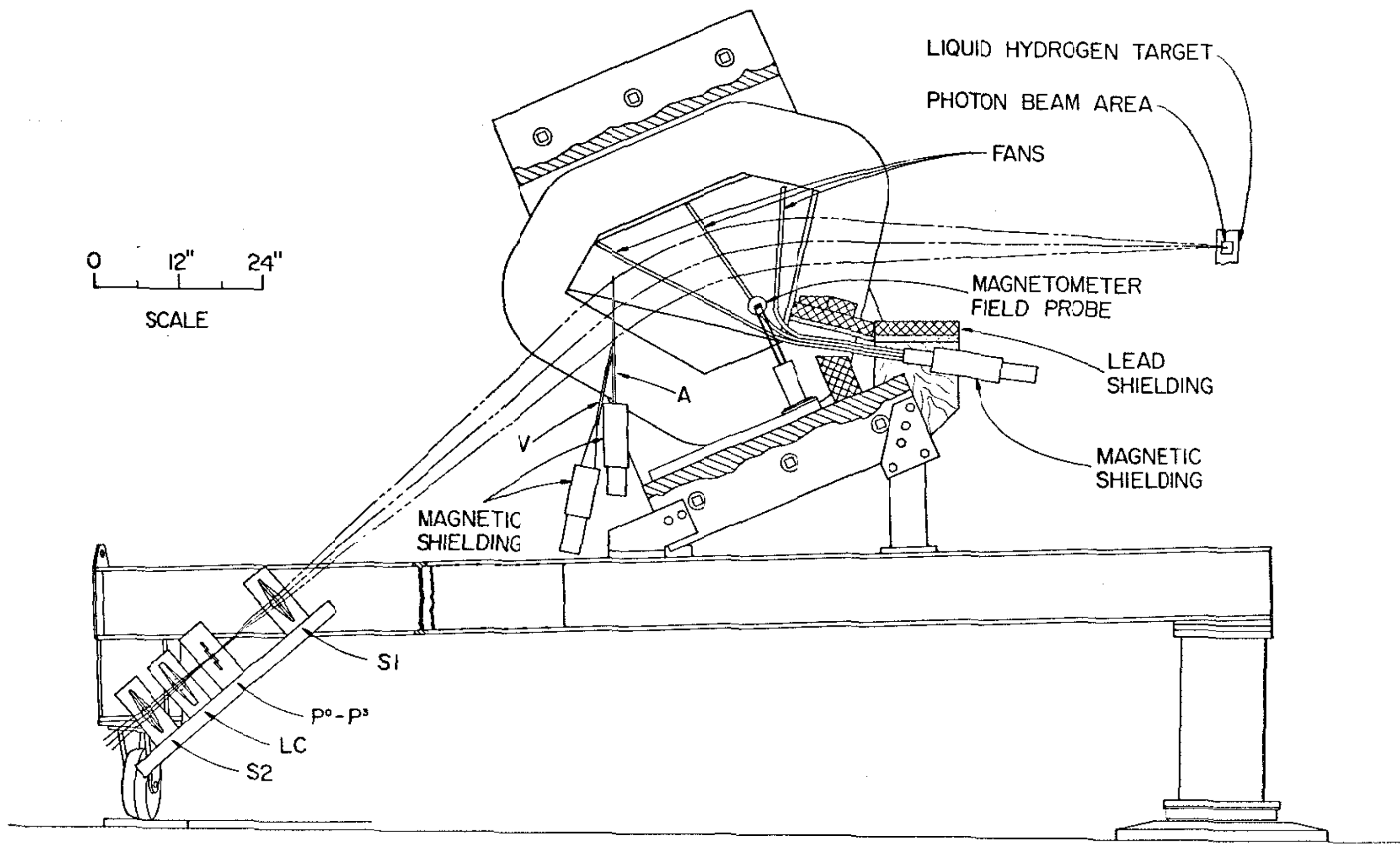

Figure 2. 600 MeV/c Magnet and Counters

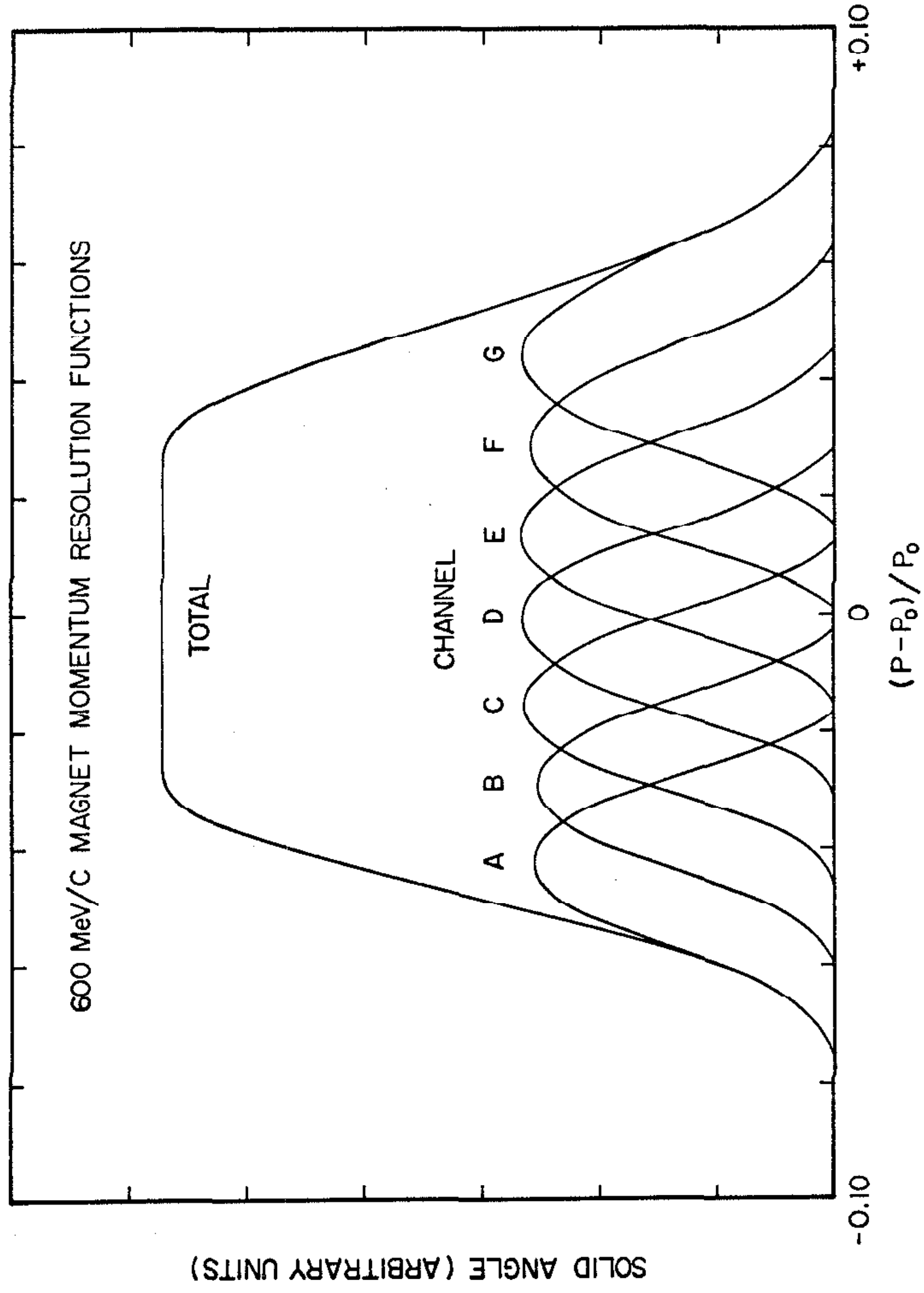
600 MeV/C MAGNET MOMENTUM RESOLUTION FUNCTIONS
TOTAL
CHANNEL
A
B
C
D
E
F
G
-0.10
0
+0.10
$(P-P_o)/P_o$
SOLID ANGLE (ARBITRARY UNITS)

Figure 3

A graphic display of the results of the magnet calibration measurements is presented in Figure 4. In this drawing, a contour map of the magnetic field is superimposed on a drawing of the pole tip structure. Three particle trajectories calculated by the ray tracing program[23] are shown. In addition, the effective edges (for a model with uniform field and zero fringe fields) computed by the same ray tracing program are shown. The accuracy of $\Delta\Omega\, \Delta P/P$ calculated from ray traces is expected to be $\pm$ 1% when a small correction for the variation with central field is included.[22]

The uniform field of the spectrometer is monitored with a nuclear resonance magnetometer. The central momentum of the spectrometer has been calibrated against the magnetometer by floating wire techniques.[22] This calibration has an absolute accuracy of $\pm$ 0.2% for a fixed location of the beam centroid. Because the beam centroid seems to wander slowly for fixed synchrotron energy, and because there is a systematic movement of the beam centroid with the synchrotron energy, the total error in the momentum calibration is taken to be $\pm$ 0.5%. The counters used with the 600 MeV/c Magnet are very similar in design and function to those which are in use on the High Energy Magnet.[9] The location of the counters is shown on Figure 3. The physical characteristics and use of each counter are given in Table 1.

The fan counters were designed so that no charged particle originating in the hydrogen target can undergo a single scattering from the pole tips and be counted in S2 without also being counted by one of the arms of the fan counters. In retrospect, it might have been useful to strengthen the specifications to include provision for vetoing neutrals which convert in the pole tips. The fan counters of the present design veto all events generated in the

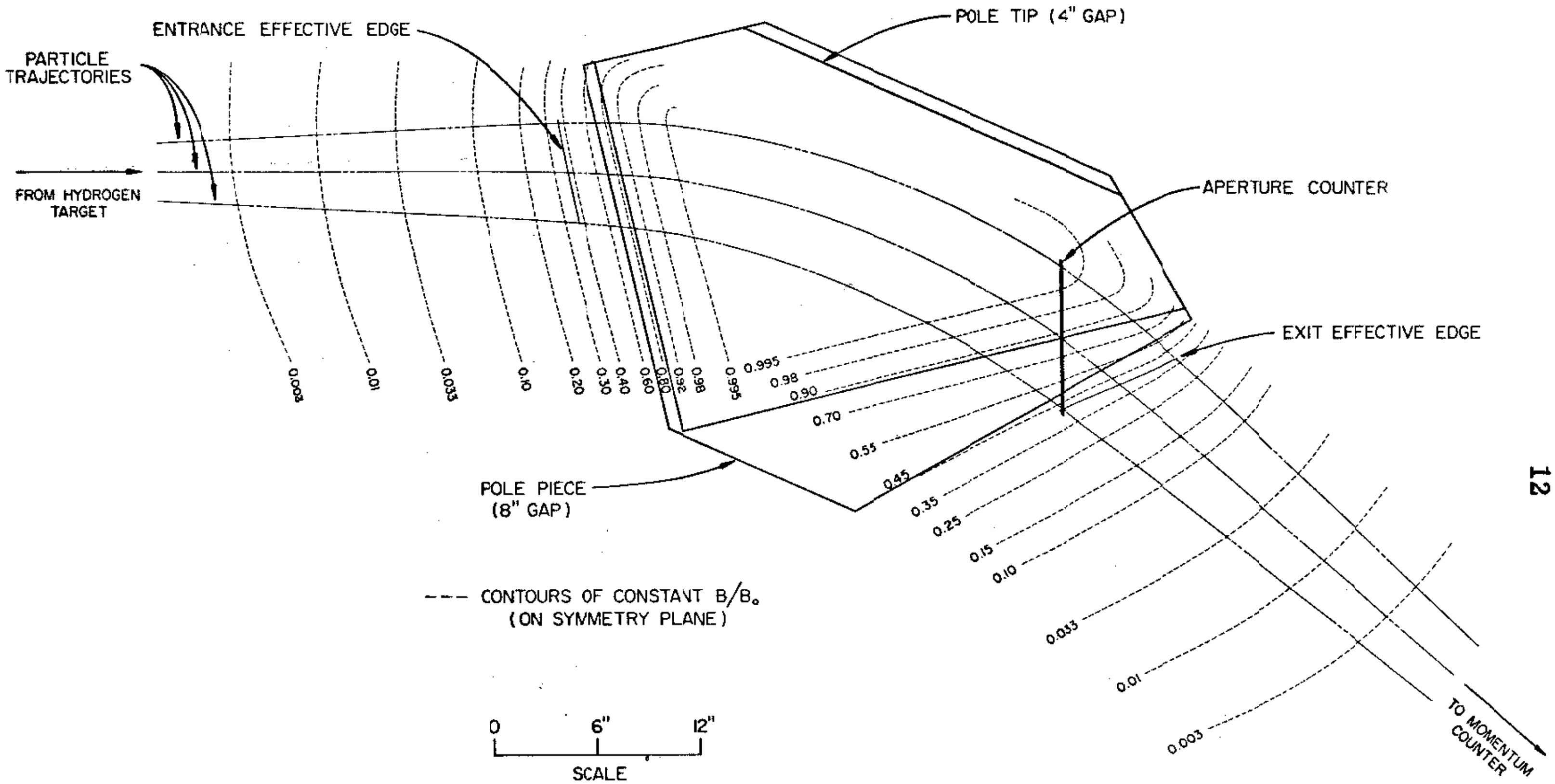

Figure 4. 600 MeV/C MAGNET OPTICS AT 10 KILOGAUSS

TABLE 1. Characteristics of 600 MeV/c Magnet Counters

Counter	Dimension (inches)	Mass (including wrapping) gm/cm^2	Type	Phototube	Comments
A	2.75 × 9.50 × 0.125	0.54	NE 102 Scintillator	1-6810A	Particles pass through at 42^{o}. Ends cut at 45^{o}. Defines solid angle of spectrometer. Mounted on long, thin lucite light pipe.
S1	7.50 × 15.00 × 0.250	0.74	NE 102 Scintillator	2-6655A	Used for particle definition and rejection of protons by dE/dx.
Average P Channel	"0.75 × 15.00 × 0.375"	1.08	NE 102 Scintillator	6655A	Defines momentum (see Figure 5).
LC	7.50 × 15.00 × 1.00	2.84	UVT Lucite	2-6810A	Cerenkov counter which rejects particles with velocity less than ~ 0.8 c.
S2	7.50 × 15.00 × 0.250	0.74	NE 102 Scintillator	2-6655A	Time-of-flight (A · S2) and dE/dx rejection of protons.
Fans	3-1/2 × 1/2 rods bent as shown in Figure 2.	not in normal path	NE 102 Scintillator	2-6810A	Veto scattering from pole faces.
V	8.00 × 12.00 × 0.250	not in normal path	NE 102 Scintillator	6655A	Veto events with particle passing through light pipe of A.

TABLE 2. Properties of Momentum Channels of 600 MeV/c Magnet

Channel	Width (inches)	$(\bar{P}-P_o)/P_o$ x 10^2	$\Delta\Omega\,\Delta P/P_o$ x 10^5	Logical Definition
A	0.759	-4.29	4.314	$P^0 \cdot \bar{P}^1 \cdot \bar{P}^2 \cdot \bar{P}^3$
B	0.734	-2.96	4.324	$P^0 \cdot P^1 \cdot \bar{P}^2 \cdot \bar{P}^3$
C	0.756	-1.58	4.612	$\bar{P}^0 \cdot P^1 \cdot \bar{P}^2 \cdot \bar{P}^3$
D	0.753	-0.13	4.800	$\bar{P}^0 \cdot P^1 \cdot P^2 \cdot \bar{P}^3$
E	0.758	1.38	4.976	$\bar{P}^0 \cdot \bar{P}^1 \cdot P^2 \cdot \bar{P}^3$
F	0.734	2.92	5.000	$\bar{P}^0 \cdot \bar{P}^1 \cdot P^2 \cdot P^3$
G	0.759	4.52	5.359	$\bar{P}^0 \cdot \bar{P}^1 \cdot \bar{P}^2 \cdot P^3$
H = TOTAL	5.253	0.19	33.65	Sum of events satisfying logic for each of above channels. (Note that this definition is not the same as $P^0+P^1+P^2+P^3$.)

$\bar{P}$ = mean momentum of particles accepted by a given channel

P_o = central momentum of magnet

pole tips by charged particles, but approximately 1/3 of the area of the pole tips is not shielded against events generated by neutrals.

The momentum-defining counter consisted of four scintillators which were mounted in the form of a seven channel hodoscope. A drawing of this counter is shown in Figure 5. The important parameters defined by the seven channels of this hodoscope are presented in Table 2. The decoding of the output of this hodoscope was done by the IBM 7094 computer. The logical definition used for this decoding is also given in Table 2.

C. Electronics

The electronics system for this experiment was broken down into three independent subblocks: a fast logic system containing the coincidence circuits; a pulse-height analysis system containing linear gates and discriminators; and a data storage system making use of a Nuclear Data 1024 channel pulse-height analyzer. The relationship between these three subsystems is shown in Figure 6.

The block diagrams of the fast logic system and the pulse-height analysis system are given in Figure 7. The modules from which these two systems were constructed have been described in the literature.[24, 25] Some of these modules were upgraded by installing more modern transistors on already existing circuit boards; otherwise these modules were the same ones which were used in the Groom-Marshall K^+ telescope experiment.[26]

The particle signature in this experiment consisted of a fast (10 nanosecond) triple coincidence, A· S1· S2, with coincidence circuit input biases of approximately 1/4 minimum ionizing. The basic trigger generated by the fast logic was

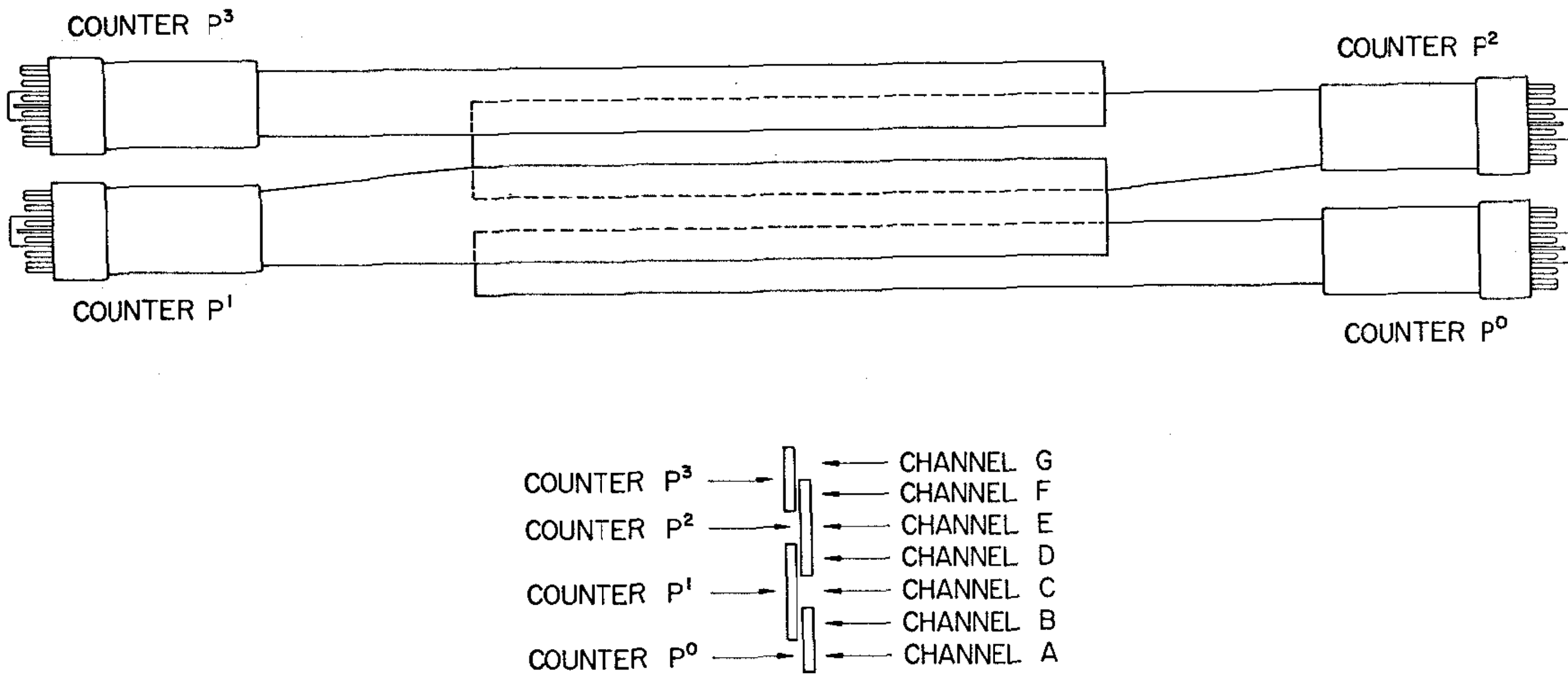

Figure 5. Momentum Hodoscope Counters P^i

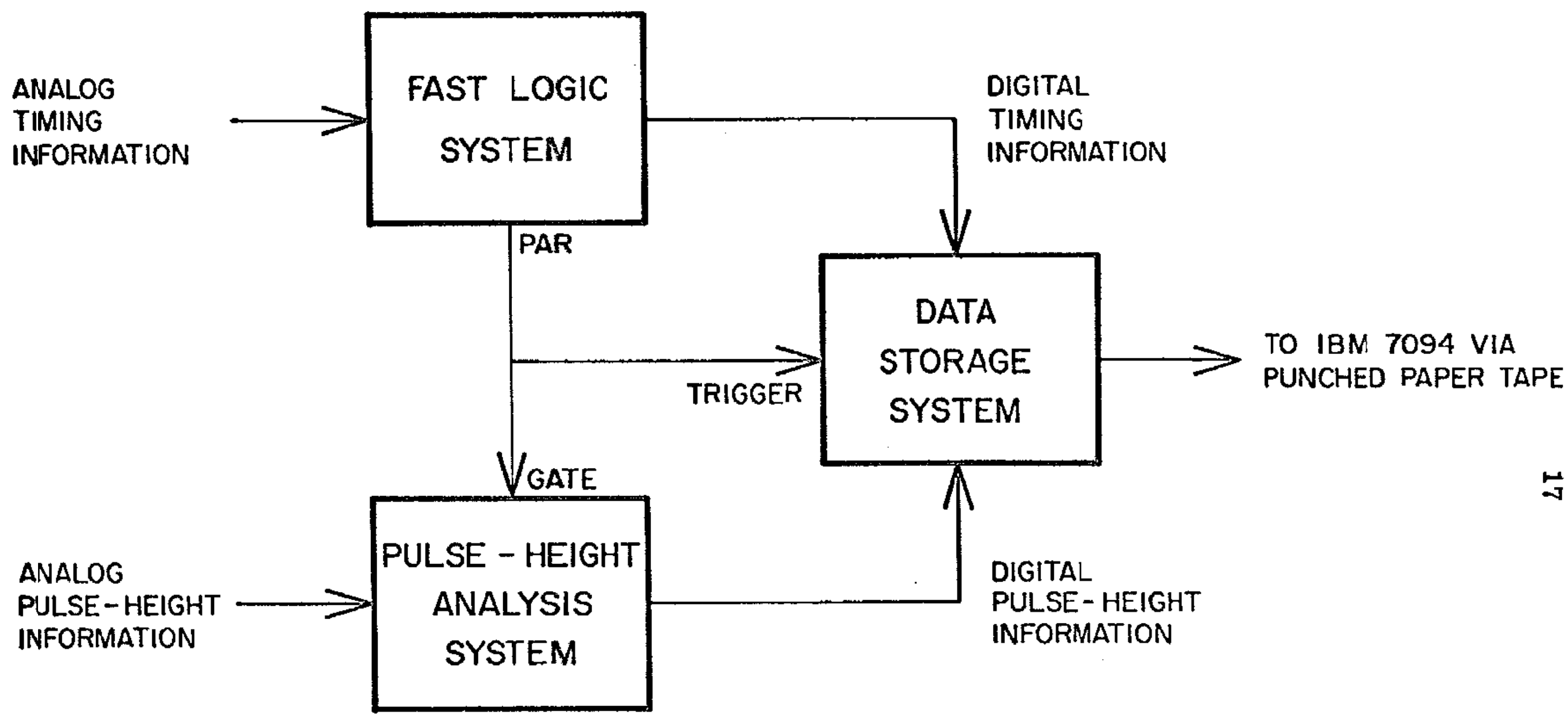

Figure 6

SYSTEM BLOCK DIAGRAM

600 MeV/C MAGNET ELECTRONICS

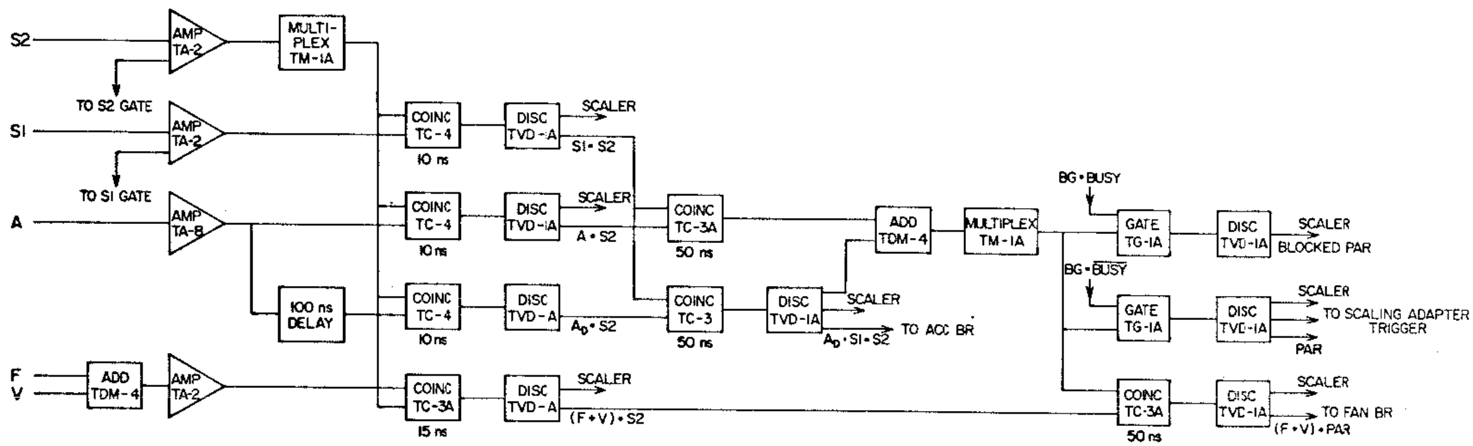

(a) TRIGGER LOGIC SYSTEM BLOCK DIAGRAM

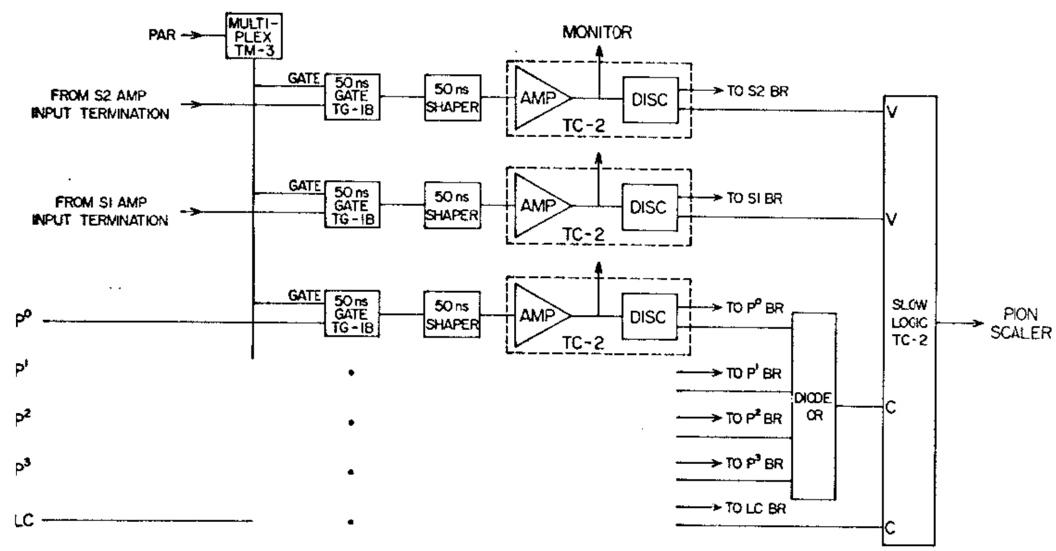

(b) PULSE HEIGHT ANALYSIS SYSTEM BLOCK DIAGRAM

Figure 7

$$PAR = A \cdot S1 \cdot S2 + A_d \cdot S1 \cdot S2$$

where A_d indicates that the A signal was delayed by 100 nanoseconds from the correct timing. The signal PAR was used to operate the linear gates of the pulse-height analysis system and to trigger the data storage system.

Several scalers were used in the fast logic system. These scalers were extremely useful for diagnostic purposes, but they did not record numbers which could be used directly in cross section calculations. The final data were recorded only by the data storage system.

The data storage system was a new feature of this experiment. This system operated on the principle that each event could be represented by a 9 bit binary number. Each bit of this binary number was controlled by a digital output from either the fast logic system or the pulse-height analysis system. For each event, a count was added to the channel whose address was the same as this binary number. After a data-taking run, the contents of the memory were punched on paper tape. The IBM 7094 computer was then used to sort the 512 possible types of events into physically useful classes.[27] A block diagram of the data storage system is presented in Figure 8. For further details of the electronics, the reader should refer to the SCALING ADAPTER instruction manual.[28]

The correspondence between digital signals and the various bits of the binary number which defines the address is explained more fully in Table 3. Note that the 2^9 bit is always set to 1 so that the result will be stored in the second half of the memory. As an example of how the address for each event is generated, consider the event

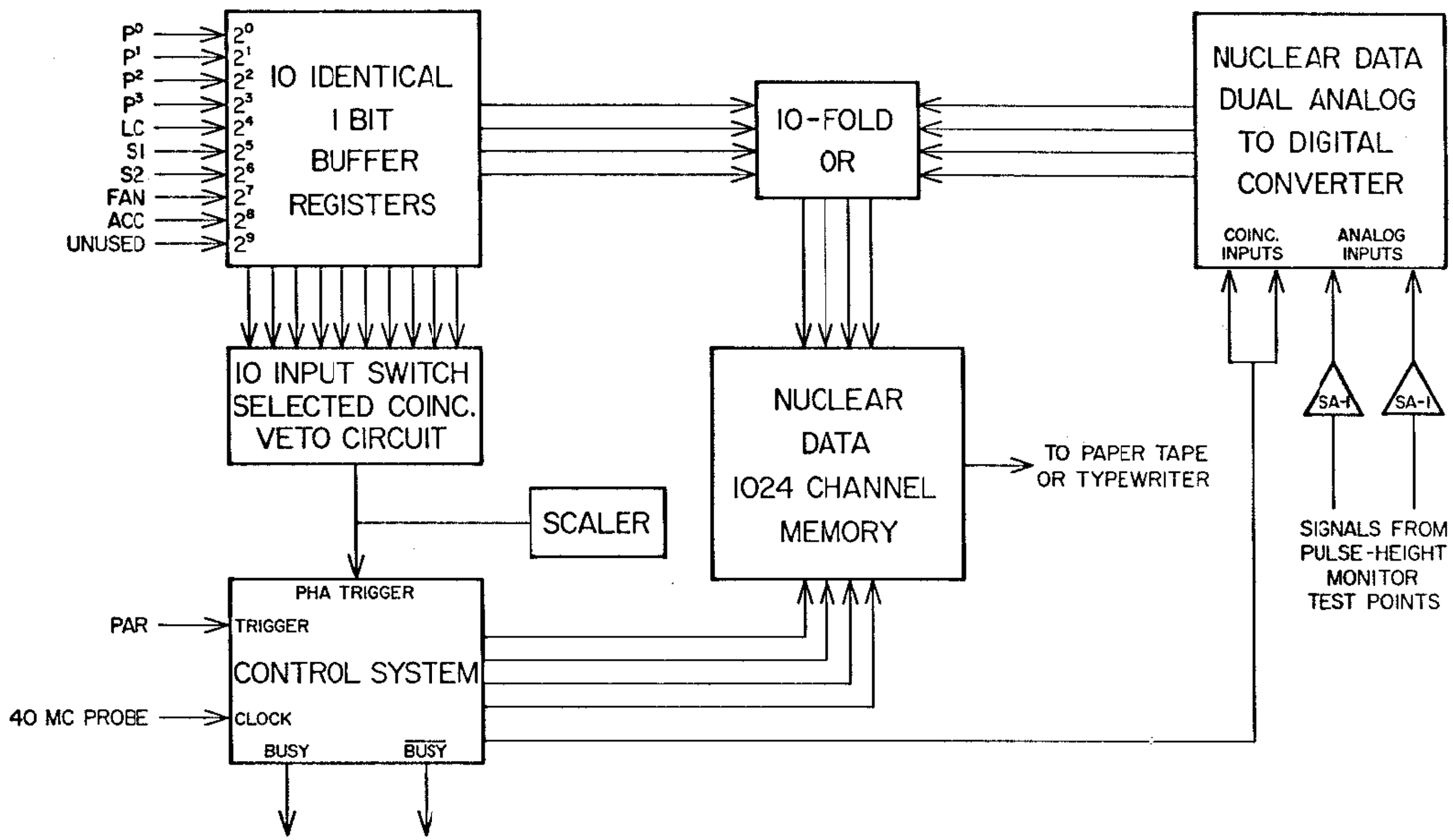

Figure 8

DATA STORAGE SYSTEM BLOCK DIAGRAM

TABLE 3. Coding of Address Register Bits

Address Bit	Signal Source	Requirement
2^0	P^0	1/2 x minimum ionizing
2^1	P^1	1/2 x minimum ionizing
2^2	P^2	1/2 x minimum ionizing
2^3	P^3	1/2 x minimum ionizing
2^4	LC	~ 1 photoelectron or $\beta \gtrsim 0.8$
2^5	S1	~ 2.5 x minimum ionizing
2^6	S2	~ 2.5 x minimum ionizing
2^7	(F+V)· PAR=FAN	F or V count within $\pm$ 8 ns of PAR
2^8	A_d· S1· S2 = ACC	PAR generated by accidental event in A
2^9	unused	always "1" so that all events are stored in second half of memory

$$\overline{ACC}\cdot \overline{FAN}\cdot \overline{S2}\cdot \overline{S1}\cdot LC\cdot \overline{P}^3\cdot P^2\cdot P^1\cdot \overline{P}^0$$

where S1 and S2 represent the high biases (~ 2.5 × minimum ionizing) on these two counters. This event is a typical pion in the central momentum channel. The address corresponding to this event is 1000010110 binary, or 534 decimal.

Because only 512 of the 1024 available channels of memory were needed for storage of the data, provision was built into the control system to allow the pulse-height analyzer to go through a normal pulse-height analysis cycle before storing the digital data for each event. The result of the pulse-height analysis was always recorded in the first half of the memory. Since the pulse-height analysis cycle did not interfere with the normal data storage cycle, the pulse-height analyzer was free for use as a diagnostic tool during data taking. Using this feature, the pulse-height distribution in each counter was checked on a daily basis.

An additional provision built into the control system permitted the use of the normal clock channel of the memory, channel zero, for recording beam monitoring information. This feature proved to be of only marginal value, however, for no single beam monitor was considered to be stable enough for use in cross section computations. This subject is discussed further in Appendix I.

IV. EXPERIMENTAL TECHNIQUE

A. Particle Identification

The major problems to be solved by the particle identification scheme were elimination of proton contamination and correction for accidentals. The proton contamination problem was most serious at small angles and high momenta where the time-of-flight requirements did not completely eliminate protons and the ratio of π^+ to protons incident on the spectrometer was 1:3. The efficiencies of the various devices which eliminated protons are given in the following table:

Typical Pion and Proton Efficiency at 570 MeV/c

Technique	ϵ_π	ϵ_P
Time-of-flight	1.00	0.1
S1 (high bias)	0.05	0.98
S2 (high bias)	0.05	0.98
LC	0.98	0.03

The time-of-flight requirement in conjunction with any two of the other counters was more than sufficient to eliminate protons under the worst conditions. The redundancy provided by LC permitted a continuous monitoring of the efficiencies of each counter for pions and protons.

The definition of π^+ used in this experiment was

$$\pi^+ = \text{PAR} \cdot (\overline{\text{S1} \cdot \text{S2}})$$

where S1 and S2 indicate the high biases on counters S1 and S2. The IBM 7094 computer automatically corrected each run for the inefficiency of the pion definition and any residual proton contamination. Both of these corrections were less than 1.0% in the worst case.

The counter system of the 600 MeV/c Magnet was designed for minimum mass in the particle trajectories in order to minimize the effects of multiple scattering on the resolution of the spectrometer. Since only one aperture counter was used, this system was particularly sensitive to events produced by an accidental in counter A and a real event in the rear counter system. Since the data recording system was triggered by $A \cdot S1 \cdot S2 + A_d \cdot S1 \cdot S2$, the IBM 7094 automatically corrected the observed number of pions for this type of accidental by subtracting the events with an A_d = ACC pulse from those events with no ACC pulse.

A correction for accidentals in the momentum defining counters was also made. This correction was based on the observed number of events with counts in the momentum hodoscope which could be generated only by accidentals or two particles passing through the hodoscope within the 50 ns. gate. An example of such an event is $P^0 \cdot \bar{P}^1 \cdot \bar{P}^2 \cdot P^3$. Eight of the sixteen possible kinds of event in the momentum hodoscope fell into this category, and these events were used to compute the corrections for each channel on the assumption that there was no correlation between the location of the true event and the second particle. The magnitude of this correction to the sum channel (H) was typically 0.5%, while the correction to individual channels was less than 2%. It is important to note that events in which a second particle passes through the channel adjacent to the true particle cannot be distinguished from single particle events. However, such events were counted only once and were counted in either the correct channel or the channel adjacent to the correct channel.

Several checks were made of the efficiency of the fast electronics. For counters A, S1, S2, and V a separate small counter was used to define a beam and test the efficiency of the coincidence circuit. In each case the efficiency was greater than 99%. The 1% of inefficient events were observed on an oscilloscope and most of these were found to have no pulse at all in the counter being tested. These events were assumed to be events due to nuclear absorption or photon conversion in the counters and the electronic efficiency was taken to be 1.00 in each case. The A· S1· S2 and A_d· S1· S2 systems were checked by installing an extra 100 ns. length of cable in the A input. The result was that the two systems gave the same number of counts to within 5%. The fan counter efficiency was tested and found to be greater than 95% for minimum ionizing particles passing through the tip of the longest arm of each counter (see Figure 2). Fan accidentals in the F + V system were found to be less than 1% under normal operating conditions. On the basis of these measurements, it was believed that the overall efficiency of the electronic system was 1.00 ± 0.01.

B. Empty Target Background

The empty target background was measured on two or more occasions for each data point. In general, empty target runs were taken within a few days of full target runs to correct for any possible buildup of solid substances on the mylar cup. For those cases in which the high energy magnet yoke was in the beam line for a full target run, an empty target run was taken under the same conditions. Typically, one-fifth of the total running time was spent measuring the empty target background.

For illustrative purposes, the observed ratios of empty target to full target rates are presented in Table 4. The data have been summed over the seven channels and averaged over the several runs taken at each point. However, the cross section computing program did not average the empty target runs; instead, it associated each full target run with a particular empty target run and calculated the cross sections independently. Only in this way would a varying empty target rate be correctly treated.

C. Negative Field Background

Since no electron detector was used in this experiment, a series of tests was made to look for possible e^+ contamination in the π^+ events. These tests were made with the normal magnet and synchrotron settings, but with the magnet field reversed. Under these conditions, the only single pion photoproduction process which can contribute is the reaction

$$\gamma + n \rightarrow \pi^- + p$$

Since neutrons are found only in the target structure, these events should be removed by an empty target subtraction. If we assume that e^- and e^+ are produced in equal numbers, as in pair production, then the e^- yield in the field reversed run should be equal to the e^+ contamination in the normal runs.

TABLE 4. Fractional Empty Target Rates Summed Over 7 Channels
(See Table 6 for Point No. Definition)

Point No.	Empty/Full	Point No.	Empty/Full
34-1	5.2 ± 0.3%	84-1	7.8 ± 1.1%
34-2	4.7 ± 0.4%	84-2	6.0 ± 0.8%
34-3	6.1 ± 0.4%	84-3	3.9 ± 0.6%
		84-4	2.9 ± 0.5%
40-1	3.9 ± 0.3%	85-5	5.4 ± 0.5%
40-2	3.8 ± 0.3%	84-6	4.9 ± 0.5%
40-3	4.6 ± 0.6%		
		94-1	7.8 ± 1.0%
48-1	3.6 ± 0.4%	94-2	5.2 ± 0.7%
48-2	3.4 ± 0.3%	94-3	4.5 ± 0.7%
48-3	4.6 ± 0.5%	94-4	2.8 ± 0.5%
48-4	4.9 ± 0.5%	94-5	6.0 ± 0.7%
56-1	4.8 ± 0.5%	106-1	8.0 ± 0.8%
56-2	4.6 ± 0.5%	106-2	5.8 ± 0.7%
56-3	4.5 ± 0.5%	106-3	4.9 ± 0.7%
56-4	3.6 ± 0.5%	106-4	4.9 ± 0.7%
		106-5	5.6 ± 0.7%
64-1	4.7 ± 0.5%		
64-2	4.6 ± 0.3%	120-1	8.2 ± 1.2%
64-3	3.6 ± 0.5%	120-2	4.7 ± 0.9%
64-4	4.6 ± 0.5%	120-3	5.9 ± 0.7%
64-5	6.4 ± 0.5%	120-4	5.3 ± 0.7%
		120-5	6.8 ± 0.8%
74-1	5.6 ± 0.8%		
74-2	4.7 ± 0.7%	134-1	6.2 ± 0.6%
74-3	4.3 ± 0.5%	134-2	6.0 ± 0.9%
74-4	4.6 ± 0.5%	134-3	4.9 ± 0.6%
74-5	4.5 ± 0.7%	134-4	5.6 ± 0.7%
74-6	3.7 ± 0.5%		
		156-1	10.7 ± 1.2%
		156-2	5.7 ± 0.8%
		156-3	7.4 ± 1.0%
		156-4	10.5 ± 1.1%

The field reversed runs were taken at several points which scanned the entire range of angles and energies used in this experiment. In order to improve the statistics, the results were summed over the seven momentum channels. The total amount of synchrotron time used for each of these points was approximately equal to half the amount of time used at each of the normal points. The results of these negative field tests are presented in Table 5. These results indicate that approximately two thirds of the observed events are produced in the target structure, but that the remainder of the events are produced in the hydrogen. Except for the points taken at the highest energies and most backwards angles, neglecting these events would result in errors which were small compared with the statistical errors of this experiment.

Several possibilities for the source of the negative field events have been considered. π^0 photoproduction with conversion of the decay photons in the target structure could result in a source of high energy electrons. However, this process can be calculated from known π^0 cross sections and gives an upper limit of 0.2% of the π^+ rate. If photons were converted in the aperture counter at the rear of the magnet, then low energy electrons could be counted. To check this effect, a 1/8" copper radiator was placed on the hydrogen target side of the aperture counter. This radiator had a thickness in radiation lengths of 29 times that of the aperture counter. For point number 134-4, the full target negative field yield was 0.17 ± 0.02 counts/QBIP, while with the radiator in place this rate increased to 0.55 ± 0.07 counts/QBIP. If we assume that half the full target events are due to π^- produced in the target walls, we would have expected an increase of a factor of 15 if all the remaining events were due to photons converting in the radiator, whereas a

TABLE 5. Summary of Negative Field Runs

Point	Full Target* π^-/QBIP**	Empty Target* π^-/QBIP**	Difference* π^-/QBIP**	$\frac{\pi^-}{\pi^+}$
34-1	0.950 ± 0.07	0.620 ± 0.06	0.330 ± 0.09	0.012 ± 0.003
48-2	0.400 ± 0.04	0.340 ± 0.04	0.060 ± 0.06	0.003 ± 0.003
64-3	0.330 ± 0.03	0.200 ± 0.02	0.130 ± 0.04	0.008 ± 0.002
84-1	0.110 ± 0.013	0.049 ± 0.009	0.061 ± 0.015	0.007 ± 0.002
84-4	0.205 ± 0.017	0.110 ± 0.015	0.095 ± 0.023	0.012 ± 0.003
106-1	0.113 ± 0.014	0.064 ± 0.010	0.049 ± 0.017	0.049 ± 0.017
106-4	0.187 ± 0.017	0.125 ± 0.016	0.062 ± 0.023	0.015 ± 0.005
134-1	0.111 ± 0.015	0.052 ± 0.009	0.059 ± 0.017	0.055 ± 0.017
134-3	0.119 ± 0.011	0.100 ± 0.012	0.019 ± 0.019	0.007 ± 0.007

* summed over momentum channels so that $\Delta\Omega\, \Delta P/P = 3.4 \times 10^{-4}$

** 1 QBIP = 1.2×10^{13} MeV

factor of 3.2 ± 0.4 was observed. Thus this process can only account for a small fraction of the observed events. The contribution of multiple pion photoproduction was also checked. Using the known shape of the tails of the resolution functions due to decay and multiple scattering and data on π^- photoproduction at 84° lab[11], we find that at most 10% of the observed events can be due to this process.

The negative field events can also be due to low energy pions or electrons which have the wrong momentum but can be counted because of wide-angle scattering processes, or the events may be due to conversion of photons in portions of the magnet iron which are not guarded by veto counters. Neither of these possibilities was investigated in any detail.

The conclusion drawn from the negative field runs was that an unexplained background exists and must be subtracted from the π^+ data. To make this subtraction, it was necessary to extrapolate to angles and energies at which no negative field runs were taken. For the purposes of this extrapolation, the negative field yield was assumed to be a function only of lab angle. The empirical formula

$$\pi^-/\mathrm{QBIP} = 0.03 + 0.05 \left(\frac{\theta - 180^\circ}{90^\circ} \right)^2$$

was found to give a good fit to the data. This function and the data of Table 5 are plotted in Figure 9. In order to indicate the expected errors in this correction, an rms error of 1/2 the correction has been included in the error bars of all the cross sections measured in this experiment.

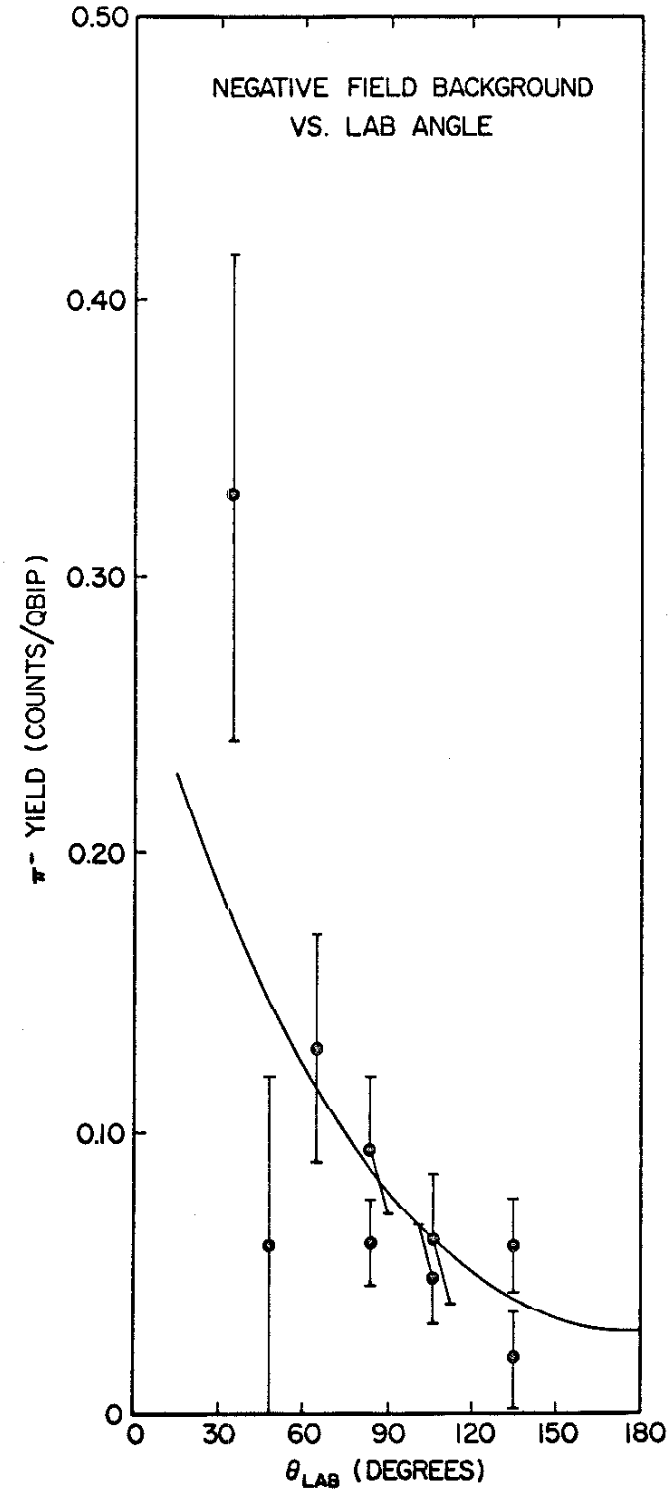
NEGATIVE FIELD BACKGROUND
VS. LAB ANGLE
π⁻ YIELD (COUNTS/QBIP)
0.50
0.40
0.30
0.20
0.10
0
0
30
60
90
120
150
180
θLAB (DEGREES)

Figure 9

Experimental evidence for a small positron contamination at large angles is lacking in previous experiments. For experiments at small angles, the positron detection system usually showed a large ratio e^+/π^+ which decreased rapidly to zero near 15^o lab. For angles between 15 and 45^o, e^+/π^+ was found to be small and neither Dixon[12] nor Kilner[13] used electron detection systems for lab angles greater than 55^o. One bit of evidence is available from the present experiment. The excitation curve taken at $\theta_{lab} = 64^o$ near K = 880 showed a background of events in the below threshold region. This background was 0.15 ± 0.02 counts/QBIP in seven channels before correction for negative field contamination. The correction used in this experiment gives 0.10 ± 0.05 counts/QBIP. By comparison, the π^+ yield was 5.0 counts/QBIP for the normal point. Thus it appears that the correction used gives a reasonable but crude approximation to the true background.

D. Excitation Functions as Proof of Particle and Reaction Identification

Two excitation functions were measured during this experiment. The first was taken near $\theta_{cm} = 95^o$ and K = 900 MeV, and the second near $\theta_{cm} = 150^o$ and K = 750 MeV. For each measurement, the magnet was set at constant momentum and lab angle while the synchrotron energy was varied. The counting rate in each channel was measured as a function of the synchrotron beam energy meter reading. The expected values of these rates were computed from the cross sections measured in this experiment and the resolution function used in reducing all the data. This resolution function includes the effects of multiple scattering, pion decay, and angular resolution. The data and the expected yields are plotted in Figures 10a - 10n. The plotted data were corrected for empty target and negative field background.

Several important conclusions can be obtained from these data. The first conclusion is that in the off kinematics region (where the expected yields were less than 3% of the peak yields), there is a background of $1.0 \pm 1.0\%$, and most of the uncertainty comes from the negative field correction. The second conclusion is that the resolution function calculation gives a reasonable approximation to the true resolution of this experiment. Finally, the best fit to the data gives a value for the energy meter calibration constant, $E_{o\ true}/E_{o\ meter} = 1.025 \pm 0.005$. This calibration agrees satisfactorily with the measurements of Stan Ecklund[9] and the new calibration of the beam energy meter electronics.[29]

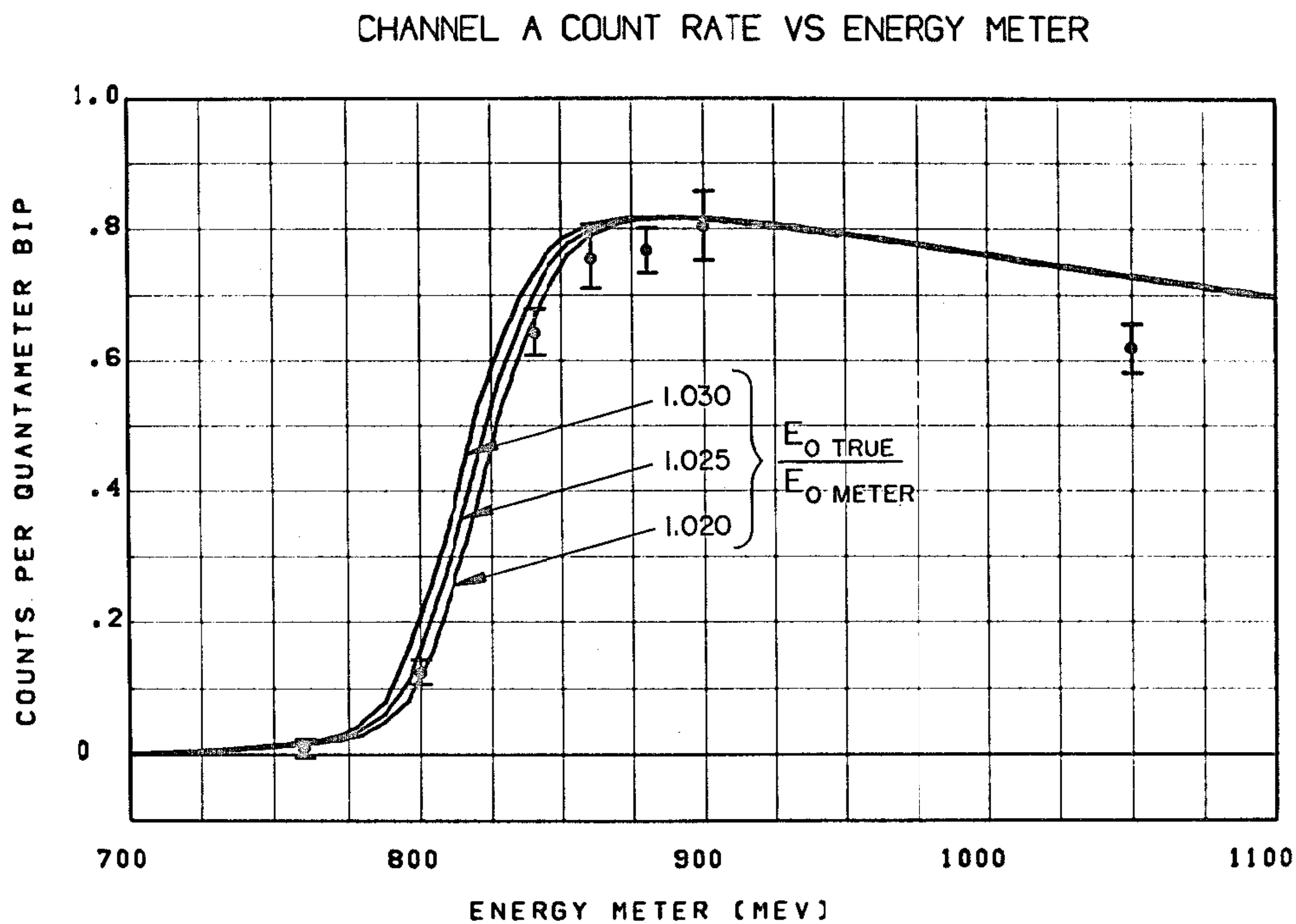

Figure 10a. Excitation Function at 64^0 Lab.

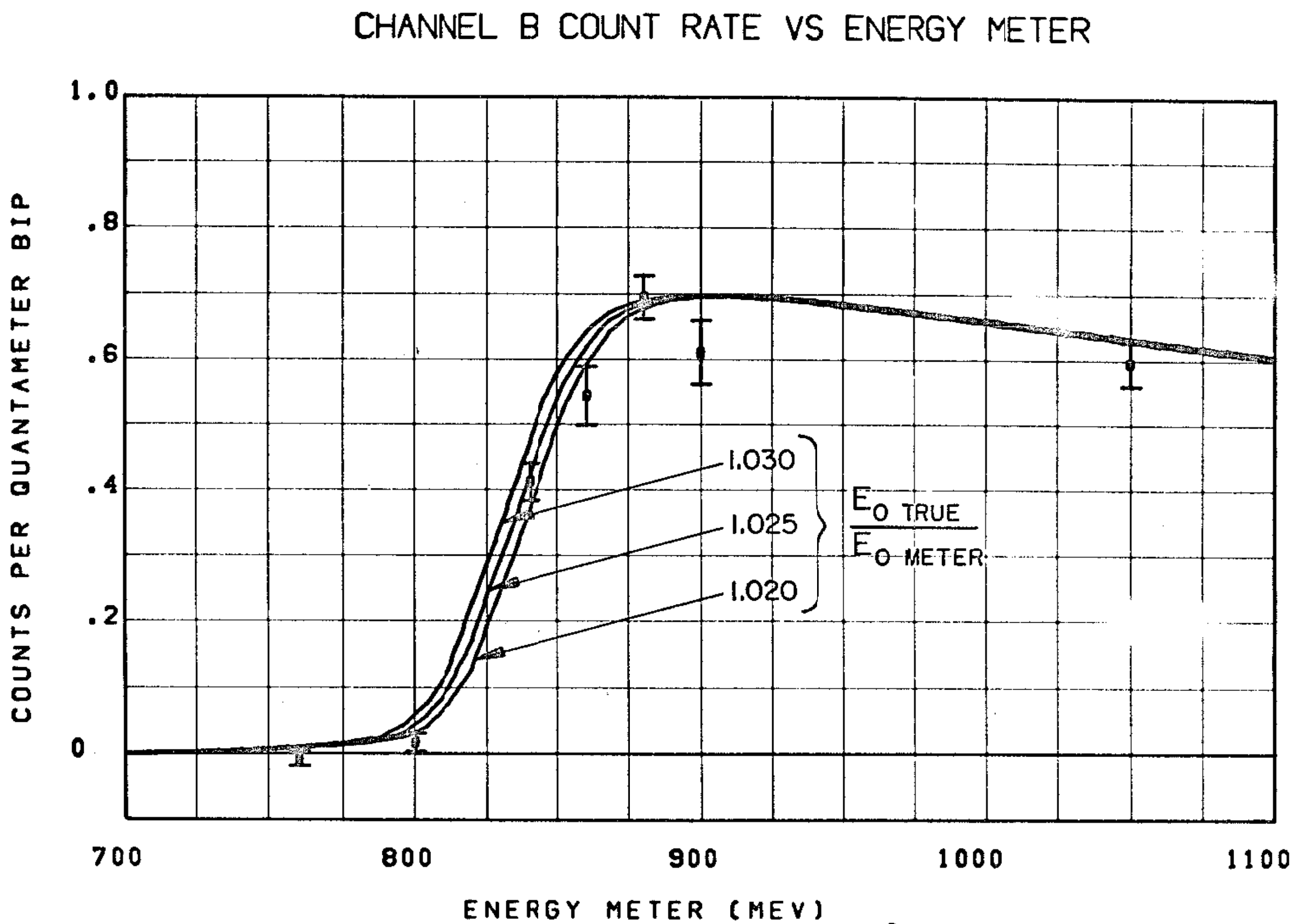

Figure 10b. Excitation Function at 64° Lab.

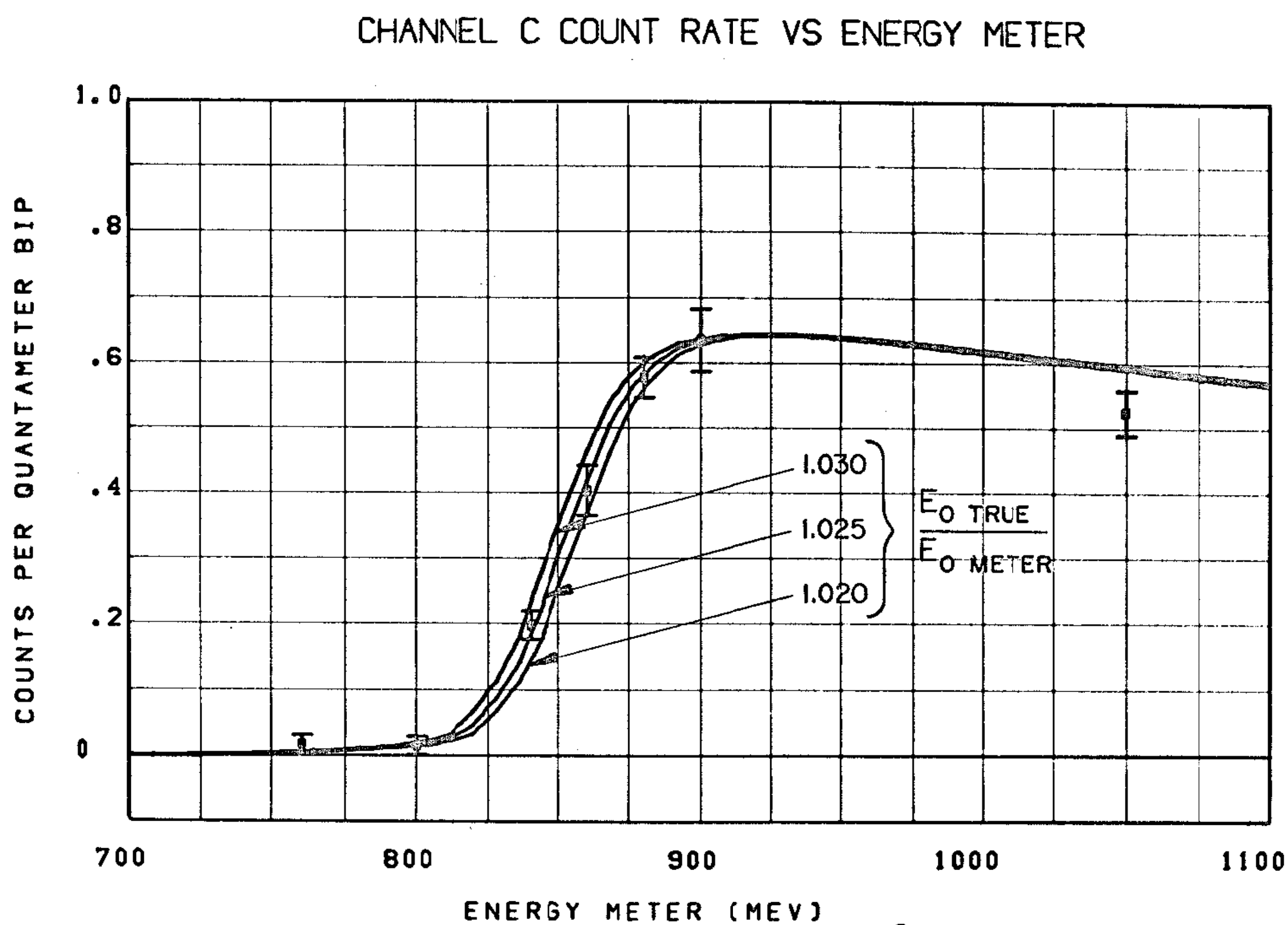

Figure 10c. Excitation Function at 64° Lab.

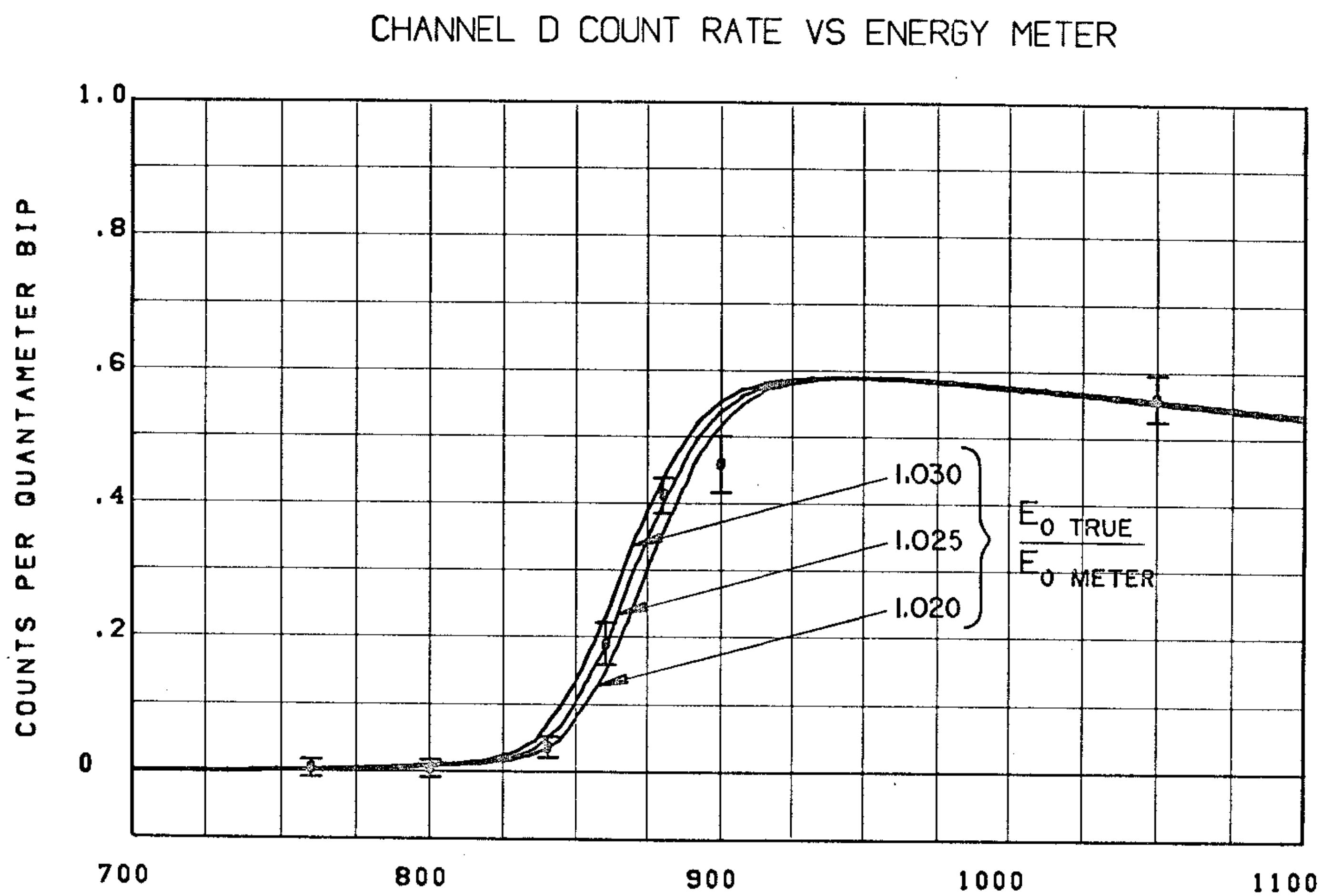

Figure 10d. Excitation Function at 64° Lab.

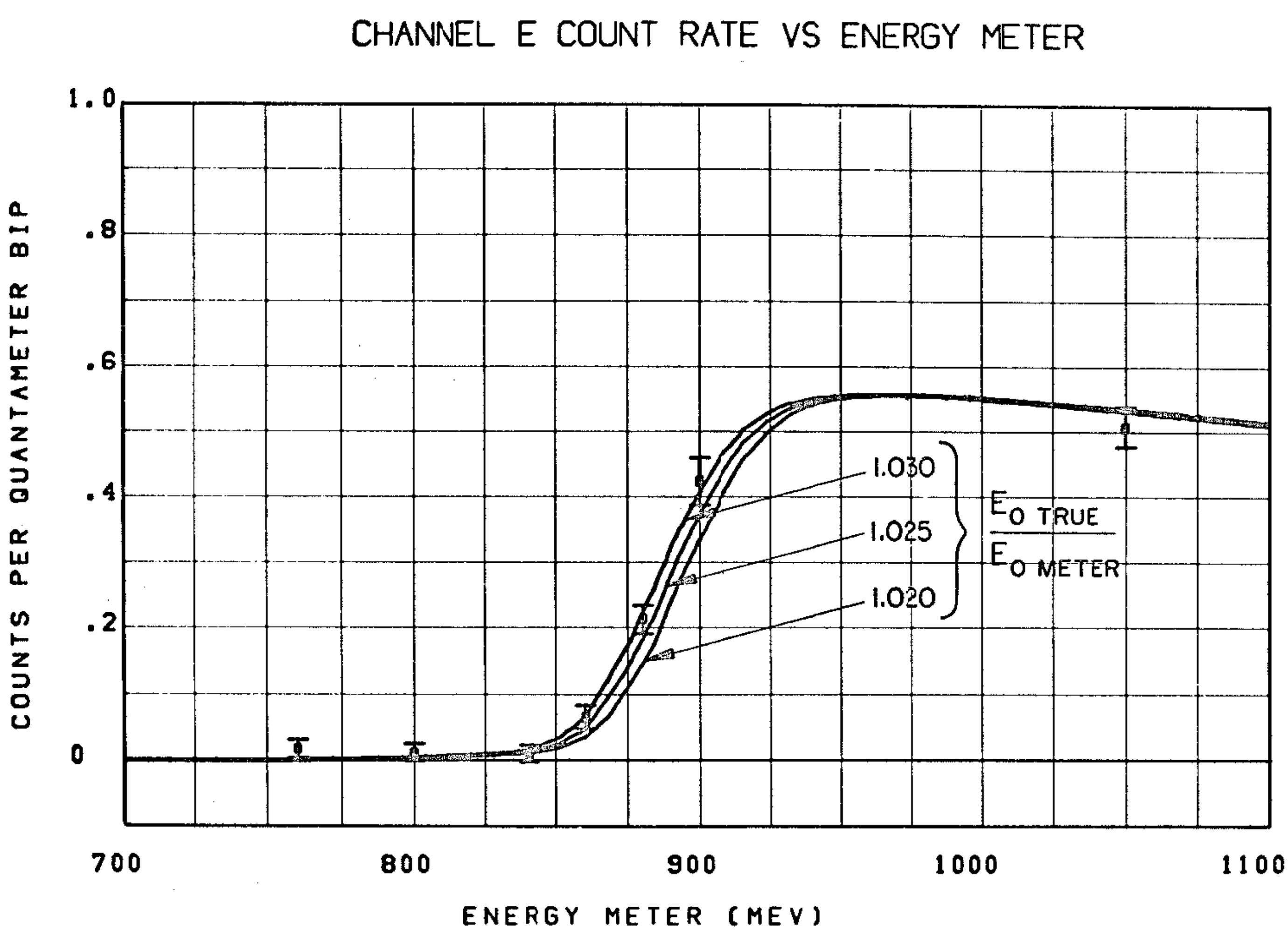

Figure 10e. Excitation Function at 64° Lab.

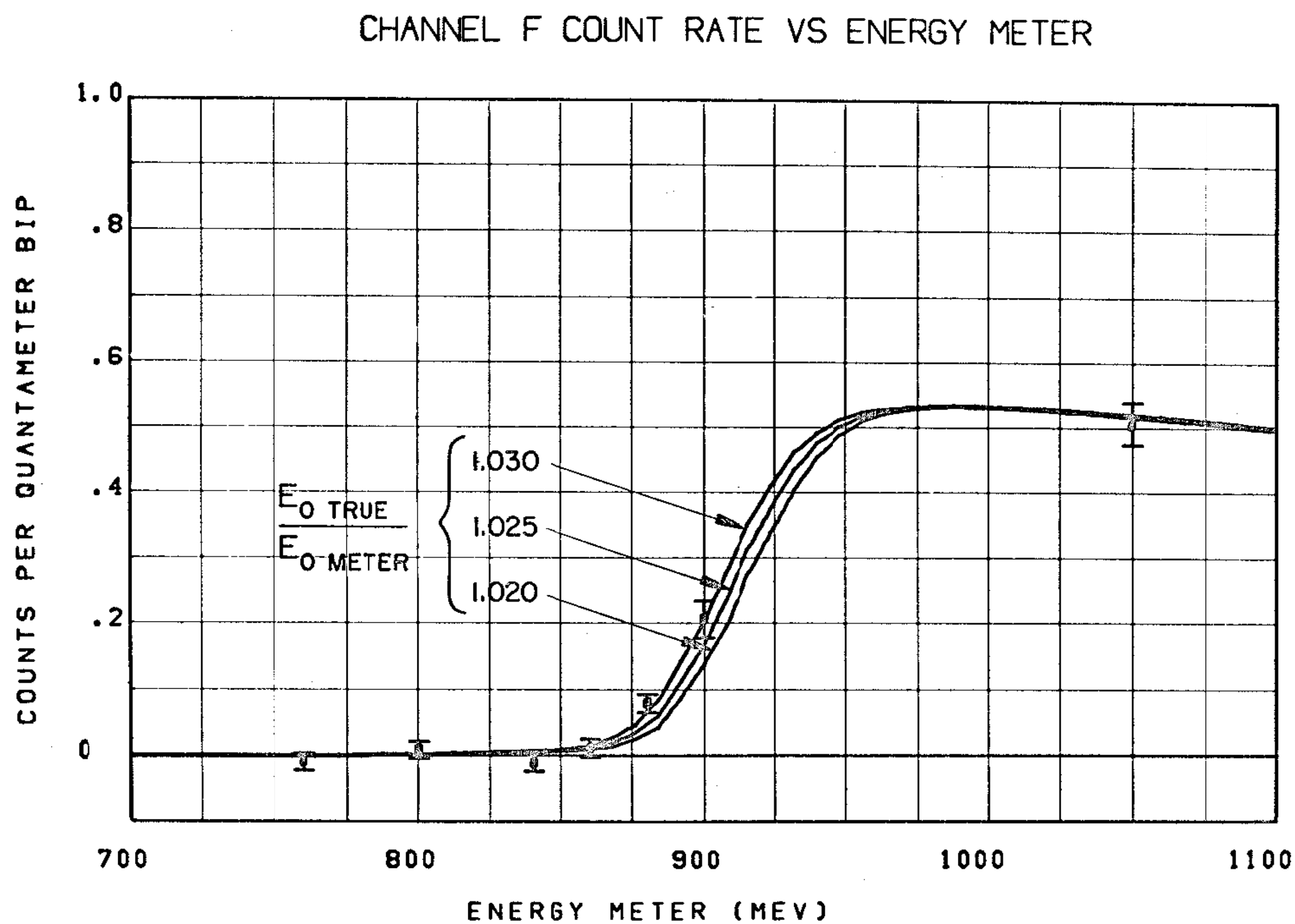

Figure 10f. Excitation Function at 64° Lab.

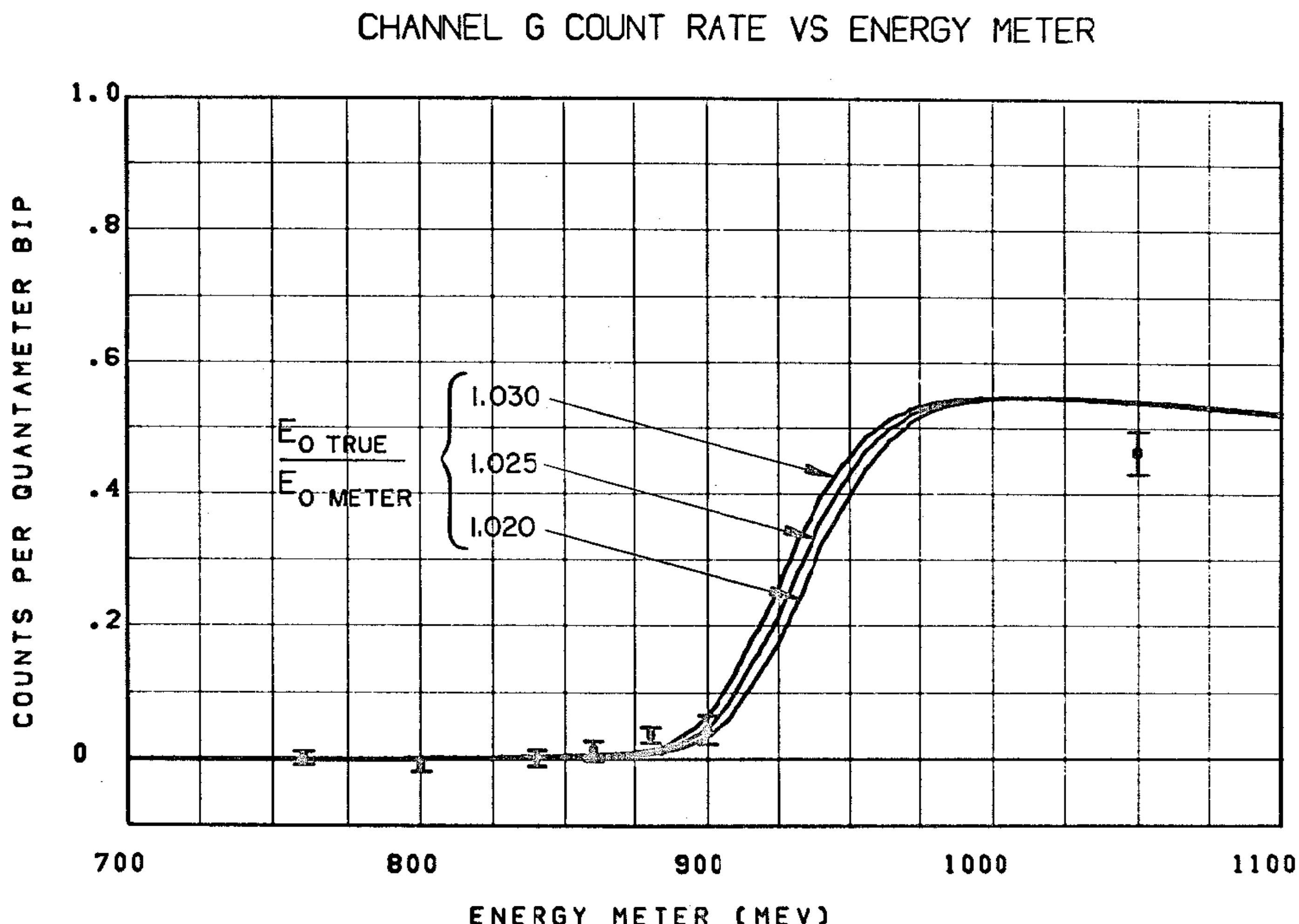

Figure 10g. Excitation Function at 64° Lab.

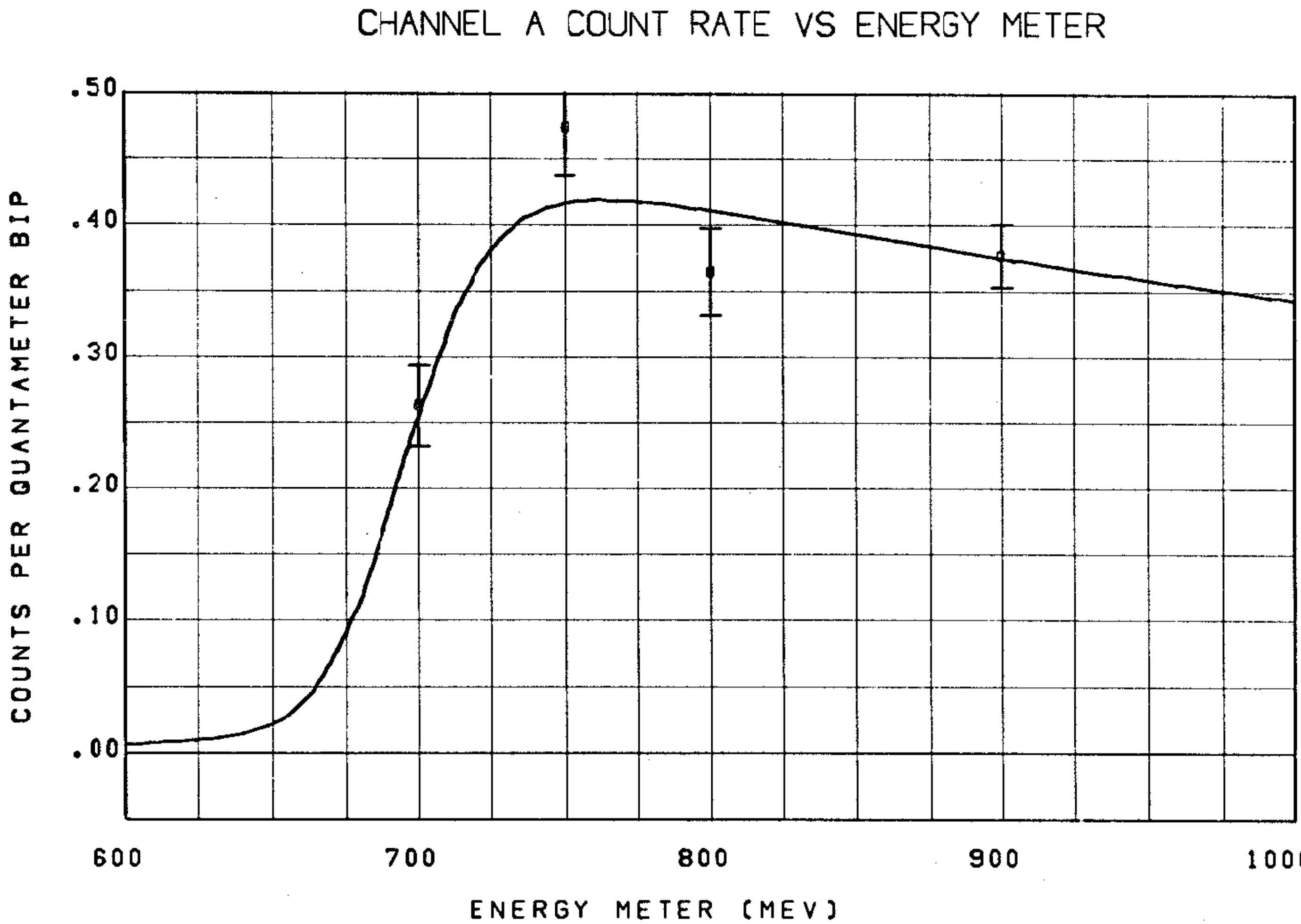

Figure 10h. Excitation Function at 134^{o} Lab. $E_{o\ true}/E_{o\ meter}$ = 1.025 for Smooth Curve

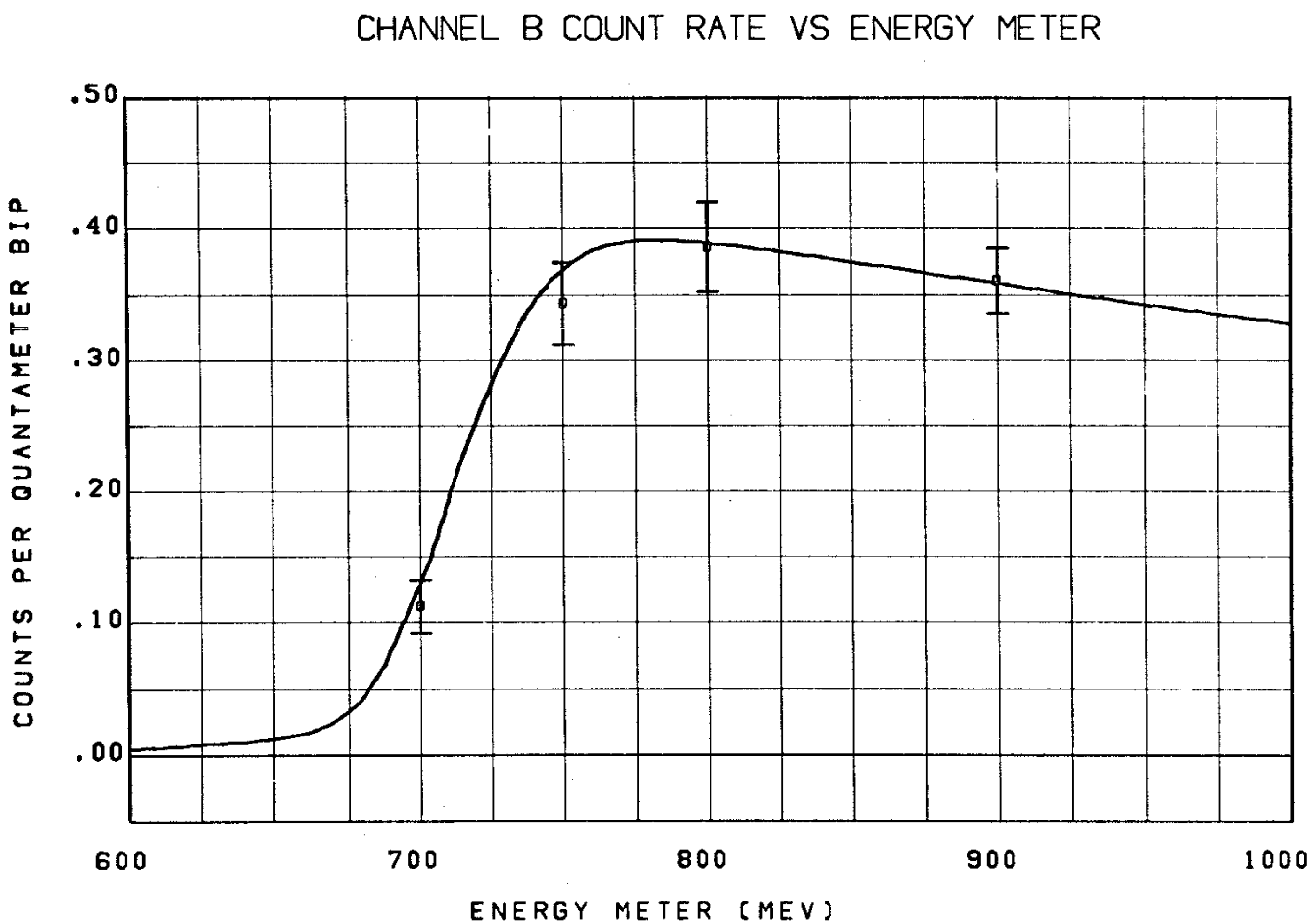

Figure 10i. Excitation Function at 134^{o} Lab. $E_{o\ true}/E_{o\ meter} = 1.025$ for Smooth Curve

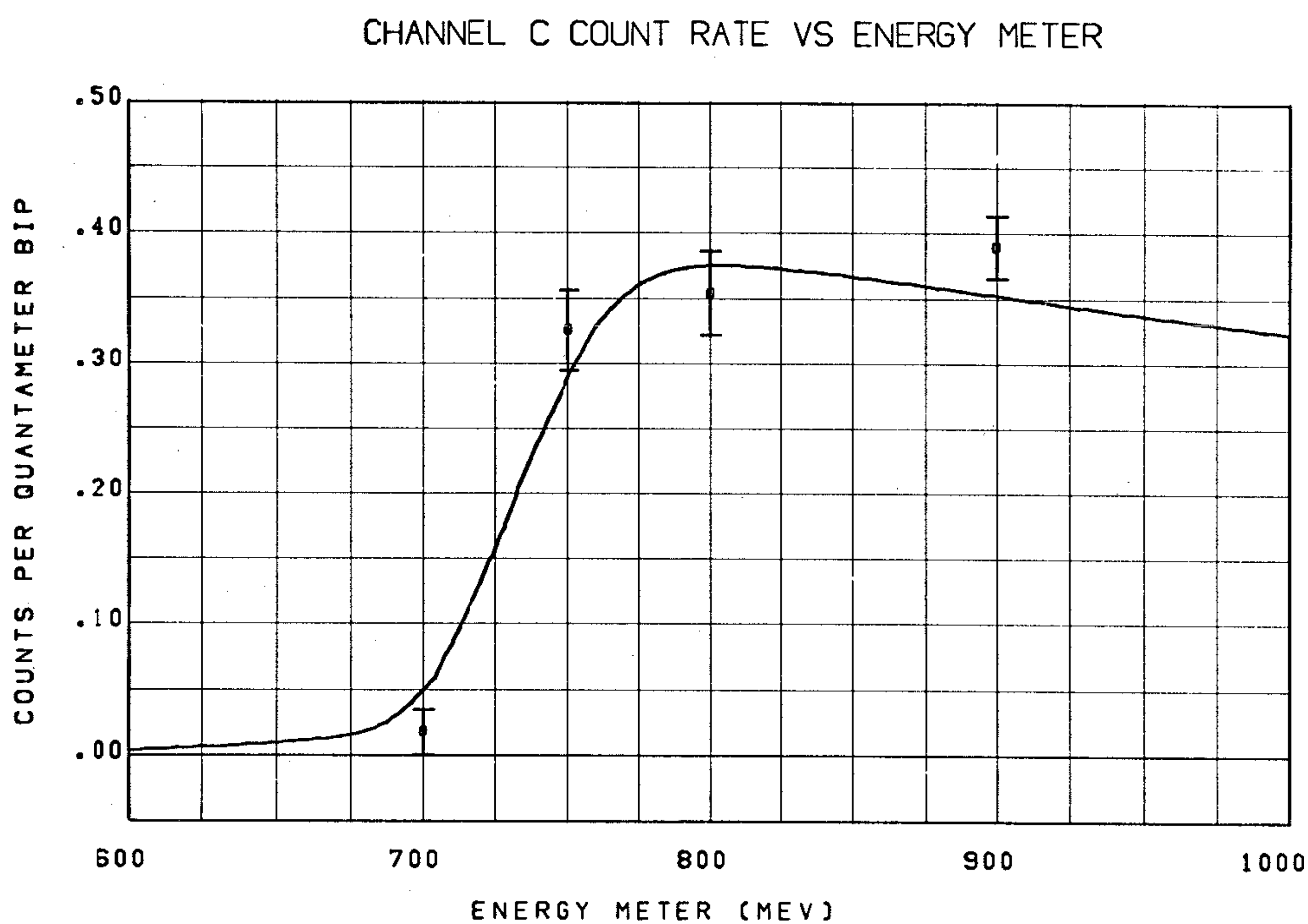

Figure 10j. Excitation Function at 134° Lab. $E_{o\ true}/E_{o\ meter}$ = 1.025 for Smooth Curve

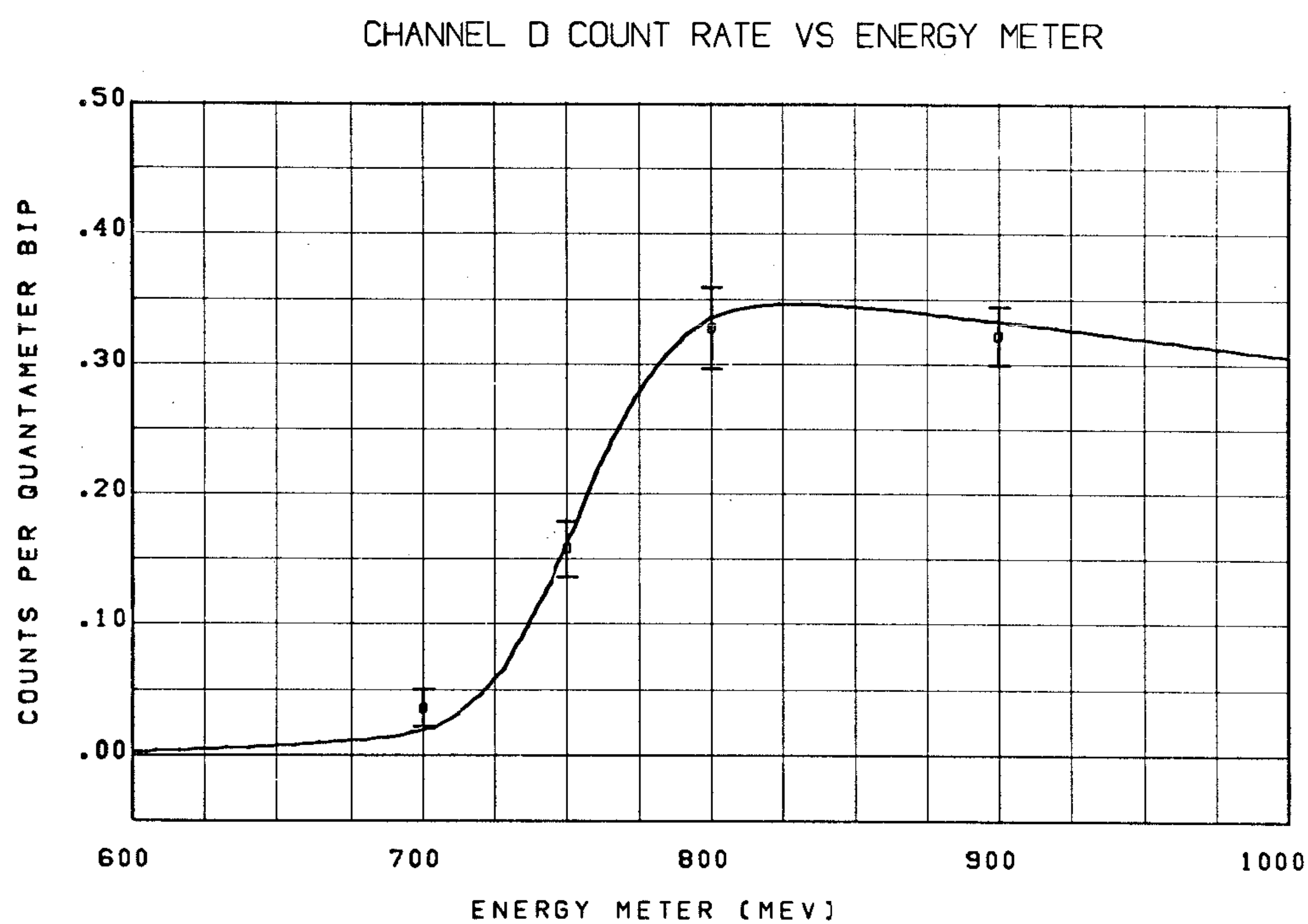

Figure 10k. Excitation Function at 134° Lab. $E_{o\ true}/E_{o\ meter}$ = 1.025 for Smooth Curve

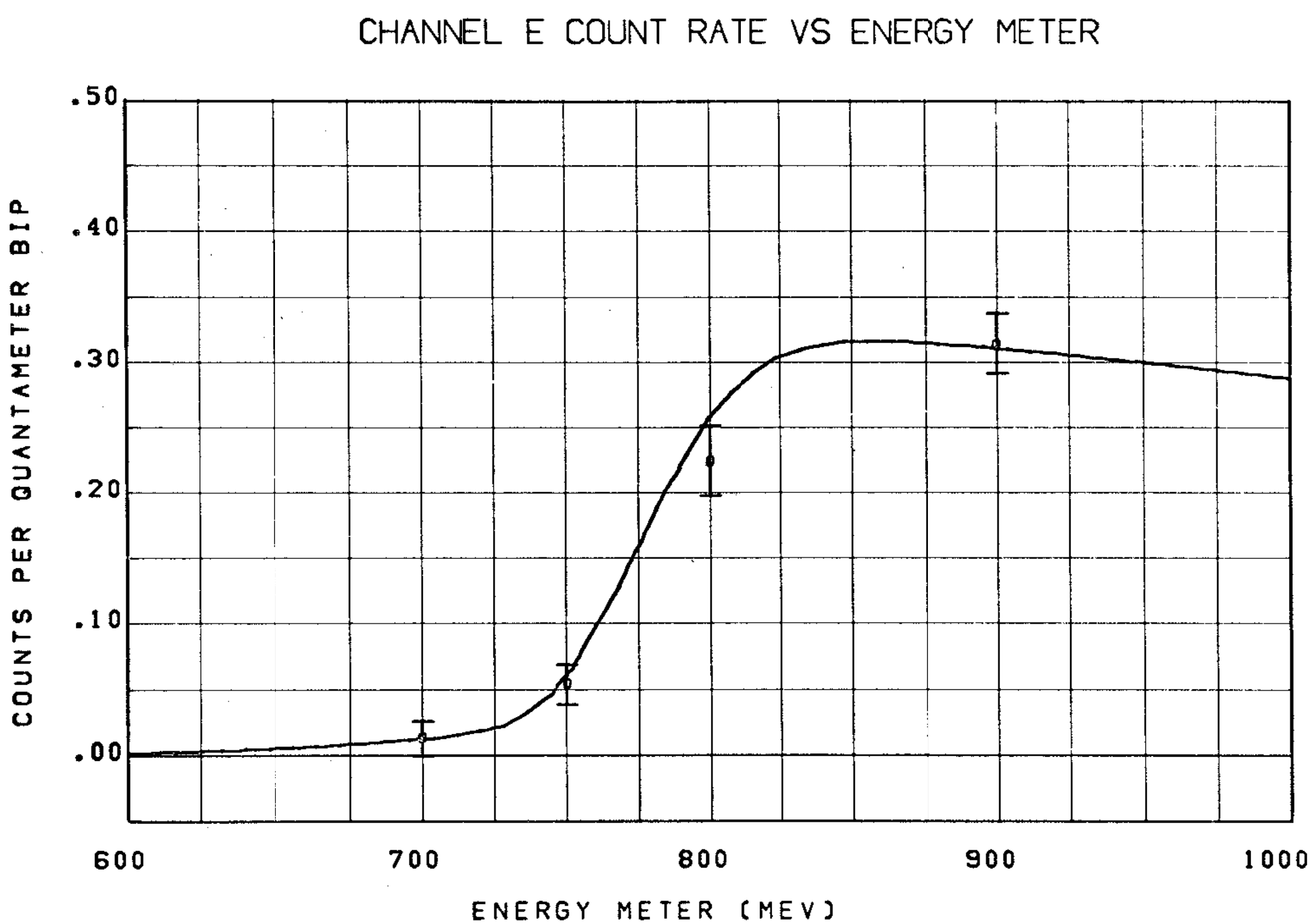

Figure 101. Excitation Function at 134°Lab. $E_{o\ true}/E_{o\ meter} = 1.025$ for Smooth Curve

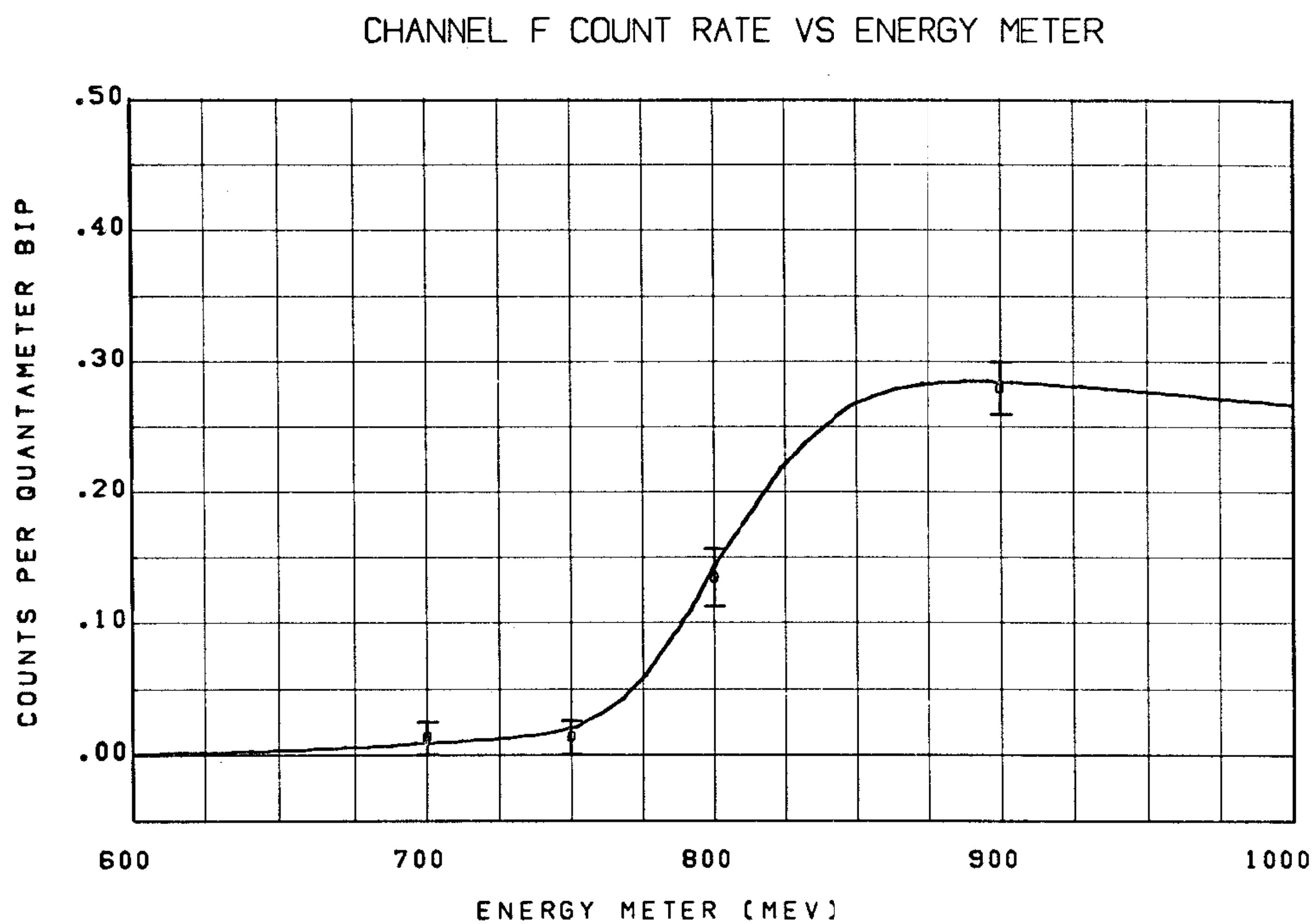

Figure 10m. Excitation Function at 134°Lab. $E_{o\ true}/E_{o\ meter} = 1.025$ for Smooth Curve

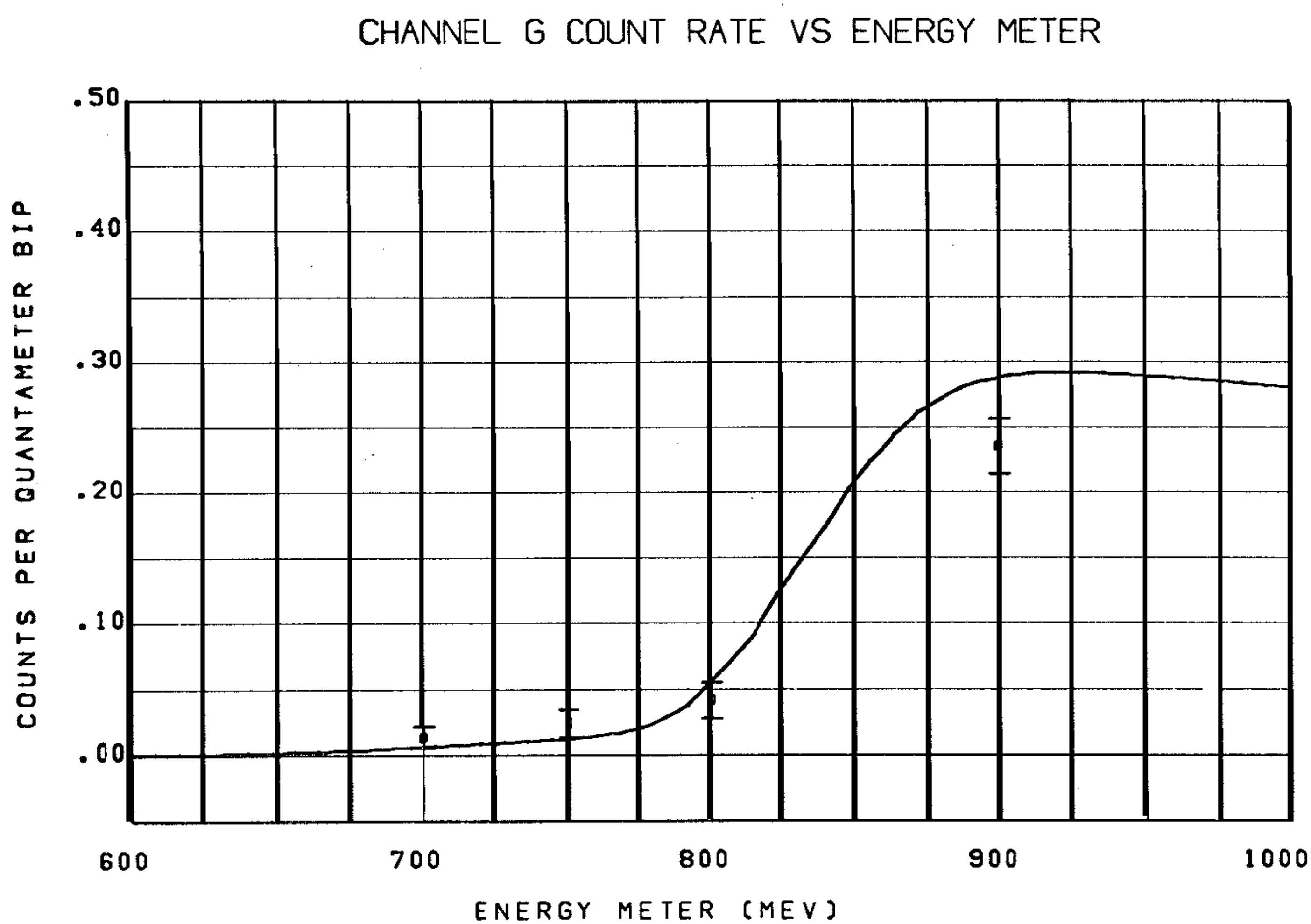

Figure 10n. Excitation Function at 134°Lab. $E_{o\ true}/E_{o\ meter} = 1.025$ for Smooth Curve

V. DATA AND DATA ANALYSIS

A. Cross Section Calculation

The observed pion counting rate in the i^{th} spectrometer channel, C_i, may be written as a multiple integral over geometrical and kinematical quantities and the cross section $\sigma(k, \theta^*)$

$$C_i = \int\int\int\int\int\int \sigma(k, \theta^*)\ G(\Omega, p)\ N(k, x, y)\ n_H(x, y, z)$$
$$\times\ A(p, \Omega)\ E_i(x, y, z, p, \Omega)\ d\Omega\ dp\ dx\ dy\ dz$$

where

C = number of events/quantameter BIP satisfying the pion definition after subtraction of backgrounds,

$\sigma(k, \theta^*)$ = differential cross section for single π^+ photoproduction from hydrogen by a photon of lab energy k producing a π^+ in $d\Omega^*$ at θ^* (* refers to c. m. system),

$G(\Omega, p)$ = the Jacobian of the transformation between the independent variables (k, Ω^*) and (p, Ω),

$N(k, x, y)$ = number of photons per BIP per cm^2 with energy between k and k + dk striking a plane perpendicular to the beam line at the hydrogen target at the point (x, y),

$n_H(x, y, z)$ = number of protons/cm^3 at the point x, y, z where the origin is at the center of the hydrogen target and the z-axis is along the beam line,

$A(p, \Omega)$ = a correction for nuclear absorption in the material in the path of particles passing through the spectrometer,

$E_i(x, y, z, p, \Omega)$ = efficiency of the ith spectrometer channel for accepting an event originating at the point x, y, z with momentum p and at lab solid angle Ω.

As this integral is defined here, the limits on the effective hydrogen target volume are contained in the functions $n_H(x, y, z)$ and $N(k, x, y)$ while the limits for the spectrometer acceptance are contained in the function $E_i(x, y, z, p, \Omega)$.

In order to simplify the evaluation of this multiple integral, several approximations were made. The first approximation involved averaging the bremsstrahlung spectrum over the target and collimator geometry. The spectrometer acceptance was taken outside of this integral and replaced with an average acceptance. This approximation may be schematically represented as follows:

$$\iiint dx\, dy\, dz \rightarrow \bar{E}_i(p, \Omega) \iiint dx\, dy\, dz \rightarrow \bar{E}_i(p, \Omega) \frac{W}{E_0} \frac{\bar{B}(k, E_0)}{k}$$

where

$\bar{E}_i(p, \Omega)$ = the spectrometer efficiency averaged over the origin of events,

W = total energy in the photon beam per quantameter BIP,

E_o = synchrotron end point energy,

$\bar{B}(k, E_o)$ = bremsstrahlung spectrum averaged over target and collimator geometry (defined below),

N_H = number of protons per square centimeter in a planar target of thickness equal to the diameter of the hydrogen target appendix.

This approximation allows the separation of the calculation of the spectrometer acceptance and the bremsstrahlung spectrum into two separate computer programs. The effect of averaging the spectrometer acceptance is a broadening of the momentum resolution, while the total volume of p, Ω phase space accepted remains constant. There is also a correlation between z and Ω which has been neglected. Since the bremsstrahlung distribution in z (along the beam line) is uniform, neglecting this correlation will have no effect on $\bar{B}(k, E_o)$.

The average bremsstrahlung spectrum, $\bar{B}(k, E_o)$, was computed from the differential spectrum, $BR(k, E_o, \theta_x, \theta_y)$, given by the program BPAKI written by Mr. Frank Wolverton.[30] $\bar{B}$ is defined by the average of BR over the target and collimator geometry, namely

$$\bar{B}(k, E_o) = \int_{\theta_{x\,min}}^{\theta_{x\,max}} \int_{\theta_{y\,min}}^{\theta_{y\,max}} BR(k, E_o, \theta_x, \theta_y) \frac{d(\theta_x, \theta_y)}{D} d\theta_x d\theta_y$$

where

θ_x, θ_y = the angle between the photon and the nominal beam line,

D = the diameter of the hydrogen target appendix,

$d(\theta_x, \theta_y)$ = the thickness of the hydrogen target at an angle θ_x, θ_y to the nominal beam line,

$\theta_{x\,min}, \theta_{x\,max}$
$\theta_{y\,min}, \theta_{y\,max}$ = limits on the photon beam angles defined by the primary collimator.

Mr. Mike Hauser coded a program to tabulate the value of $\overline{B}(k, E_o)$ for several values of k and E_o.[31] A second short subroutine, also coded by Mr. Hauser, was able to compute $\overline{B}(k, E_o)$ by interpolation on the tabular values.[31] This subroutine was used for all the data analysis of this experiment.

Using this first approximation, the counting rate integral was reduced from a six fold integral to a three fold integral over $d\Omega\, dp$. This integral contains the effects of the finite resolution of the spectrometer in the quantities k and θ^*. Since the unfolding of two dimentional resolution is a difficult numerical analysis problem, an approximation was made to reduce the integral to an integral over a single variable, k. This approximation consisted of replacing θ, φ, and θ^* by the mean values $\overline{\theta}$, $\overline{\varphi}$, and $\overline{\theta}^*$, and may be schematically represented as follows

$$\iint d\,\Omega \rightarrow R_i(p, p_o, \overline{\theta})\; G(p, \overline{\theta})\; \sigma(k, \overline{\theta}^*)$$

wherc

$R_i(p, p_o, \bar{\theta})$ = the effective momentum resolution function for the i^{th} spectrometer channel,

p_o = the spectrometer central momentum.

The effective resolution function defined here is normalized so that the integral over p gives $\Delta\Omega\,\Delta p$, i. e.

$$\int_0^\infty \frac{R_i(p, p_o, \bar{\theta})}{p_o}\, d\,p = \left(\frac{\Delta\Omega\,\Delta p}{p_o}\right)_i$$

where

$\left(\frac{\Delta\Omega\,\Delta p}{p_o}\right)_i$ = the volume of $\Delta\Omega\,\Delta p/p_o$ phase space accepted by spectrometer channel i.

The details of the calculation of the effective resolution function are described in Appendix V.

This second approximation results in ignoring any effects of finite resolution in θ^*. Because the observed angular distributions were smooth and the resolution in angle was good (less than 1.5 degrees r. m. s.), these effects were expected to be small.

After changing the variable of integration from p to k, the counting rate integral may be written

$$C(\bar{k}, \bar{\theta}^*) = \int_0^\infty \sigma(k, \bar{\theta}^*)\, R_i(p(k, \bar{\theta}), p_o, \bar{\theta})\, \frac{d\Omega^*}{d\Omega}(k, \bar{\theta})\, A(p(k, \bar{\theta}), \bar{\theta})\, N_H \frac{W}{E_o}$$

$$\times \frac{\bar{B}(k, E_o)}{k}\, dk$$

where

$C(\overline{k}, \overline{\theta}^*)$ = the pion counting rate per quantameter BIP explicitly labelled with $\overline{k}$ and $\overline{\theta}^*$,

and

$\overline{k}$ = the photon lab energy calculated from $\overline{\theta}$ and the mean momentum of particles accepted by the i^{th} spectrometer channel.

The equation was solved in two steps. First, σ was assumed to be slowly varying in the region for which R is non-zero and was taken outside the integral. This approximation to σ, which will be called $\overline{\sigma}$, is related to C by an easily calculable factor, namely

$$\overline{\sigma}(\overline{k}, \overline{\theta}^*) = \frac{C(\overline{k}, \overline{\theta}^*)}{\int_0^\infty R_i(k, p_o, \overline{\theta}) \frac{d\Omega^*}{d\Omega}(k, \overline{\theta})\, A\, p_o \overline{\theta})\, N_H \frac{W}{E_o} \frac{B(k, E_o)}{k}\, dk}$$

or

$$\overline{\sigma}(\overline{k}, \overline{\theta}^*) = \frac{C(\overline{k}, \overline{\theta}^*)}{\varkappa}$$

The average cross section, $\overline{\sigma}$, was calculated for each point by evaluating $\varkappa$ numerically. The computer program which computed $\overline{\sigma}$ was called CRØS, and was a joint effort of the author and Mr. Stan Ecklund.[9]

The second step in the process of calculating σ was to start with the measured values of $\overline{\sigma}$ and correct for the effects of the finite resolution of the spectrometer. The details of this process, which is called unfolding, are the subject of Section V-B.

B. Resolution Unfolding

The equation for σ may be rewritten in the form of a Fredholm equation of the first kind, namely

$$\overline{\sigma}(\overline{k},\theta) = \int_0^\infty \sigma(k, \overline{\theta})\ K(k, \overline{k}, \overline{\theta})\ dk$$

where the kernel is given by the normalized resolution function, i. e.,

$$K(k, \overline{k}, \overline{\theta}) = \frac{R_i(k,\ p_o, \overline{\theta})\ \frac{d\Omega^*}{d\Omega}\ (k, \overline{\theta})\ \frac{\overline{B}(k, E_o)}{k}}{\int_0^\infty R_i(k, p_o, \overline{\theta})\ \frac{d\Omega^*}{d\Omega}\ (k, \overline{\theta})\ \frac{\overline{B}(k, E_o)}{k}\ dk}$$

where $\overline{k}$ is the photon energy corresponding to the mean momentum and angle accepted by the i^{th} spectrometer channel. The limits of the integrals are not actually infinite as shown, for there were no photons of energy greater than the maximum possible energy of the synchrotron, namely, 1. 5 GeV. This integral equation may be converted into a sum if an appropriate numerical quadrature method is used. The method chosen was to assume that σ could be sufficiently accurately represented by straight line segments connecting the experimental points and then to use Simpson's rule to calculate the integrals. For regions in which no experimental data existed, namely, for energies below the lowest energy measured or energies above the highest energy measured, $\bar{\sigma}$ was assumed to be constant and have the same value as $\bar{\sigma}$ at the nearest measured point. We may then write a matrix equation in which σ and $\bar{\sigma}$ represent vectors whose components are the values of σ and $\bar{\sigma}$ at the measured points. This equation may be written as follows

$$\bar{\sigma}_i(\bar{\theta}) = \sum_j K_{ij}(\bar{\theta})\,\sigma_j(\bar{\theta})$$

or in simplified notation

$$\bar{\sigma}(\bar{\theta}) = K(\bar{\theta})\,\sigma(\bar{\theta})$$

The solution to this equation is

$$K^{-1}(\bar{\theta})\,\bar{\sigma}(\bar{\theta}) = \sigma(\bar{\theta})$$

A computer program was written to compute K and K^{-1}. The matrix inversion was computed in double precision and elements of the matrix E, where

$$E = K\,K^{-1} - 1$$

were typically of order 10^{-12}. Then the vector σ was computed from the vector $\bar{\sigma}$. The resulting solution for σ was violently oscillatory. In a typical example, $\bar{\sigma}$ was nearly constant at about

3 microbarns/steradian while σ would vary between $\pm$ 2000 microbarns/steradian.

There are three possible sources for errors which can build up into the observed violent oscillations. These sources include statistical errors in $\bar{\sigma}$, inaccuracy of the numerical integration method, and the near singularity inherent in the solution of the Fredholm equation. The statistical errors are much greater than the errors of the quadrature method, so that we may safely neglect this source of oscillations.

Gold[32] has made extensive studies of a method which has shown some success in eliminating the singularities of the Fredholm equation. This method was tried, but it was found that the statistical errors in $\bar{\sigma}$ were greatly magnified in computing σ. Twomey[33] has invented a method which attempts to filter out the oscillations and obtain a smooth unfolded result. This method was also coded for the computer. However, the smoothing function required to eliminate the oscillations was as broad as the resolution functions of the spectrometer. Intuitively, no gain may be obtained by this method.

Some success was obtained when the response matrix, K, was written as the sum of a diagonal matrix and another "small" matrix. The diagonal matrix was associated with the normal part of the resolution functions and the "small" matrix was associated with the tails of the resolution functions which result from the $\pi \rightarrow \mu + \nu$ decay process (see Appendix IV). In the integral equation, this approximation is equivalent to assuming that the normal part of the resolution function is a delta function. Using this approximation, the inverted response matrix gave reasonable results, and the error bars for σ came out about 10% greater than the error bars for $\bar{\sigma}$. Since the effects of the resolution function tails on the peaks and valleys was about 2%, it was felt that this correction would be worthwhile. Because there may be objections to the details of the unfolding method used, both the values of $\bar{\sigma}$ and σ were tabulated.

One may wonder why the method previously used by R. Diebold[34] was not tried. Diebold fit the data with a theory which was folded with the resolution. The parameters of the theory determined in this fit were used to compute the unfolded cross sections. Since any reasonable theory must also work for regions not measured in this experiment, all available data must be fit simultaneously, and the program which does this job must be more complicated than the phenomenological analysis programs presently used by S. Ecklund[9] and C. Clinesmith[10]. Since the other data which are available at the present time have similar or worse resolution, it is unreasonable to attempt this task now.

If it is necessary to completely unfold the resolution at some later date, one may start with the unfolded data (in which the effects of the tails have been corrected) and approximate the resolution functions by Gaussians with standard deviations given by the values of $\Delta k_{r.m.s.}$ from Table 7. A sample calculation has shown that a Gaussian will be within $\pm$ 10% of the exact resolution functions (without decay tails) for values of $(k - \bar{k})$ less than $2\ \Delta k_{r.m.s.}$.

C. Data Point Summary and Internal Consistency of Data

The data were obtained from 12 momentum scans at 12 lab angles. At each lab angle, from three to six spectrometer central momentum settings were required to cover the range of

TABLE 6-a and 6-b

Kinematic Parameters and Some Intermediate Results
of the Cross Section Calculation

θ_{lab}	is the mean spectrometer lab angle in degrees.
f	is the nuclear resonance magnetometer frequency in mc.
P_o	is the mean momentum of the seven momentum channels (taken as one channel) referred to pion momentum at the center of the hydrogen target.
θ^*	is the mean pion C. M. angle in degrees.
k_{min}	is the mean photon lab energy in MeV accepted by Channel A.
k_{max}	is the mean photon lab energy in MeV accepted by Channel G.
$k_{2\pi}$	is the photon energy threshold in MeV for double pion photoproduction in Channel A.
E_o	is the synchrotron end point energy in MeV.
π^+	is the observed number of pions summed over the seven channels in a pair of full and empty target runs.
QAVG	is the number of Quantameter BIPS in each run determined by the average of the other monitors (see Appendix I).

κ	is the constant relating cross sections in microbarns per Steradian and pion yield in counts per Quantameter BIP (pions summed over all seven channels). The total energy/BIP was 1.214×10^{13} MeV/BIP and the number of hydrogen atoms/cm^2 in one diameter of the hydrogen target was 3.138×10^{23} for all the runs shown in this table.
CCORR	is the correction for the field reversed background in units of microbarns/steradian.
$\overline{\sigma}_1$	is the cross section in microbarns/steradian calculated from the run shown (averaged over the seven channels) with no correction for resolution effects.
$\overline{\sigma}$	is the cross section in microbarns/steradian computed for all data available at the given point.
$d\overline{\sigma}$	is the statistical error associated with $\overline{\sigma}$ (see Section V-F).
χ^2	is the value of χ-squared obtained for the several runs at the given point.
deg f	is the number of degrees of freedom (number of runs -1) associated with χ-squared at the given point.

TABLE 6a

Point No.	θ_{lab}	f	P_0	θ^*	K_{min}	K_{max}	$K_{2\gamma}$	E_0	Full Target π^+	Full Target QAVG	Empty Target π^+	Empty Target QAVG	χ	CCORR	$\bar{\sigma}_1$	$\bar{\sigma}$	$d\bar{\sigma}$	χ^2	Deg. f.
34-3	34.0	54.86	462.	49.1	508.	545.	675.	677.	3357	129.9	40	28.8	2.521	0.065	9.601	9.551	0.123	0.48	3
34-2	34.0	61.11	513.	50.3	564.	628.	733.	677.	3349	117.2	37	28.8	2.623	0.063	10.288	10.353	0.130	4.90	3
34-1	34.0	68.26	570.	51.6	629.	690.	799.	769.	4499	151.9	78	50.9	2.486	0.066	11.209	11.061	0.180	0.60	1
40-3	40.0	54.86	462.	57.5	525.	575.	698.	677.	3689	149.8	28	28.7	2.518	0.061	9.313	9.182	0.173	0.80	1
40-2	40.0	61.11	513.	58.9	585.	644.	761.	677.	3099	121.3	28	28.8	2.545	0.060	9.570	9.716	0.184	0.84	1
40-1	40.0	68.26	570.	60.4	656.	723.	834.	769.	5659	199.5	63	48.3	2.424	0.064	11.083	11.132	0.181	0.09	1
48-4	48.0	49.28	417.	67.1	496.	544.	661.	677.	3154	156.5	30	38.1	2.315	0.060	8.272	8.360	0.162	0.42	1
48-3	48.0	54.86	462.	68.6	554.	611.	737.	677.	2824	132.9	30	28.8	2.411	0.058	8.281	8.498	0.168	2.36	1
48-2	48.0	61.11	513.	70.2	622.	689.	809.	769.	4622	194.5	41	50.3	2.280	0.061	9.963	9.963	0.226		0
48-1	48.0	68.26	570.	72.1	703.	781.	893.	871.	1999	103.4	69	103.4	2.140	0.065	8.624	8.743	0.130	0.64	2
56-4	56.0	49.28	417.	77.6	525.	580.	716.	677.	3124	185.8	22	38.4	2.204	0.058	7.265	7.468	0.142	2.89	1
56-3	56.0	54.86	462.	79.4	592.	657.	787.	769.	5263	295.0	73	97.0	2.079	0.061	8.117	7.971	0.122	4.79	2
56-2	56.0	61.11	513.	81.4	670.	748.	871.	871.	3775	204.7	87	103.3	1.956	0.065	8.888	8.754	0.164	0.89	1
56-1	56.0	68.26	571.	83.6	765.	859.	969.	974.	3580	423.1	40	111.4	1.852	0.069	4.297	4.260	0.089	0.31	1
64-5	64.0	44.25	375.	86.1	496.	550.	695.	677.	2214	168.3	20	38.0	2.004	0.058	6.238	6.506	0.109	6.13	2
64-4	64.0	49.28	417.	87.9	562.	626.	766.	769.	3569	263.3	72	101.9	1.886	0.061	6.730	6.528	0.088	2.54	3
64-3	64.0	54.86	462.	89.9	639.	716.	850.	769.	6009	388.6	54	96.5	1.929	0.060	7.629	7.757	0.113	1.57	2
64-2	64.0	61.11	513.	92.2	732.	826.	951.	871.	1770	171.0	211	423.5	1.795	0.064	5.412	5.560	0.095	1.42	2
64-1	64.0	68.26	570.	94.9	847.	964.	1177.	1076.	1888	458.0	27	116.3	1.594	0.072	2.361	2.324	0.053	1.62	3
74-6	74.0	39.84	338.	96.5	477.	531.	686.	677.	2858	270.1	33	72.2	1.759	0.057	5.674	5.555	0.137	0.09	2
74-5	74.0	44.25	375.	98.2	541.	606.	757.	677.	2802	268.9	37	70.7	1.851	0.055	5.270	5.283	0.106	0.02	1
74-4	74.0	49.28	417.	100.3	620.	700.	845.	769.	5140	452.5	45	96.9	1.731	0.058	6.203	6.234	0.101	0.39	2
74-3	74.0	54.86	462.	102.7	716.	815.	952.	871.	1947	192.9	45	106.8	1.606	0.063	5.936	5.677	0.083	3.94	3
74-2	74.0	61.11	513.	105.4	836.	962.	1086.	1076.	1899	459.2	25	114.8	1.416	0.071	2.687	2.706	0.068	0.11	1
74-1	74.0	68.26	570.	108.5	991.	1155.	1259.	1179.	1067	461.8	22	119.7	1.233	0.082	1.639	1.732	0.065	4.85	1

TABLE 6b

Point No.	θ_{lab}	f	P_0	Θ^*	K_{min}	K_{max}	$K_{\gamma\gamma}$	E_0	Full Target γ's	Full Target QAVG	Empty Target γ's	Empty Target QAVG	χ	CCORR	$\bar{\sigma}_1$	$\bar{\sigma}$	$d\bar{\sigma}$	χ^2	Deg. f.
84-6	84.0	37.82	321.	106.9	487.	545.	710.	677.	2799	360.6	34	94.0	1.592	0.056	4.587	4.336	0.092	9.03	1
84-5	84.0	41.98	356.	108.7	556.	628.	789.	769.	2996	400.5	46	99.3	1.519	0.058	4.547	4.441	0.080	3.19	2
84-4	84.0	46.77	395.	110.9	645.	736.	894.	871.	3460	412.1	23	103.5	1.428	0.062	5.640	5.683	0.109	3.23	1
84-3	84.0	52.08	439.	113.4	756.	874.	1039.	974.	2411	431.2	24	110.3	1.341	0.066	3.932	3.958	0.085	0.11	1
84-2	84.0	57.91	487.	116.3	896.	1051.	1178.	1179.	1730	476.1	24	119.5	1.177	0.075	2.833	2.884	0.071	6.07	2
84-1	84.0	64.57	541.	119.7	1085.	1320.	1394.	1384.	441	453.3	12	222.0	1.035	0.086	0.801	0.736	0.047	10.17	5
94-5	94.0	37.82	321.	117.4	532.	603.	876.	769.	2212	389.7	31	95.7	1.328	0.058	3.955	3.875	0.092	1.21	1
94-4	94.0	41.98	356.	119.5	617.	708.	894.	871.	2427	410.5	13	103.5	1.265	0.061	4.500	4.590	0.096	1.28	1
94-3	94.0	46.77	395.	121.9	729.	848.	1006.	974.	2176	429.0	28	109.8	1.195	0.065	3.961	4.008	0.088	0.43	2
94-2	94.0	52.08	439.	124.7	875.	1038.	1178.	1179.	1653	473.9	16	119.1	1.044	0.074	3.132	3.058	0.074	0.97	2
94-1	94.0	57.91	487.	128.0	1070.	1300.	1407.	1384.	634	527.6	29	235.6	0.912	0.085	1.097	1.047	0.051	7.27	3
106-5	106.0	34.02	289.	127.4	512.	582.	767.	769.	1709	389.5	26	95.8	1.154	0.056	3.491	3.528	0.079	0.67	2
106-4	106.0	37.82	321.	129.3	597.	690.	871.	871.	1811	409.8	25	103.0	1.094	0.059	3.745	3.698	0.083	0.31	1
106-3	106.0	41.98	356.	131.4	708.	831.	1003.	974.	1768	423.5	21	111.6	1.043	0.062	3.749	3.789	0.090	0.66	2
106-2	106.0	46.77	395.	134.1	861.	1035.	1188.	1179.	1301	473.1	13	119.3	0.912	0.071	2.816	2.836	0.075	0.52	2
106-1	106.0	52.08	439.	137.3	1075.	1334.	1447.	1384.	504	452.3	5	106.0	0.766	0.085	1.303	1.247	0.054	1.47	4
120-5	120.0	30.59	260.	138.3	492.	561.	758.	769.	1442	399.0	21	95.2	1.021	0.052	3.262	3.234	0.073	8.92	2
120-4	120.0	34.02	289.	139.9	577.	669.	865.	769.	1326	389.0	16	95.7	1.043	0.051	3.038	3.084	0.073	3.89	2
120-3	120.0	37.82	321.	141.7	690.	818.	1005.	871.	1416	413.2	22	104.1	0.959	0.055	3.280	3.298	0.078	0.05	1
120-2	120.0	41.98	356.	144.0	843.	1027.	1195.	1179.	1083	474.7	11	119.5	0.790	0.067	2.695	2.630	0.075	0.79	2
120-1	120.0	46.77	395.	146.8	1073.	1361.	1481.	1384.	468	474.4	13	135.0	0.638	0.083	1.307	1.329	0.060	2.64	3
134-4	134.0	30.59	260.	149.5	541.	584.	835.	769.	1163	392.1	17	96.4	0.940	0.047	2.909	2.906	0.060	8.82	4
134-3	134.0	34.02	289.	151.0	648.	769.	972.	871.	1190	411.3	16	104.5	0.861	0.051	3.118	3.147	0.066	0.14	3
134-2	134.0	37.82	321.	152.7	796.	974.	1161.	1076.	884	456.0	43	376.0	0.741	0.059	2.390	2.365	0.059	1.62	3
134-1	134.0	41.98	356.	154.9	1010.	1290.	1433.	1384.	704	666.7	11	159.3	0.607	0.072	1.548	1.491	0.045	7.04	5
156-4	155.4	27.53	234.	163.9	510.	592.	767.	769.	1599	582.4	26	96.3	0.842	0.041	2.884	2.934	0.064	6.17	4
156-3	155.4	30.59	260.	164.6	609.	724.	943.	871.	970	410.4	20	103.1	0.767	0.045	2.757	2.760	0.065	0.07	2
156-2	155.4	34.02	289.	165.6	750.	920.	1129.	1076.	1063	645.5	10	164.4	0.653	0.053	2.368	2.306	0.061	4.48	3
156-1	155.4	37.82	321.	166.8	960.	1234.	1405.	1384.	536	601.7	15	161.6	0.538	0.064	1.420	1.424	0.050	1.17	5

photon energies available. The region of the (k, θ^*) plane which was investigated in this experiment is shown in Figure 11. In addition, the region scanned by S. Ecklund[9] is also shown.

The basic experimental parameters for each data point are given in Table 6. The momentum was calculated from the magnetometer calibration and includes a 2.7 MeV/c correction for momentum lost in the hydrogen target structure. Several useful kinematic quantities derived from the basic parameters are also given.

The observed π^+ rates and a few intermediate results of the cross section calculation are also presented in Table 6. These quantities may be used to check the cross section computation or to estimate count rates for similar experiments using the 600 MeV/c Magnet. The π^+ rates shown are for a typical pair of full and empty target runs only. At least twice this much data was used for the final results which are presented in Section V-D.

The internal consistency of the data was investigated by comparing the yields for the sum of the seven momentum channels at each point. This method should show up normalization inconsistencies more clearly than investigating the channels separately because of the better statistics of the sum. The observed value of χ-squared and the number of degrees of freedom at each point are presented in Table 6. The integral χ-squared probability distribution is presented in Figure 12. This figure indicates that the quoted errors are approximately correct, but that there is an excess of runs in the low probability tail. This effect is probably a result of the fact that the normalization errors do not have a Gaussian distribution. Three runs deserve special comment. The cross section for point 48-2 was computed from

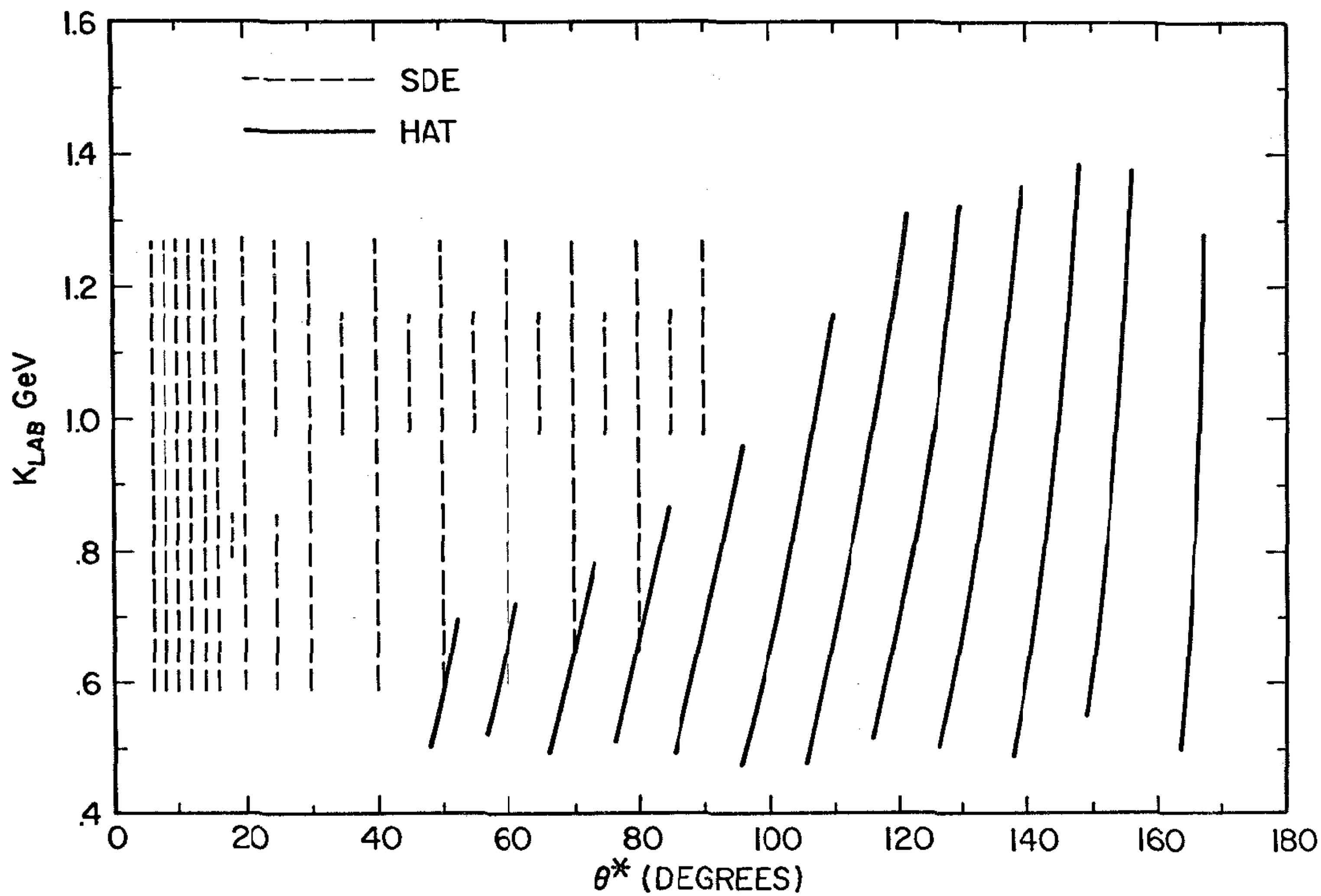

Figure 11. Location of Data Points on k, θ* Plane

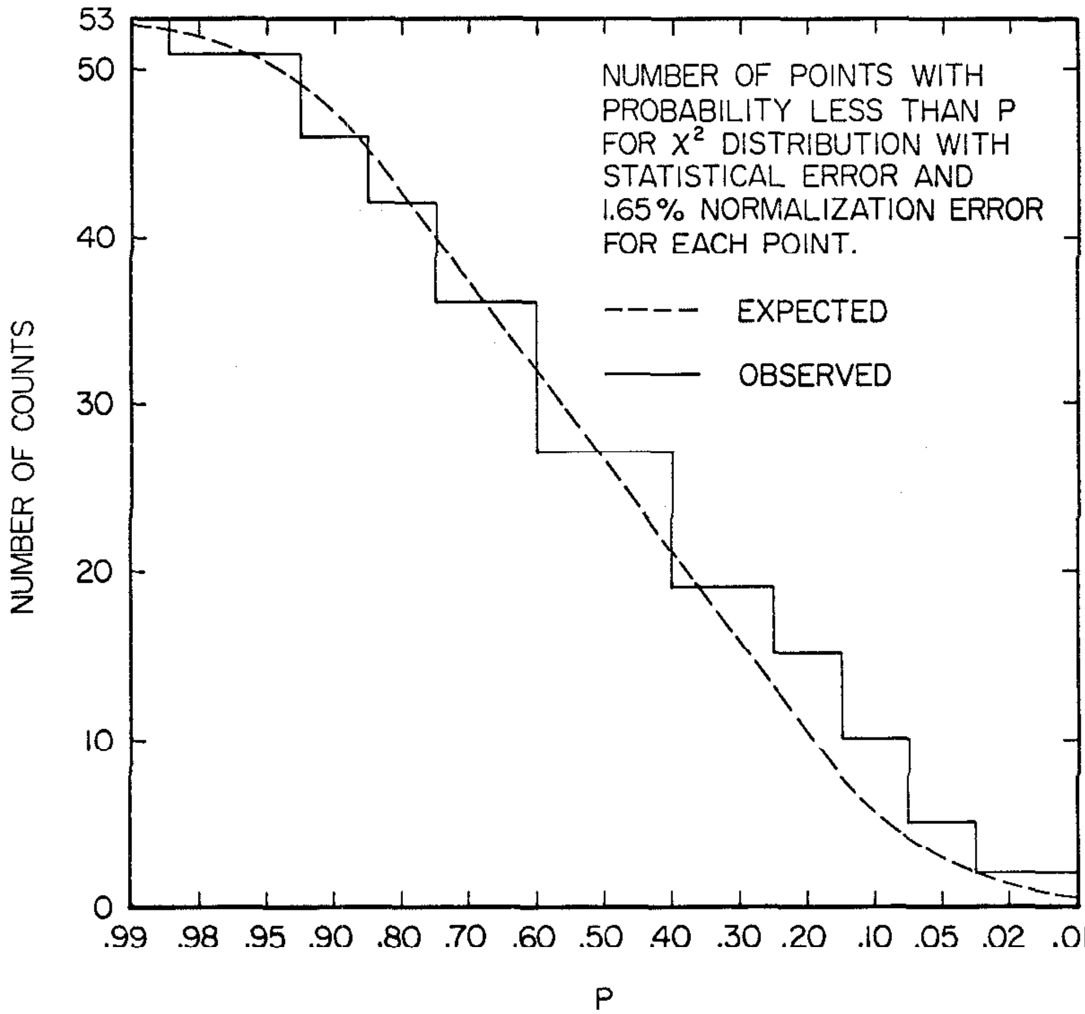
NUMBER OF POINTS WITH PROBABILITY LESS THAN P FOR X^2 DISTRIBUTION WITH STATISTICAL ERROR AND 1.65% NORMALIZATION ERROR FOR EACH POINT.
EXPECTED
OBSERVED
NUMBER OF COUNTS
53
50
40
30
20
10
0
.99 .98 .95 .90 .80 .70 .60 .50 .40 .30 .20 .10 .05 .02 .01
P

Figure 12

one run because the second run at this point had inconsistencies in beam monitoring which could not be resolved. Point 84-6, which is one of the two points with χ-squared probability less than 1%, is a point at which the high energy magnet was in the beam line for one of the two runs, and the two runs disagreed by 10%. Since this effect was not observed for other points, it was assumed that each of the two runs was equally likely to be wrong and thus neither run was thrown away. Point 120-5, which was the other point with probability less than 1%, consisted of three runs. After the first two runs were taken, it was observed that there was a 15% discrepancy for 3% statistics. A third run was taken and the results of this run fell almost exactly at the mean of the two preceeding runs. Thus, there was no way of distinguishing the observed discrepancy at this point from a large statistical fluctuation.

D. Tabulation of Data

The data are presented in Tables 7A - 7L, in which the spectrometer lab angle is a constant for each table. The (unfolded) data are also plotted in Figures 13a - 13l, and the spectrometer lab angle is also a constant for each figure. A smooth curve has been drawn through the data on five of these figures. The same smooth curves are also shown on Figures 13m - 13q, along with a representative set of data from other experiments.[9, 12, 13, 15, 16, 37] Since all of the data from this experiment have been plotted in Stan Ecklund's thesis[9], only a small part of the data available from his experiment is shown here.

TABLES 7A - 7L

Average and Unfolded Cross Sections

POINT NO.	corresponds to the designation of the kinematical parameters given in Tables 6-a and 6-b.
THETA LAB	is the mean laboratory angle of the spectrometer in degrees.
K	is the mean photon lab energy in MeV.
W	is the total c. m. energy in MeV.
THETA C. M.	is the pion laboratory angle in degrees.
SIGMA AVERAGE	is the measured c. m. cross section in microbarns/steradian without resolution corrections.
DSIGMA AVERAGE	is the statistical error associated with Sigma Average (see Section V-F).
SIGMA UNFOLDED	is the measured c. m. cross section in microbarns/steradian including a correction for the "tails" of the resolution functions (see Section V-B).
DSIGMA UNFOLDED	is the statistical error associated with Sigma Unfolded (see Section V-F).
ΔK_{rms}	is the r. m. s. resolution in photon energy in MeV after correction for the tails of the resolution functions.

TABLE 7a

AVERAGE AND UNFOLDED CROSS SECTIONS

POINT NO.	THETA LAB	K	W	THETA C.M.	SIGMA AVERAGE	DSIGMA AVERAGE	SIGMA UNFOLDED	DSIGMA UNFOLDED	ΔK RMS
34-3	34.0	508.	1354.	48.6	9.791	0.254	9.787	0.289	6.8
34-3	34.0	515.	1359.	48.8	9.349	0.253	9.290	0.281	6.8
34-3	34.0	522.	1364.	48.9	9.607	0.253	9.581	0.280	6.9
34-3	34.0	530.	1369.	49.1	9.321	0.246	9.254	0.273	7.0
34-3	34.0	539.	1374.	49.2	9.661	0.248	9.631	0.275	7.2
~~34-3~~	~~34.0~~	~~546.~~	~~1380.~~	~~49.4~~	~~10.028~~	~~0.245~~	~~10.033~~	~~0.271~~	~~7.4~~
34-3	34.0	555.	1386.	49.6	9.805	0.234	9.773	0.258	7.8
34-2	34.0	564.	1392.	49.7	10.463	0.266	10.500	0.293	7.6
34-2	34.0	572.	1397.	49.9	9.810	0.262	9.764	0.288	7.6
34-2	34.0	580.	1403.	50.1	10.517	0.266	10.542	0.291	7.7
~~34-2~~	~~34.0~~	~~589.~~	~~1409.~~	~~50.2~~	~~10.680~~	~~0.263~~	~~10.712~~	~~0.287~~	~~7.9~~
34-2	34.0	598.	1415.	50.4	9.776	0.250	9.712	0.271	8.1
34-2	34.0	608.	1421.	50.6	10.913	0.266	10.955	0.287	8.4
34-2	34.0	617.	1428.	50.8	10.422	0.248	10.411	0.266	8.8
34-1	34.0	629.	1435.	51.0	10.995	0.353	11.017	0.382	8.6
~~34-1~~	~~34.0~~	~~638.~~	~~1441.~~	~~51.2~~	~~10.536~~	~~0.351~~	~~10.509~~	~~0.379~~	~~8.6~~
34-1	34.0	648.	1447.	51.3	10.470	0.341	10.435	0.367	8.8
34-1	34.0	658.	1454.	51.5	10.684	0.341	10.663	0.365	8.9
34-1	34.0	668.	1461.	51.7	11.094	0.343	11.095	0.365	9.2
34-1	34.0	679.	1468.	51.9	11.931	0.349	11.981	0.370	9.5
34-1	34.0	690.	1475.	52.1	11.634	0.337	11.650	0.362	10.0

TABLE 7b

AVERAGE AND UNFOLDED CROSS SECTIONS

POINT NO.	THETA LAB	K	W	THETA C.M.	SIGMA AVERAGE	DSIGMA AVERAGE	SIGMA UNFOLDED	DSIGMA UNFOLDED	Δ K RMS
40-3	40.0	525.	1366.	57.0	9.729	0.392	9.761	0.445	7.4
40-3	40.0	533.	1371.	57.1	9.650	0.387	9.672	0.428	7.4
40-3	40.0	540.	1376.	57.3	9.085	0.361	9.046	0.398	7.5
40-3	40.0	549.	1382.	57.5	8.984	0.370	8.942	0.408	7.7
40-3	40.0	557.	1388.	57.7	8.662	0.346	8.583	0.382	7.9
40-3	40.0	566.	1394.	57.9	8.990	0.356	8.950	0.392	8.1
40-3	40.0	576.	1400.	58.1	9.384	0.340	9.380	0.374	8.5
40-2	40.0	585.	1407.	58.3	9.146	0.399	9.106	0.436	8.4
40-2	40.0	594.	1412.	58.5	9.693	0.402	9.707	0.438	8.4
40-2	40.0	603.	1418.	58.7	10.406	0.407	10.476	0.442	8.5
40-2	40.0	613.	1425.	58.9	9.615	0.384	9.600	0.415	8.7
40-2	40.0	623.	1431.	59.1	9.347	0.382	9.301	0.411	9.0
40-2	40.0	633.	1438.	59.3	10.215	0.400	10.241	0.427	9.2
40-2	40.0	644.	1445.	59.5	9.684	0.384	9.658	0.407	9.6
40-1	40.0	656.	1453.	59.8	10.667	0.346	10.681	0.374	9.6
40-1	40.0	666.	1459.	60.0	11.126	0.363	11.163	0.391	9.6
40-1	40.0	677.	1466.	60.2	11.392	0.356	11.435	0.382	9.8
40-1	40.0	688.	1473.	60.4	11.269	0.351	11.289	0.374	10.0
40-1	40.0	699.	1480.	60.6	11.324	0.346	11.341	0.367	10.3
40-1	40.0	711.	1488.	60.9	11.807	0.357	11.855	0.377	10.7
40-1	40.0	723.	1496.	61.1	10.389	0.326	10.336	0.348	11.1

TABLE 7c

AVERAGE AND UNFOLDED CROSS SECTIONS

POINT NO.	THETA LAB	K	W	THETA C.M.	SIGMA AVERAGE	DSIGMA AVERAGE	SIGMA UNFOLDED	DSIGMA UNFOLDED	ΔK RMS
48-4	48.0	496.	1345.	66.5	8.940	0.366	8.999	0.421	7.5
48-4	48.0	503.	1350.	66.7	8.036	0.353	7.969	0.395	7.5
48-4	48.0	510.	1356.	66.9	8.716	0.354	8.747	0.395	7.6
48-4	48.0	518.	1361.	67.1	8.207	0.342	8.175	0.382	7.7
48-4	48.0	527.	1367.	67.3	8.239	0.347	8.211	0.389	7.9
48-4	48.0	535.	1373.	67.5	8.240	0.336	8.214	0.376	8.2
48-4	48.0	544.	1379.	67.7	8.031	0.320	7.978	0.357	8.5
48-3	48.0	554.	1386.	67.9	7.969	0.365	7.904	0.406	8.5
48-3	48.0	563.	1391.	68.1	8.369	0.370	8.350	0.411	8.5
48-3	48.0	571.	1397.	68.3	8.503	0.358	8.494	0.396	8.7
48-3	48.0	581.	1404.	68.6	8.431	0.366	8.404	0.404	8.8
48-3	48.0	591.	1410.	68.8	8.256	0.354	8.202	0.388	9.1
48-3	48.0	601.	1417.	69.0	9.201	0.377	9.235	0.412	9.4
48-3	48.0	611.	1424.	69.3	8.427	0.351	8.367	0.381	9.8
48-2	48.0	622.	1431.	69.5	9.228	0.437	9.213	0.482	9.8
48-2	48.0	632.	1437.	69.7	10.641	0.470	10.770	0.517	9.8
48-2	48.0	642.	1444.	70.0	9.831	0.452	9.847	0.496	10.0
48-2	48.0	653.	1451.	70.2	9.549	0.441	9.529	0.482	10.2
48-2	48.0	665.	1459.	70.5	9.596	0.427	9.572	0.464	10.5
48-2	48.0	676.	1466.	70.7	10.587	0.452	10.651	0.489	10.9
48-2	48.0	689.	1474.	71.0	10.361	0.436	10.387	0.469	11.4
48-1	48.0	703.	1483.	71.3	10.853	0.285	10.972	0.308	11.4
48-1	48.0	715.	1490.	71.6	10.095	0.278	10.151	0.300	11.5
48-1	48.0	727.	1498.	71.8	10.164	0.271	10.242	0.291	11.7
48-1	48.0	739.	1506.	72.1	9.418	0.253	9.457	0.271	12.0
48-1	48.0	753.	1514.	72.4	7.686	0.229	7.625	0.244	12.4
48-1	48.0	767.	1523.	72.7	7.329	0.222	7.286	0.235	12.8
48-1	48.0	781.	1532.	73.0	6.196	0.197	6.096	0.211	13.5

TABLE 7d

AVERAGE AND UNFOLDED CROSS SECTIONS

POINT NO.	THETA LAB	K	W	THETA C.M.	SIGMA AVERAGE	DSIGMA AVERAGE	SIGMA UNFOLDED	DSIGMA UNFOLDED	ΔK RMS
56-4	56.0	525.	1366.	77.0	7.815	0.312	7.843	0.357	8.6
56-4	56.0	533.	1371.	77.2	7.455	0.310	7.435	0.345	8.6
56-4	56.0	542.	1377.	77.4	7.693	0.305	7.706	0.339	8.8
56-4	56.0	551.	1383.	77.6	7.143	0.295	7.091	0.328	8.9
56-4	56.0	560.	1390.	77.9	7.293	0.291	7.262	0.323	9.2
56-4	56.0	570.	1396.	78.1	7.237	0.292	7.199	0.324	9.5
56-4	56.0	580.	1403.	78.4	7.480	0.287	7.467	0.317	9.9
56-3	56.0	592.	1411.	78.6	7.396	0.246	7.341	0.275	9.9
56-3	56.0	601.	1417.	78.9	7.517	0.248	7.469	0.277	10.0
56-3	56.0	611.	1424.	79.1	7.844	0.246	7.827	0.274	10.2
56-3	56.0	622.	1431.	79.4	8.308	0.255	8.334	0.283	10.4
56-3	56.0	633.	1438.	79.6	7.742	0.238	7.687	0.263	10.7
56-3	56.0	645.	1446.	79.9	8.155	0.250	8.137	0.275	11.1
56-3	56.0	657.	1454.	80.2	8.855	0.251	8.902	0.275	11.7
56-2	56.0	670.	1462.	80.5	8.434	0.348	8.477	0.385	11.7
56-2	56.0	682.	1469.	80.8	9.040	0.358	9.154	0.395	11.8
56-2	56.0	694.	1477.	81.0	8.876	0.352	8.965	0.387	12.0
56-2	56.0	706.	1485.	81.3	9.829	0.363	10.029	0.398	12.3
56-2	56.0	720.	1494.	81.6	8.525	0.335	8.591	0.366	12.7
56-2	56.0	734.	1502.	81.9	9.397	0.350	9.580	0.380	13.2
56-2	56.0	748.	1511.	82.3	7.385	0.299	7.396	0.323	13.9
56-1	56.0	765.	1522.	82.6	6.976	0.238	7.040	0.258	14.0
56-1	56.0	779.	1530.	82.9	5.576	0.216	5.557	0.233	14.1
56-1	56.0	793.	1539.	83.3	4.918	0.194	4.893	0.209	14.4
56-1	56.0	808.	1548.	83.6	4.006	0.172	3.955	0.184	14.8
56-1	56.0	825.	1558.	83.9	3.343	0.157	3.286	0.167	15.4
56-1	56.0	841.	1568.	84.3	3.103	0.149	3.065	0.158	16.0
56-1	56.0	859.	1578.	84.6	2.432	0.133	2.366	0.143	16.8

TABLE 7e

AVERAGE AND UNFOLDED CROSS SECTIONS

POINT NO.	THETA LAB	K	W	THETA C.M.	SIGMA AVERAGE	DSIGMA AVERAGE	SIGMA UNFOLDED	DSIGMA UNFOLDED	ΔK RMS
64-5	64.0	496.	1346.	85.4	6.517	0.247	6.513	0.287	8.6
64-5	64.0	504.	1351.	85.7	6.938	0.251	6.996	0.284	8.7
64-5	64.0	513.	1357.	85.9	6.537	0.239	6.534	0.269	8.8
64-5	64.0	521.	1363.	86.1	6.299	0.233	6.265	0.263	9.0
64-5	64.0	531.	1370.	86.3	6.388	0.227	6.370	0.256	9.2
64-5	64.0	540.	1376.	86.6	6.584	0.231	6.594	0.260	9.5
64-5	64.0	550.	1383.	86.8	6.344	0.219	6.319	0.246	9.9
64-4	64.0	562.	1391.	87.1	6.572	0.181	6.561	0.205	10.0
64-4	64.0	571.	1397.	87.4	6.246	0.173	6.184	0.196	10.1
64-4	64.0	581.	1404.	87.6	5.971	0.169	5.865	0.191	10.3
64-4	64.0	591.	1411.	87.9	6.912	0.176	6.933	0.198	10.5
64-4	64.0	602.	1418.	88.2	6.334	0.170	6.262	0.191	10.9
64-4	64.0	614.	1425.	88.4	6.599	0.168	6.554	0.188	11.2
64-4	64.0	626.	1433.	88.7	6.993	0.169	6.986	0.188	11.8
64-3	64.0	639.	1442.	89.0	7.459	0.219	7.496	0.243	11.9
64-3	64.0	650.	1449.	89.3	7.001	0.215	6.969	0.237	12.0
64-3	64.0	662.	1457.	89.6	7.254	0.216	7.240	0.238	12.2
64-3	64.0	675.	1465.	89.9	7.831	0.222	7.864	0.243	12.5
64-3	64.0	688.	1474.	90.2	8.035	0.221	8.074	0.240	13.0
64-3	64.0	702.	1482.	90.5	8.292	0.233	8.344	0.252	13.4
64-3	64.0	716.	1491.	90.9	8.273	0.222	8.315	0.239	14.0
64-2	64.0	732.	1501.	91.2	7.963	0.245	8.083	0.268	14.3
64-2	64.0	746.	1510.	91.5	7.081	0.230	7.135	0.251	14.5
64-2	64.0	760.	1519.	91.8	6.383	0.219	6.399	0.237	14.8
64-2	64.0	776.	1528.	92.2	5.466	0.199	5.441	0.215	15.2
64-2	64.0	792.	1538.	92.5	4.605	0.179	4.549	0.192	15.8
64-2	64.0	809.	1548.	92.9	4.131	0.173	4.080	0.185	16.3
64-2	64.0	826.	1559.	93.3	3.631	0.159	3.580	0.169	16.6
64-1	64.0	847.	1572.	93.7	2.765	0.111	2.716	0.120	17.6
64-1	64.0	864.	1582.	94.1	2.641	0.106	2.612	0.114	17.9
64-1	64.0	882.	1592.	94.4	2.328	0.099	2.296	0.106	18.4
64-1	64.0	901.	1603.	94.8	2.140	0.095	2.112	0.101	19.0
64-1	64.0	921.	1615.	95.2	2.034	0.090	2.011	0.096	19.8
64-1	64.0	942.	1627.	95.6	2.327	0.094	2.333	0.100	20.6
64-1	64.0	964.	1640.	96.0	2.075	0.088	2.064	0.094	21.7

TABLE 7f

AVERAGE AND UNFOLDED CROSS SECTIONS

POINT NO.	THETA LAB	K	W	THETA C.M.	SIGMA (AVERAGE)	DSIGMA (AVERAGE)	SIGMA (UNFOLDED)	DSIGMA (UNFOLDED)	ΔK RMS
74-6	74.0	477.	1333.	95.8	6.076	0.315	6.145	0.371	8.9
74-6	74.0	485.	1338.	96.0	5.672	0.317	5.671	0.363	9.0
74-6	74.0	493.	1344.	96.2	5.595	0.296	5.588	0.337	9.1
74-6	74.0	502.	1350.	96.4	5.758	0.303	5.781	0.346	9.3
74-6	74.0	511.	1356.	96.7	5.812	0.290	5.849	0.331	9.6
74-6	74.0	521.	1363.	96.9	5.349	0.296	5.320	0.337	9.9
74-6	74.0	531.	1370.	97.2	5.445	0.272	5.440	0.309	10.3
74-5	74.0	541.	1377.	97.4	5.146	0.238	5.097	0.270	10.4
74-5	74.0	550.	1383.	97.7	5.309	0.232	5.289	0.263	10.5
74-5	74.0	560.	1390.	97.9	5.368	0.232	5.361	0.261	10.7
74-5	74.0	571.	1397.	98.2	5.328	0.225	5.313	0.253	11.0
74-5	74.0	582.	1404.	98.5	5.294	0.221	5.280	0.246	11.3
74-5	74.0	594.	1412.	98.7	5.219	0.225	5.190	0.250	11.7
74-5	74.0	606.	1420.	99.0	5.322	0.221	5.302	0.244	12.3
74-4	74.0	620.	1429.	99.4	5.587	0.198	5.556	0.222	12.5
74-4	74.0	631.	1437.	99.7	5.690	0.203	5.662	0.227	12.7
74-4	74.0	644.	1445.	100.0	5.848	0.203	5.827	0.226	12.9
74-4	74.0	657.	1453.	100.3	5.999	0.197	5.981	0.218	13.3
74-4	74.0	670.	1462.	100.6	6.756	0.206	6.807	0.227	13.7
74-4	74.0	685.	1471.	100.9	6.888	0.211	6.934	0.231	14.3
74-4	74.0	700.	1481.	101.2	6.745	0.207	6.759	0.225	15.0
74-3	74.0	716.	1491.	101.6	7.536	0.201	7.710	0.222	15.3
74-3	74.0	730.	1500.	101.9	6.834	0.192	6.910	0.211	15.5
74-3	74.0	746.	1510.	102.3	6.256	0.181	6.297	0.198	15.9
74-3	74.0	762.	1520.	102.6	5.690	0.171	5.692	0.186	16.4
74-3	74.0	779.	1530.	103.0	5.101	0.157	5.083	0.170	17.0
74-3	74.0	797.	1541.	103.4	4.696	0.152	4.670	0.164	17.7
74-3	74.0	816.	1553.	103.8	3.825	0.137	3.758	0.146	18.3
74-2	74.0	836.	1565.	104.2	3.298	0.151	3.264	0.166	19.2
74-2	74.0	854.	1576.	104.5	2.849	0.150	2.800	0.165	19.6
74-2	74.0	873.	1587.	104.9	2.487	0.133	2.429	0.145	20.1
74-2	74.0	894.	1599.	105.3	2.639	0.134	2.618	0.146	20.8
74-2	74.0	915.	1612.	105.7	2.622	0.129	2.612	0.140	21.7
74-2	74.0	938.	1625.	106.2	2.586	0.131	2.583	0.141	22.7
74-2	74.0	962.	1639.	106.6	2.515	0.127	2.511	0.136	24.1
74-1	74.0	991.	1655.	107.1	2.829	0.157	2.875	0.169	24.9
74-1	74.0	1014.	1668.	107.6	2.388	0.148	2.404	0.159	25.5
74-1	74.0	1039.	1682.	108.0	2.126	0.133	2.131	0.142	26.3
74-1	74.0	1065.	1697.	108.5	1.701	0.123	1.688	0.131	27.2
74-1	74.0	1093.	1712.	108.9	1.331	0.112	1.309	0.118	28.1
74-1	74.0	1123.	1728.	109.4	0.763	0.101	0.720	0.106	27.1
74-1	74.0	1155.	1746.	109.9	0.696	0.114	0.656	0.122	28.3

TABLE 7g

AVERAGE AND UNFOLDED CROSS SECTIONS

POINT NO.	THETA LAB	K	W	THETA C.M.	SIGMA AVERAGE	DSIGMA AVERAGE	SIGMA UNFOLDED	DSIGMA UNFOLDED	ΔK RMS
84-6	84.0	487.	1339.	106.2	4.749	0.218	4.792	0.258	9.9
84-6	84.0	496.	1345.	106.4	4.279	0.204	4.243	0.234	10.0
84-6	84.0	505.	1352.	106.6	4.662	0.208	4.693	0.237	10.2
84-6	84.0	514.	1358.	106.8	4.268	0.196	4.240	0.223	10.4
84-6	84.0	524.	1365.	107.1	4.254	0.187	4.227	0.213	10.7
84-6	84.0	535.	1372.	107.3	4.323	0.186	4.309	0.212	11.0
84-6	84.0	545.	1380.	107.6	4.039	0.177	3.980	0.202	11.5
84-5	84.0	556.	1387.	107.9	4.719	0.174	4.744	0.200	11.8
84-5	84.0	567.	1394.	108.1	4.464	0.173	4.441	0.199	11.9
84-5	84.0	578.	1402.	108.4	3.902	0.162	3.786	0.185	12.1
84-5	84.0	589.	1409.	108.7	4.362	0.162	4.313	0.185	12.4
84-5	84.0	602.	1418.	109.0	4.436	0.161	4.389	0.183	12.9
84-5	84.0	615.	1426.	109.3	4.735	0.171	4.718	0.194	13.3
84-5	84.0	628.	1435.	109.6	4.537	0.163	4.479	0.183	14.0
84-4	84.0	645.	1446.	109.9	5.279	0.222	5.324	0.252	14.4
84-4	84.0	658.	1454.	110.2	5.418	0.230	5.468	0.261	14.6
84-4	84.0	672.	1463.	110.5	5.214	0.218	5.223	0.246	15.0
84-4	84.0	687.	1473.	110.9	5.928	0.228	6.025	0.256	15.4
84-4	84.0	702.	1483.	111.2	5.776	0.223	5.842	0.250	16.0
84-4	84.0	719.	1493.	111.6	6.329	0.233	6.458	0.259	16.7
84-4	84.0	736.	1504.	111.9	5.728	0.219	5.783	0.242	17.6
84-3	84.0	756.	1516.	112.3	5.595	0.216	5.697	0.241	18.1
84-3	84.0	773.	1526.	112.7	5.032	0.204	5.084	0.227	18.4
84-3	84.0	791.	1537.	113.0	4.276	0.181	4.261	0.200	19.0
84-3	84.0	810.	1549.	113.4	3.739	0.173	3.696	0.191	19.6
84-3	84.0	830.	1561.	113.8	3.499	0.160	3.463	0.175	20.5
84-3	84.0	851.	1574.	114.2	2.980	0.157	2.919	0.171	21.4
84-3	84.0	874.	1587.	114.6	2.909	0.143	2.868	0.155	22.7
84-2	84.0	896.	1601.	115.0	2.823	0.150	2.803	0.166	23.4
84-2	84.0	918.	1613.	115.4	2.942	0.156	2.952	0.172	24.0
84-2	84.0	941.	1627.	115.8	2.903	0.147	2.914	0.161	24.8
84-2	84.0	966.	1641.	116.3	3.048	0.150	3.083	0.164	25.8
84-2	84.0	993.	1656.	116.7	3.028	0.146	3.066	0.158	27.1
84-2	84.0	1021.	1672.	117.2	2.973	0.150	3.018	0.162	28.5
84-2	84.0	1051.	1689.	117.7	2.418	0.133	2.425	0.143	30.3
84-1	84.0	1085.	1707.	118.2	1.636	0.087	1.624	0.094	31.6
84-1	84.0	1114.	1724.	118.7	1.054	0.076	1.016	0.082	32.6
84-1	84.0	1146.	1741.	119.2	0.800	0.068	0.765	0.073	34.0
84-1	84.0	1180.	1759.	119.7	0.481	0.061	0.442	0.065	35.5
84-1	84.0	1216.	1778.	120.2	0.432	0.058	0.407	0.062	37.5
84-1	84.0	1255.	1799.	120.8	0.391	0.056	0.375	0.059	39.3
84-1	84.0	1297.	1820.	121.3	0.377	0.058	0.366	0.062	39.4

TABLE 7h

AVERAGE AND UNFOLDED CROSS SECTIONS

POINT NO.	THETA LAB	K	W	THETA C.M.	SIGMA AVERAGE	DSIGMA AVERAGE	SIGMA UNFOLDED	DSIGMA UNFOLDED	Δ K RMS
94-5	94.0	532.	1371.	116.7	4.151	0.215	4.162	0.254	11.9
94-5	94.0	542.	1378.	116.9	3.952	0.216	3.931	0.248	12.1
94-5	94.0	553.	1385.	117.2	3.720	0.204	3.666	0.233	12.3
94-5	94.0	565.	1393.	117.4	3.535	0.200	3.452	0.228	12.6
94-5	94.0	577.	1401.	117.7	3.435	0.189	3.333	0.216	13.1
94-5	94.0	590.	1410.	118.0	4.202	0.207	4.214	0.236	13.5
94-5	94.0	603.	1419.	118.3	4.109	0.195	4.093	0.222	14.2
94-4	94.0	617.	1427.	118.6	4.166	0.202	4.156	0.232	14.6
94-4	94.0	630.	1436.	118.8	4.057	0.200	4.021	0.229	14.8
94-4	94.0	643.	1445.	119.1	4.226	0.203	4.211	0.232	15.2
94-4	94.0	658.	1454.	119.4	4.629	0.206	4.664	0.234	15.6
94-4	94.0	674.	1464.	119.7	4.617	0.203	4.640	0.230	16.2
94-4	94.0	690.	1475.	120.1	5.416	0.217	5.539	0.245	16.9
94-4	94.0	708.	1486.	120.4	4.885	0.203	4.927	0.228	17.9
94-3	94.0	729.	1499.	120.8	5.610	0.233	5.793	0.263	18.5
94-3	94.0	746.	1510.	121.2	4.504	0.215	4.533	0.242	18.9
94-3	94.0	764.	1521.	121.5	4.232	0.204	4.243	0.229	19.5
94-3	94.0	783.	1533.	121.9	4.087	0.197	4.099	0.220	20.2
94-3	94.0	804.	1545.	122.2	3.648	0.183	3.627	0.203	21.1
94-3	94.0	825.	1558.	122.6	3.244	0.176	3.199	0.194	22.1
94-3	94.0	848.	1572.	123.0	2.929	0.162	2.873	0.178	23.5
94-2	94.0	875.	1588.	123.5	2.938	0.156	2.914	0.174	24.4
94-2	94.0	898.	1601.	123.9	3.022	0.160	3.023	0.178	25.1
94-2	94.0	922.	1616.	124.3	3.009	0.156	3.015	0.173	26.0
94-2	94.0	948.	1631.	124.7	2.842	0.153	2.836	0.169	27.1
94-2	94.0	976.	1647.	125.1	3.456	0.159	3.523	0.174	28.5
94-2	94.0	1006.	1664.	125.6	3.279	0.155	3.334	0.169	30.2
94-2	94.0	1038.	1682.	126.1	2.809	0.143	2.827	0.155	32.2
94-1	94.0	1070.	1699.	126.6	2.207	0.110	2.220	0.120	33.5
94-1	94.0	1102.	1717.	127.0	1.678	0.098	1.661	0.107	34.7
94-1	94.0	1135.	1735.	127.5	1.006	0.085	0.951	0.092	36.3
94-1	94.0	1172.	1755.	128.0	0.758	0.073	0.708	0.079	38.1
94-1	94.0	1212.	1776.	128.5	0.630	0.070	0.592	0.075	40.4
94-1	94.0	1254.	1798.	129.0	0.592	0.070	0.567	0.074	42.3
94-1	94.0	1300.	1822.	129.6	0.533	0.072	0.513	0.077	41.8

TABLE 7i

AVERAGE AND UNFOLDED CROSS SECTIONS

POINT NO.	THETA LAB	K	W	THETA C.M.	SIGMA AVERAGE	DSIGMA AVERAGE	SIGMA UNFOLDED	DSIGMA UNFOLDED	ΔK RMS
106-5	106.0	512.	1357.	126.7	3.773	0.190	3.791	0.228	12.3
106-5	106.0	522.	1364.	126.9	3.948	0.192	3.999	0.223	12.4
106-5	106.0	533.	1371.	127.1	3.639	0.178	3.637	0.206	12.7
106-5	106.0	544.	1379.	127.4	3.399	0.178	3.361	0.206	13.0
106-5	106.0	556.	1387.	127.6	3.006	0.164	2.904	0.190	13.4
106-5	106.0	569.	1396.	127.9	3.491	0.167	3.479	0.194	13.9
106-5	106.0	582.	1405.	128.1	3.450	0.167	3.426	0.194	14.5
106-4	106.0	597.	1415.	128.4	3.441	0.180	3.410	0.209	15.1
106-4	106.0	611.	1423.	128.7	3.636	0.189	3.635	0.219	15.3
106-4	106.0	624.	1432.	129.0	3.284	0.171	3.218	0.198	15.7
106-4	106.0	639.	1442.	129.2	3.606	0.171	3.591	0.197	16.2
106-4	106.0	655.	1453.	129.5	3.873	0.178	3.895	0.204	16.9
106-4	106.0	672.	1463.	129.8	3.798	0.177	3.795	0.202	17.6
106-4	106.0	690.	1475.	130.1	4.118	0.183	4.157	0.208	18.6
106-3	106.0	708.	1486.	130.5	4.931	0.234	5.115	0.268	19.2
106-3	106.0	725.	1497.	130.8	4.479	0.230	4.584	0.262	19.6
106-3	106.0	743.	1508.	131.1	4.486	0.219	4.596	0.249	20.3
106-3	106.0	763.	1521.	131.4	3.489	0.195	3.463	0.220	21.0
106-3	106.0	785.	1534.	131.7	3.839	0.199	3.884	0.223	22.0
106-3	106.0	807.	1547.	132.1	3.033	0.187	2.987	0.208	23.1
106-3	106.0	831.	1562.	132.5	2.567	0.159	2.487	0.176	24.6
106-2	106.0	861.	1580.	132.9	2.759	0.168	2.737	0.189	25.8
106-2	106.0	885.	1594.	133.3	2.679	0.169	2.657	0.190	26.5
106-2	106.0	910.	1609.	133.7	2.648	0.159	2.627	0.177	27.6
106-2	106.0	938.	1625.	134.1	2.931	0.160	2.956	0.178	28.9
106-2	106.0	968.	1642.	134.5	2.846	0.158	2.862	0.174	30.5
106-2	106.0	1000.	1661.	134.9	2.828	0.163	2.852	0.179	32.4
106-2	106.0	1035.	1680.	135.4	3.031	0.166	3.079	0.180	34.8
106-1	106.0	1075.	1702.	135.9	2.341	0.121	2.368	0.133	36.6
106-1	106.0	1110.	1721.	136.3	1.563	0.103	1.524	0.113	38.1
106-1	106.0	1147.	1742.	136.8	1.104	0.090	1.042	0.098	40.0
106-1	106.0	1189.	1764.	137.2	1.048	0.086	1.004	0.093	42.2
106-1	106.0	1234.	1787.	137.7	1.053	0.084	1.028	0.090	44.7
106-1	106.0	1282.	1813.	138.3	0.797	0.082	0.764	0.088	44.9
106-1	106.0	1334.	1840.	138.8	0.764	0.097	0.734	0.106	44.9

TABLE 7j

AVERAGE AND UNFOLDED CROSS SECTIONS

POINT NO.	THETA LAB	K	W	THETA C.M.	SIGMA AVERAGE	DSIGMA AVERAGE	SIGMA UNFOLDED	DSIGMA UNFOLDED	ΔK RMS
120-5	120.0	492.	1343.	137.7	3.467	0.180	3.510	0.216	12.6
120-5	120.0	501.	1349.	137.9	3.163	0.165	3.148	0.192	12.7
120-5	120.0	512.	1357.	138.1	3.505	0.173	3.554	0.200	13.0
120-5	120.0	523.	1365.	138.3	3.292	0.166	3.307	0.191	13.3
120-5	120.0	535.	1373.	138.5	3.257	0.160	3.270	0.184	13.7
120-5	120.0	548.	1381.	138.7	2.838	0.155	2.788	0.178	14.2
120-5	120.0	561.	1390.	138.9	3.168	0.153	3.182	0.174	14.9
120-4	120.0	577.	1401.	139.1	2.805	0.161	2.741	0.187	15.5
120-4	120.0	590.	1410.	139.4	2.679	0.166	2.597	0.192	15.8
120-4	120.0	604.	1419.	139.6	3.304	0.174	3.327	0.201	16.2
120-4	120.0	619.	1429.	139.8	2.984	0.163	2.949	0.187	16.7
120-4	120.0	635.	1439.	140.1	3.195	0.165	3.189	0.188	17.4
120-4	120.0	651.	1450.	140.3	3.011	0.166	2.973	0.188	18.1
120-4	120.0	669.	1462.	140.6	3.482	0.170	3.504	0.191	19.1
120-3	120.0	690.	1475.	140.9	3.577	0.185	3.620	0.210	20.0
120-3	120.0	707.	1486.	141.2	3.887	0.191	3.975	0.217	20.5
120-3	120.0	726.	1498.	141.4	3.718	0.182	3.774	0.205	21.1
120-3	120.0	747.	1511.	141.7	3.539	0.172	3.575	0.193	21.9
120-3	120.0	769.	1524.	142.0	3.384	0.164	3.405	0.182	23.0
120-3	120.0	792.	1539.	142.3	2.550	0.157	2.483	0.173	23.9
120-3	120.0	818.	1554.	142.6	2.625	0.147	2.583	0.161	23.8
120-2	120.0	843.	1569.	143.0	2.424	0.174	2.377	0.198	27.0
120-2	120.0	868.	1584.	143.3	2.656	0.173	2.654	0.196	27.9
120-2	120.0	895.	1600.	143.6	2.557	0.165	2.543	0.186	29.0
120-2	120.0	924.	1617.	143.9	2.576	0.159	2.574	0.178	30.5
120-2	120.0	956.	1635.	144.3	2.598	0.168	2.601	0.187	32.3
120-2	120.0	990.	1655.	144.7	2.686	0.172	2.708	0.190	34.4
120-2	120.0	1027.	1675.	145.1	2.795	0.167	2.834	0.183	37.1
120-1	120.0	1073.	1701.	145.6	2.212	0.140	2.229	0.155	39.4
120-1	120.0	1111.	1722.	145.9	1.771	0.132	1.754	0.146	41.2
120-1	120.0	1152.	1744.	146.3	1.547	0.121	1.524	0.133	43.4
120-1	120.0	1197.	1768.	146.8	1.165	0.105	1.122	0.114	46.1
120-1	120.0	1247.	1795.	147.2	0.794	0.094	0.735	0.102	48.3
120-1	120.0	1301.	1823.	147.7	0.874	0.109	0.838	0.117	46.8
120-1	120.0	1361.	1853.	148.2	0.747	0.129	0.698	0.143	54.5

TABLE 7k

AVERAGE AND UNFOLDED CROSS SECTIONS

POINT NO.	THETA LAB	K	W	THETA C.M.	SIGMA AVERAGE	DSIGMA AVERAGE	SIGMA UNFOLDED	DSIGMA UNFOLDED	ΔK RMS
134-4	134.0	541.	1377.	149.0	3.046	0.139	3.059	0.167	15.2
134-4	134.0	554.	1385.	149.1	2.701	0.138	2.651	0.160	15.5
134-4	134.0	567.	1394.	149.3	2.837	0.135	2.815	0.156	15.8
134-4	134.0	581.	1403.	149.5	2.876	0.137	2.860	0.158	16.3
134-4	134.0	596.	1413.	149.7	2.995	0.134	2.997	0.154	16.9
134-4	134.0	611.	1424.	149.9	3.020	0.132	3.023	0.151	17.6
134-4	134.0	628.	1435.	150.1	2.688	0.124	2.636	0.142	18.6
134-3	134.0	648.	1448.	150.3	2.990	0.151	3.003	0.175	19.5
134-3	134.0	665.	1459.	150.5	3.200	0.153	3.246	0.178	19.9
134-3	134.0	683.	1470.	150.7	3.238	0.158	3.285	0.182	20.6
134-3	134.0	702.	1482.	150.9	3.570	0.154	3.673	0.177	21.4
134-3	134.0	723.	1496.	151.2	3.280	0.147	3.333	0.168	22.4
134-3	134.0	745.	1509.	151.4	2.838	0.141	2.831	0.160	23.5
134-3	134.0	769.	1524.	151.7	2.785	0.132	2.783	0.148	25.1
134-2	134.0	796.	1541.	151.9	2.413	0.136	2.377	0.156	26.3
134-2	134.0	820.	1555.	152.2	2.131	0.127	2.064	0.145	27.2
134-2	134.0	846.	1571.	152.4	2.204	0.129	2.160	0.146	28.4
134-2	134.0	874.	1588.	152.7	2.503	0.130	2.509	0.146	29.7
134-2	134.0	905.	1606.	153.0	2.503	0.127	2.511	0.142	31.5
134-2	134.0	938.	1625.	153.3	2.491	0.128	2.500	0.142	33.5
134-2	134.0	974.	1646.	153.6	2.195	0.124	2.174	0.136	35.3
134-1	134.0	1010.	1666.	153.9	2.358	0.093	2.407	0.105	38.2
134-1	134.0	1047.	1687.	154.2	1.992	0.086	2.002	0.096	39.9
134-1	134.0	1087.	1709.	154.5	1.703	0.080	1.692	0.089	42.1
134-1	134.0	1131.	1733.	154.8	1.255	0.070	1.208	0.077	44.8
134-1	134.0	1179.	1759.	155.2	1.057	0.067	1.008	0.073	48.2
134-1	134.0	1232.	1787.	155.5	1.116	0.067	1.088	0.073	51.1
134-1	134.0	1290.	1817.	155.9	0.877	0.066	0.829	0.073	50.5

TABLE 7 1

AVERAGE AND UNFOLDED CROSS SECTIONS

POINT NO.	THETA LAB	K	W	THETA C.M.	SIGMA AVERAGE	DSIGMA AVERAGE	SIGMA UNFOLDED	DSIGMA UNFOLDED	ΔK RMS
156-4	155.4	510.	1355.	163.6	3.057	0.160	3.088	0.196	15.1
156-4	155.4	522.	1363.	163.7	3.225	0.161	3.288	0.190	15.3
156-4	155.4	534.	1372.	163.8	2.742	0.152	2.709	0.178	15.6
156-4	155.4	547.	1381.	163.9	2.662	0.144	2.621	0.169	16.1
156-4	155.4	561.	1390.	164.0	2.855	0.147	2.855	0.172	16.6
156-4	155.4	576.	1400.	164.1	3.104	0.147	3.152	0.172	17.3
156-4	155.4	592.	1411.	164.2	2.841	0.139	2.835	0.161	18.2
156-3	155.4	609.	1422.	164.3	2.782	0.158	2.782	0.185	19.1
156-3	155.4	625.	1433.	164.4	3.077	0.156	3.137	0.183	19.6
156-3	155.4	642.	1444.	164.5	2.700	0.146	2.692	0.170	20.2
156-3	155.4	660.	1456.	164.6	2.816	0.151	2.835	0.176	20.9
156-3	155.4	680.	1468.	164.7	2.541	0.141	2.517	0.163	21.9
156-3	155.4	701.	1482.	164.9	2.929	0.154	2.978	0.177	23.0
156-3	155.4	724.	1496.	165.0	2.455	0.138	2.431	0.156	24.4
156-2	155.4	750.	1513.	165.1	2.410	0.149	2.398	0.173	25.8
156-2	155.4	773.	1527.	165.3	2.173	0.137	2.129	0.159	26.7
156-2	155.4	798.	1542.	165.4	2.544	0.145	2.570	0.167	27.8
156-2	155.4	825.	1558.	165.6	2.370	0.137	2.373	0.157	29.1
156-2	155.4	854.	1576.	165.7	2.164	0.131	2.140	0.149	30.9
156-2	155.4	886.	1594.	165.9	2.069	0.136	2.040	0.153	32.9
156-2	155.4	920.	1615.	166.0	2.348	0.131	2.362	0.146	35.5
156-1	155.4	965.	1637.	166.2	2.298	0.129	2.353	0.147	37.7
156-1	155.4	995.	1658.	166.4	2.185	0.130	2.233	0.147	39.4
156-1	155.4	1034.	1679.	166.5	1.834	0.119	1.845	0.134	41.7
156-1	155.4	1077.	1703.	166.7	1.329	0.103	1.293	0.115	44.4
156-1	155.4	1125.	1729.	166.9	1.075	0.091	1.030	0.100	48.0
156-1	155.4	1177.	1757.	167.1	0.848	0.082	0.796	0.090	51.9
156-1	155.4	1234.	1788.	167.3	0.452	0.072	0.364	0.080	55.2

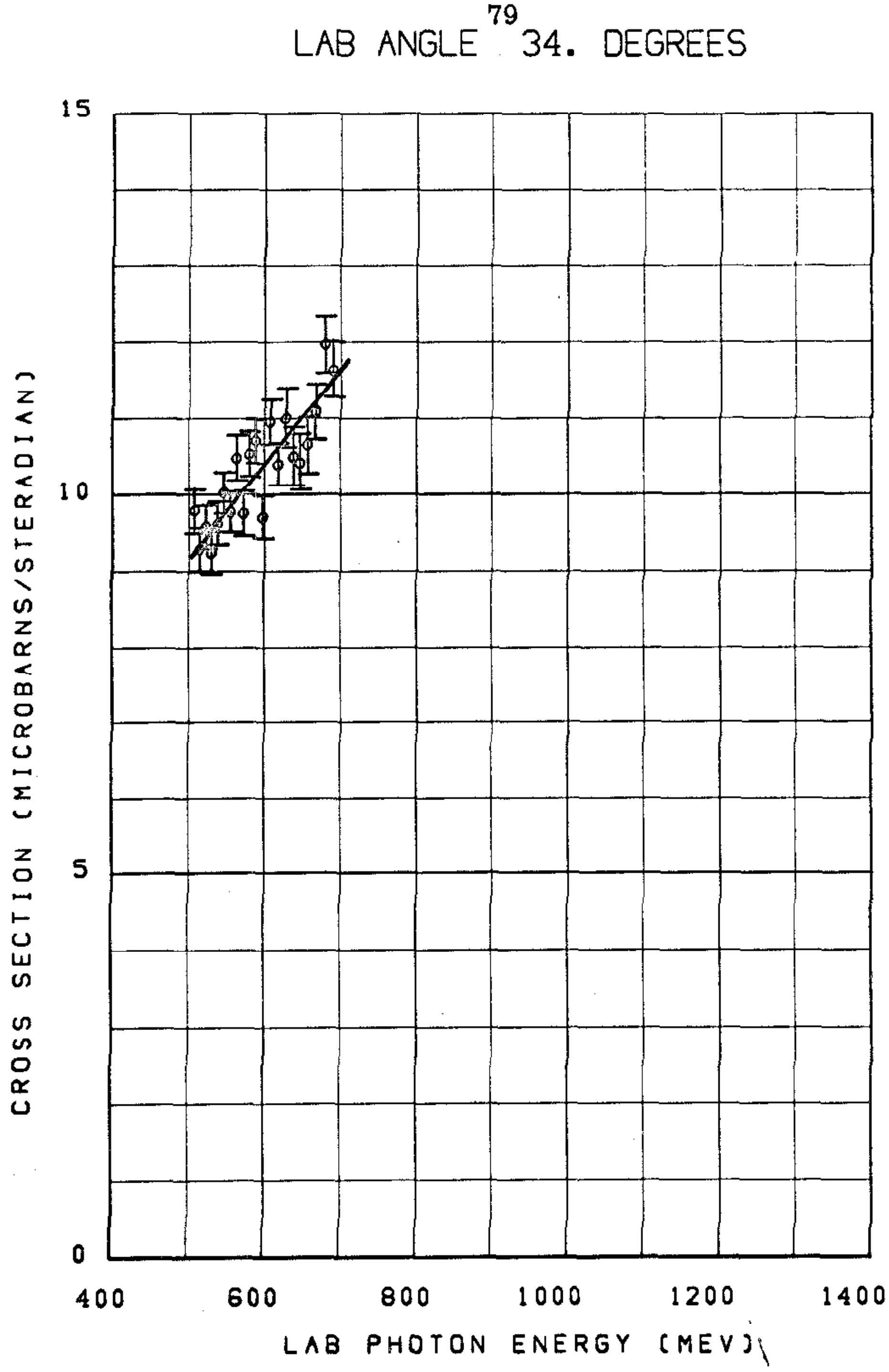
LAB ANGLE 34. DEGREES
15
10
5
0
CROSS SECTION (MICROBARNS/STERADIAN)
400
600
800
1000
1200
1400
LAB PHOTON ENERGY (MEV)

Figure 13a

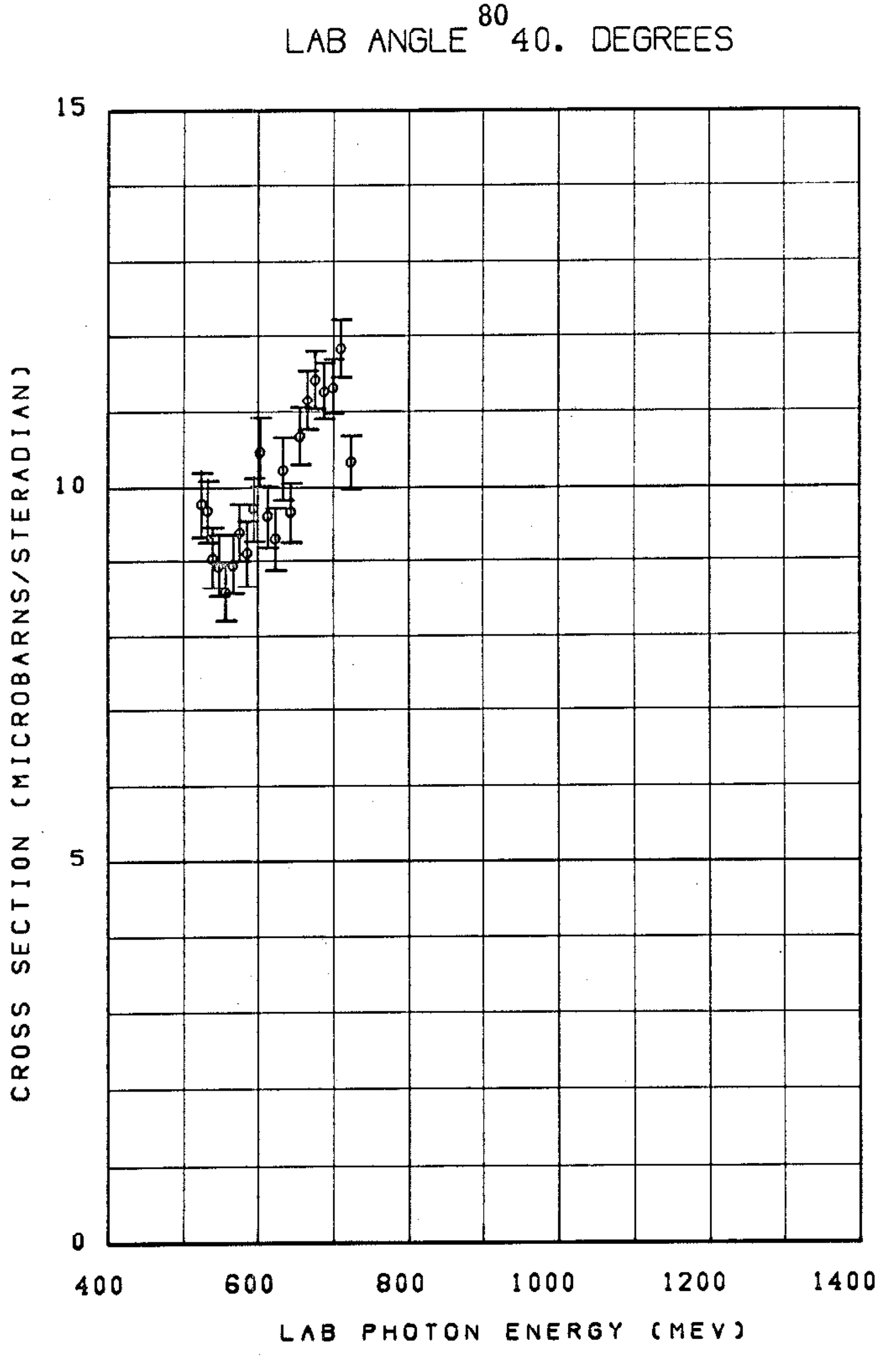
LAB ANGLE 40. DEGREES
15
10
5
0
400
600
800
1000
1200
1400
LAB PHOTON ENERGY (MEV)
CROSS SECTION (MICROBARNS/STERADIAN)

Figure 13b.

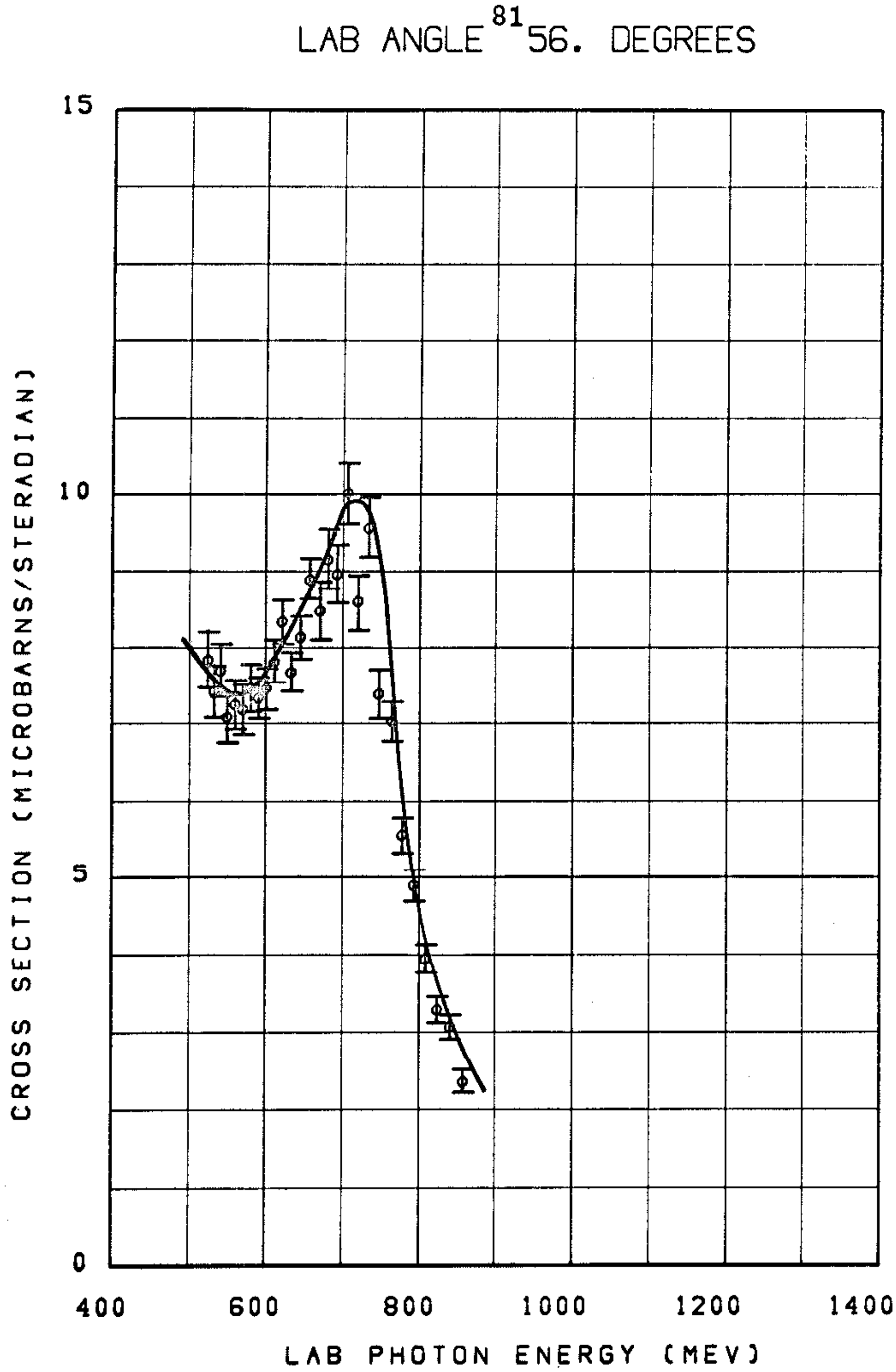

LAB ANGLE 56. DEGREES
81
CROSS SECTION (MICROBARNS/STERADIAN)
15
10
5
0
400
600
800
1000
1200
1400
LAB PHOTON ENERGY (MEV)

Figure 13c

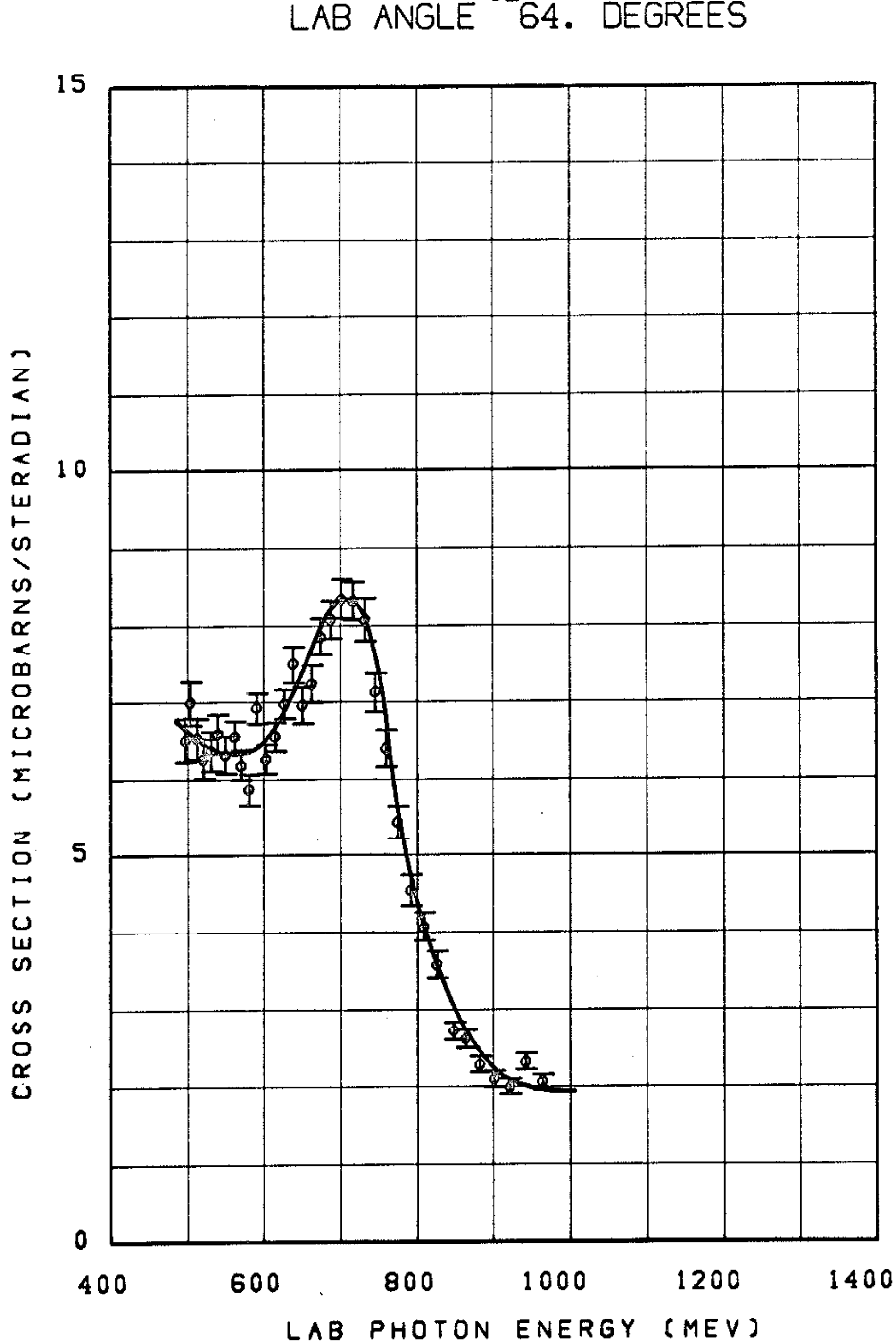
LAB ANGLE 64. DEGREES
15
10
5
0
400
600
800
1000
1200
1400
LAB PHOTON ENERGY (MEV)
CROSS SECTION (MICROBARNS/STERADIAN)

Figure 13d

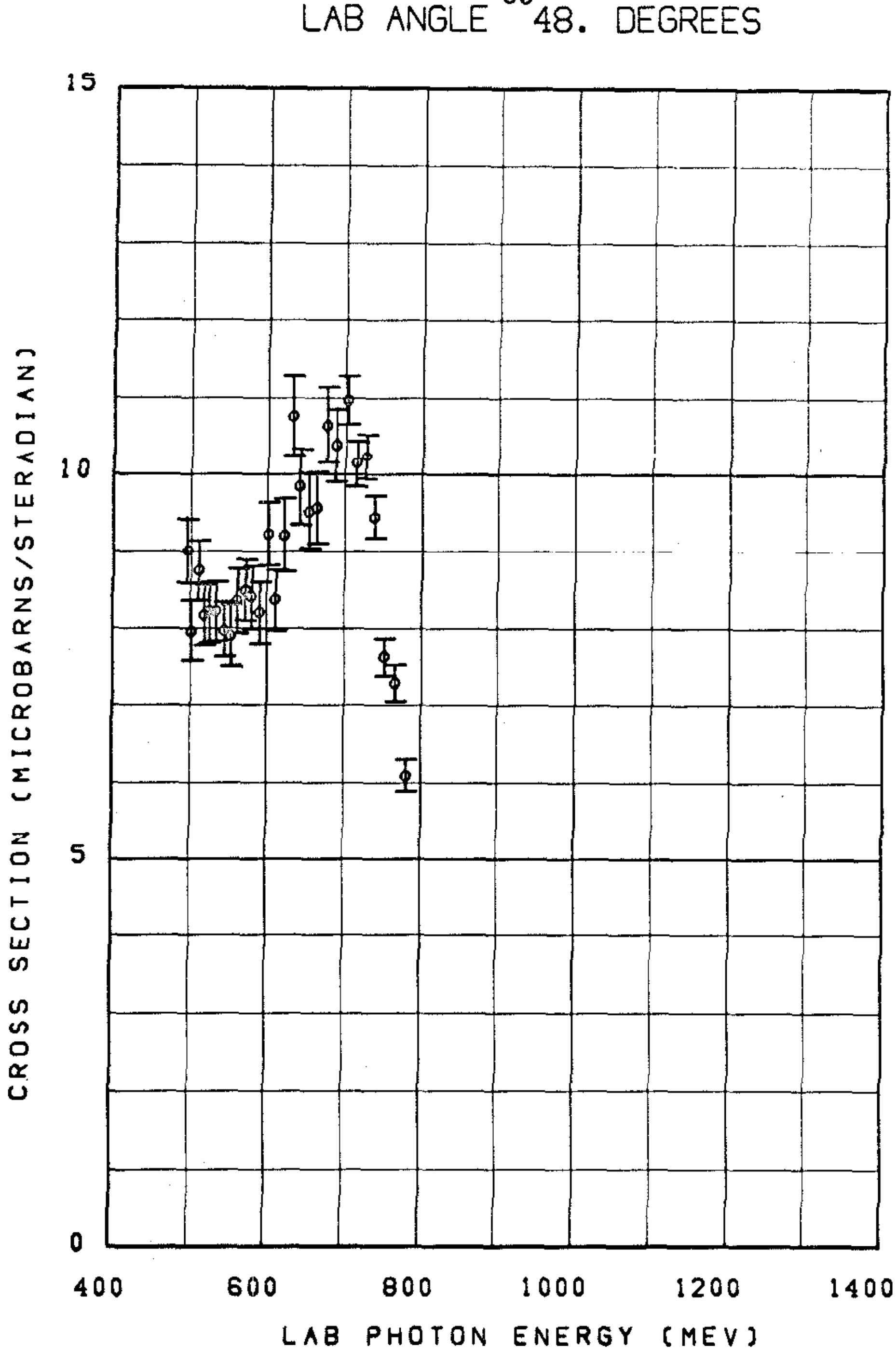
LAB ANGLE 48. DEGREES
15
10
5
0
CROSS SECTION (MICROBARNS/STERADIAN)
400
600
800
1000
1200
1400
LAB PHOTON ENERGY (MEV)

Figure 13e

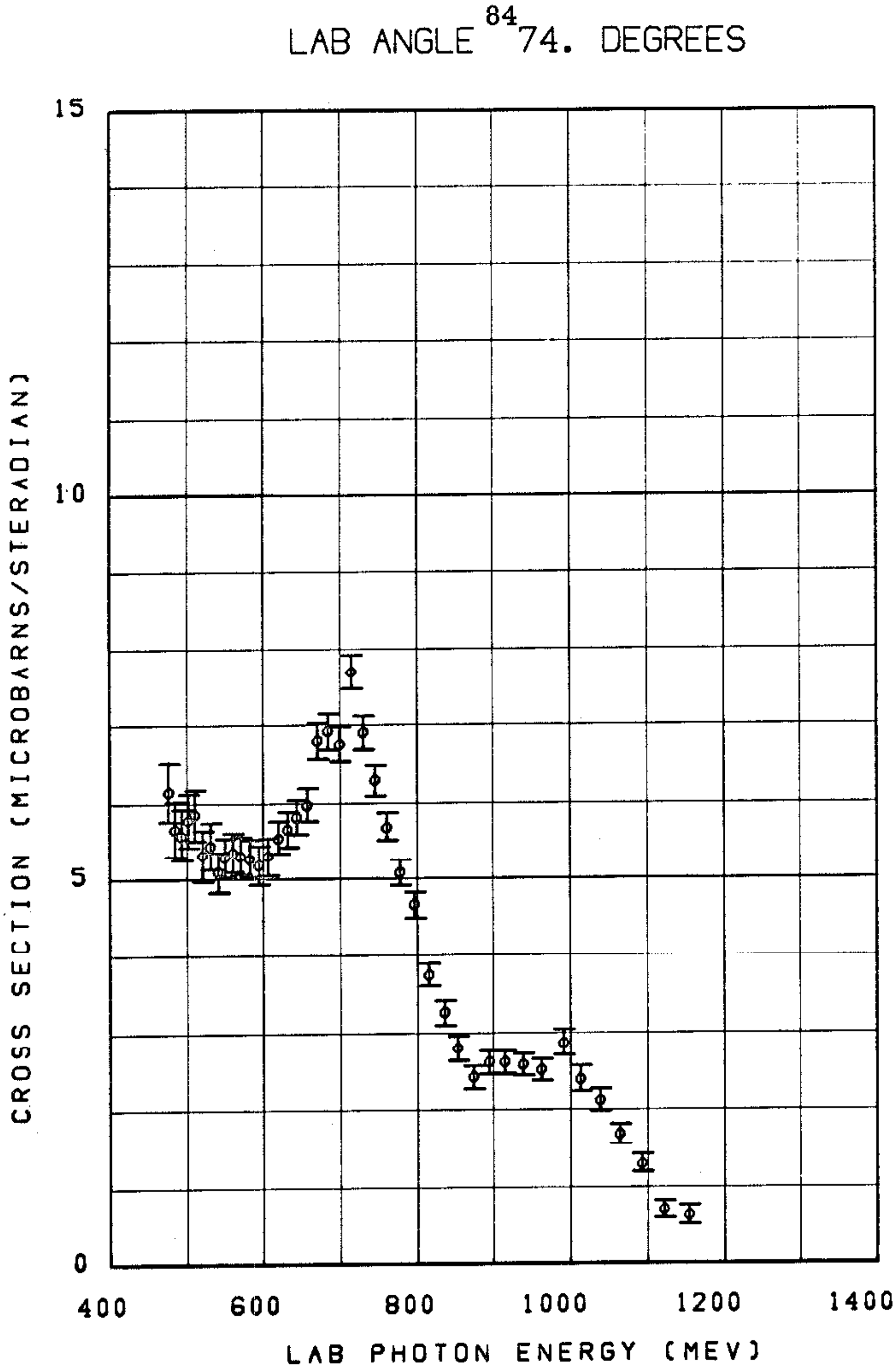
LAB ANGLE 84.74. DEGREES
15
10
5
0
400
600
800
1000
1200
1400
LAB PHOTON ENERGY (MEV)
CROSS SECTION (MICROBARNS/STERADIAN)

Figure 13f

85

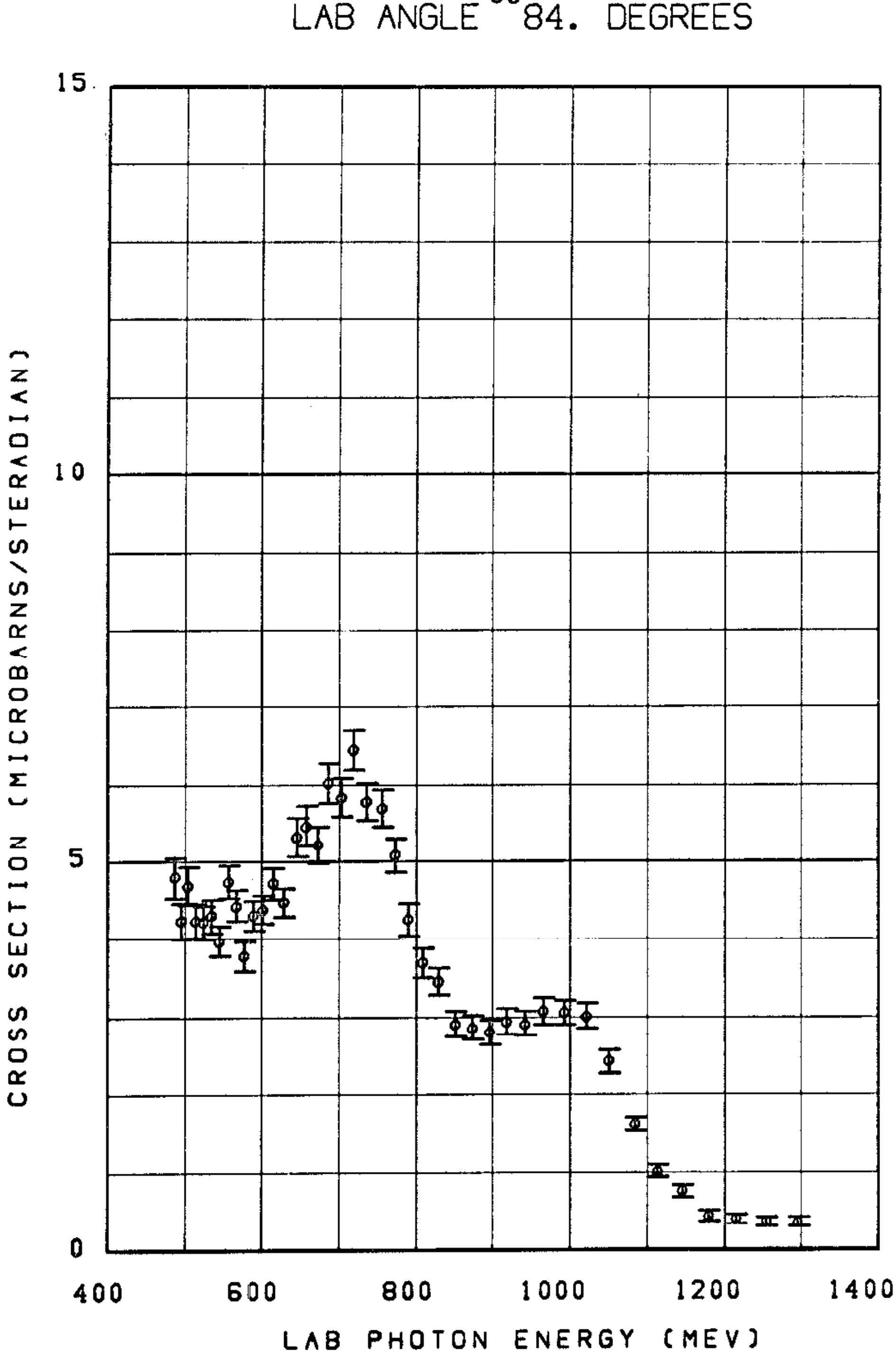

Figure 13g

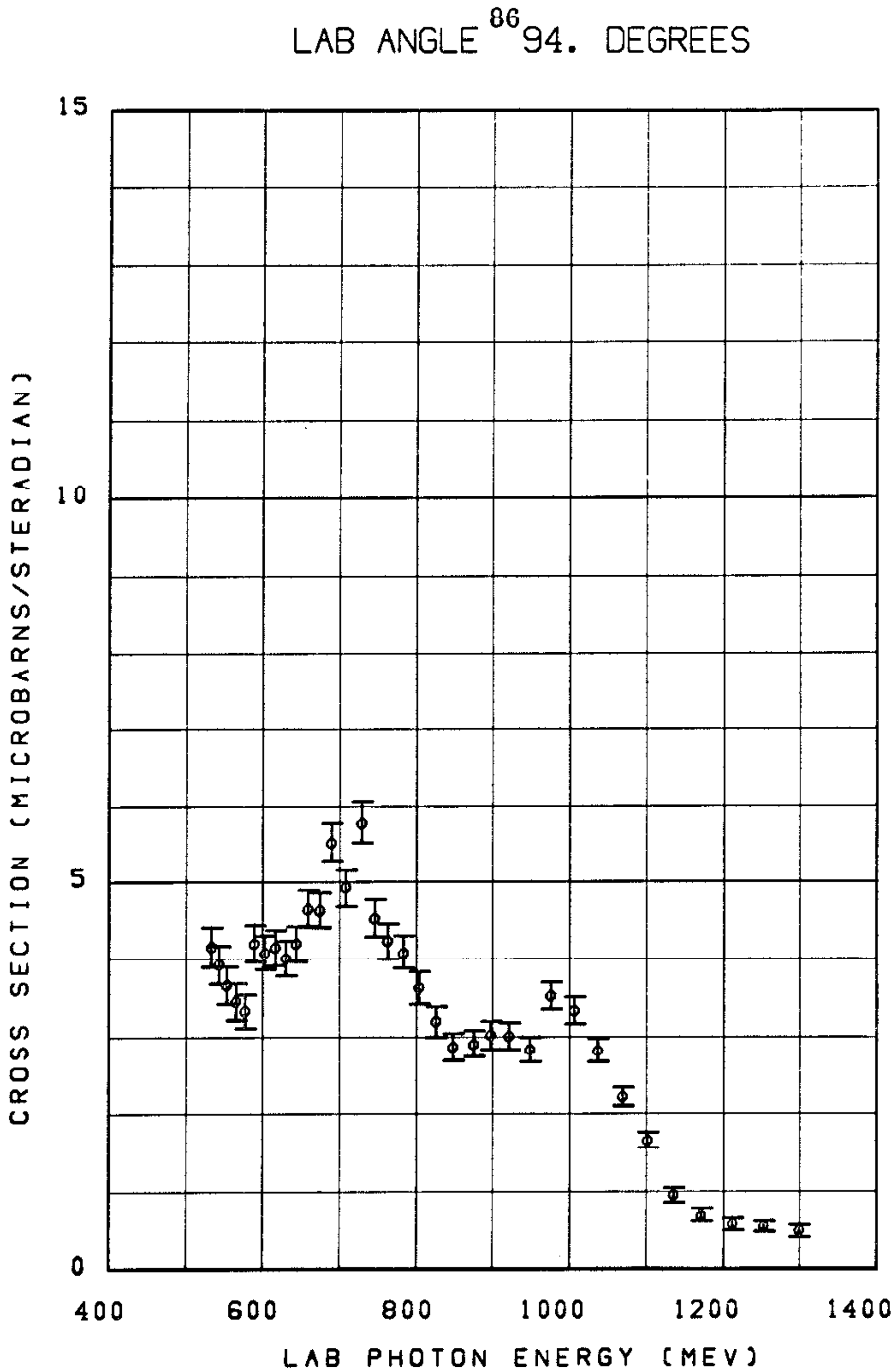
LAB ANGLE 86 94. DEGREES
15
10
5
0
CROSS SECTION (MICROBARNS/STERADIAN)
400
600
800
1000
1200
1400
LAB PHOTON ENERGY (MEV)

Figure 13h

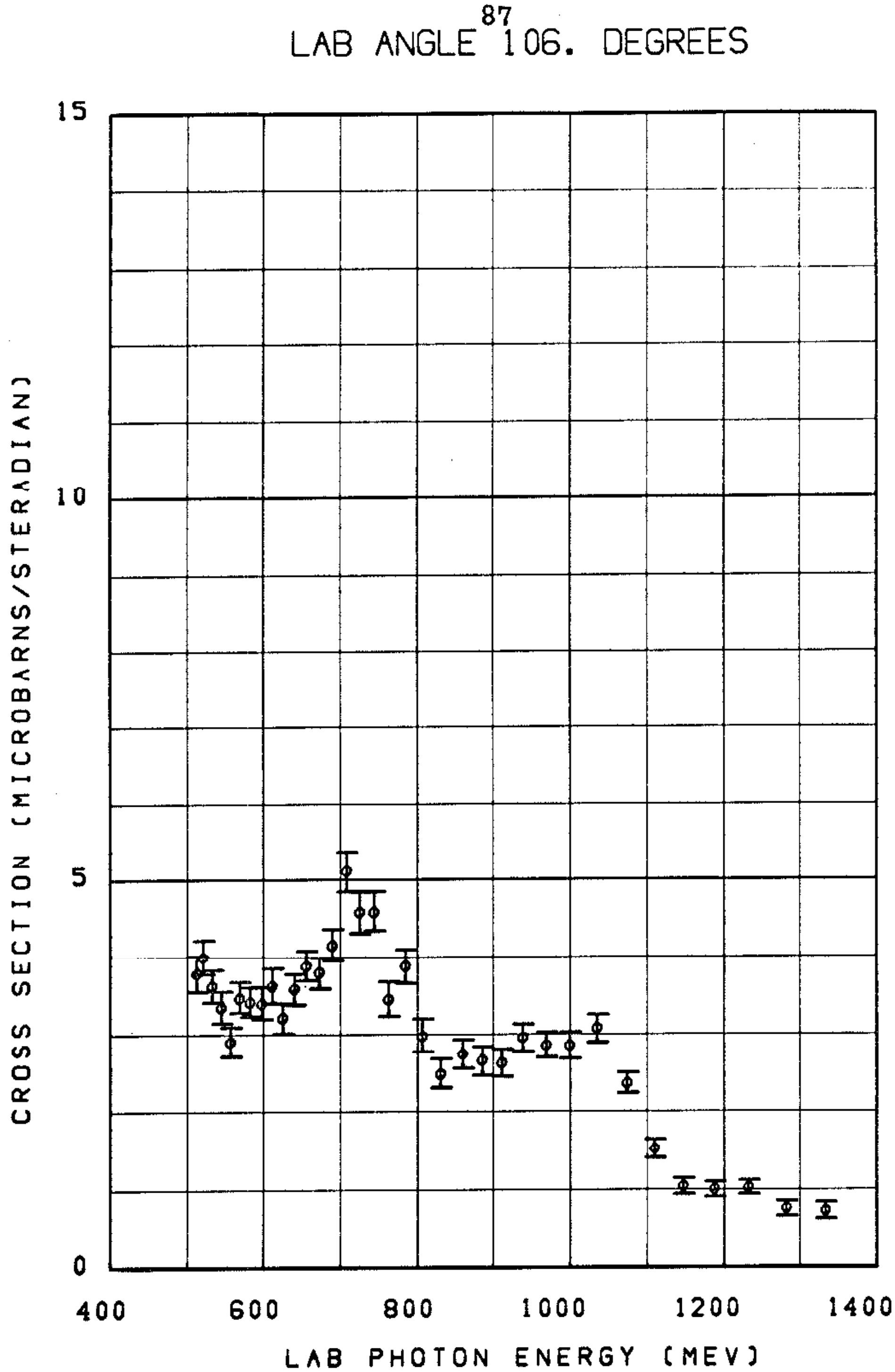
LAB ANGLE 106. DEGREES
15
10
5
0
CROSS SECTION (MICROBARNS/STERADIAN)
400
600
800
1000
1200
1400
LAB PHOTON ENERGY (MEV)

Figure 13i

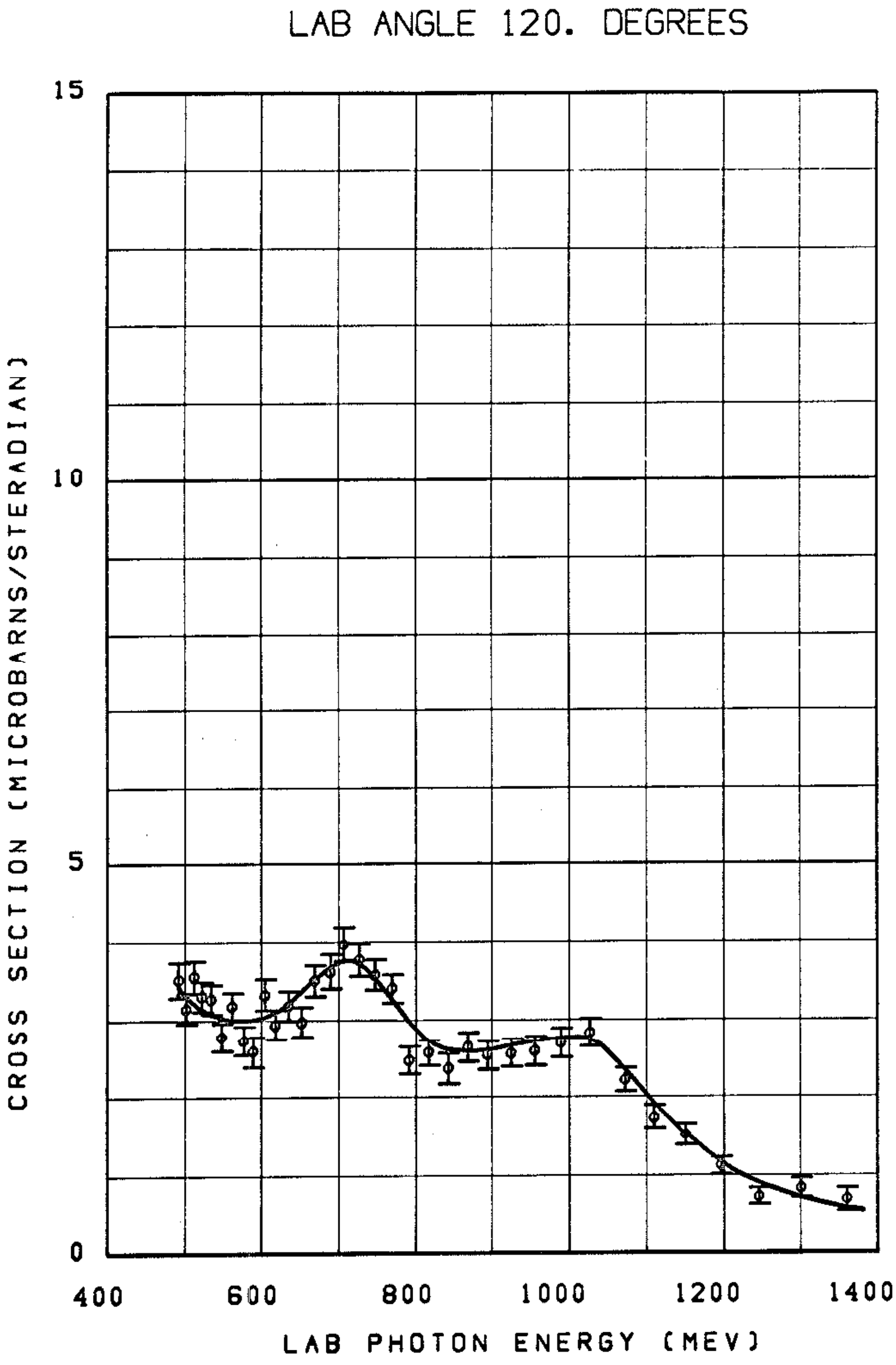
LAB ANGLE 120. DEGREES
CROSS SECTION (MICROBARNS/STERADIAN)
15
10
5
0
400
600
800
1000
1200
1400
LAB PHOTON ENERGY (MEV)

Figure 13j

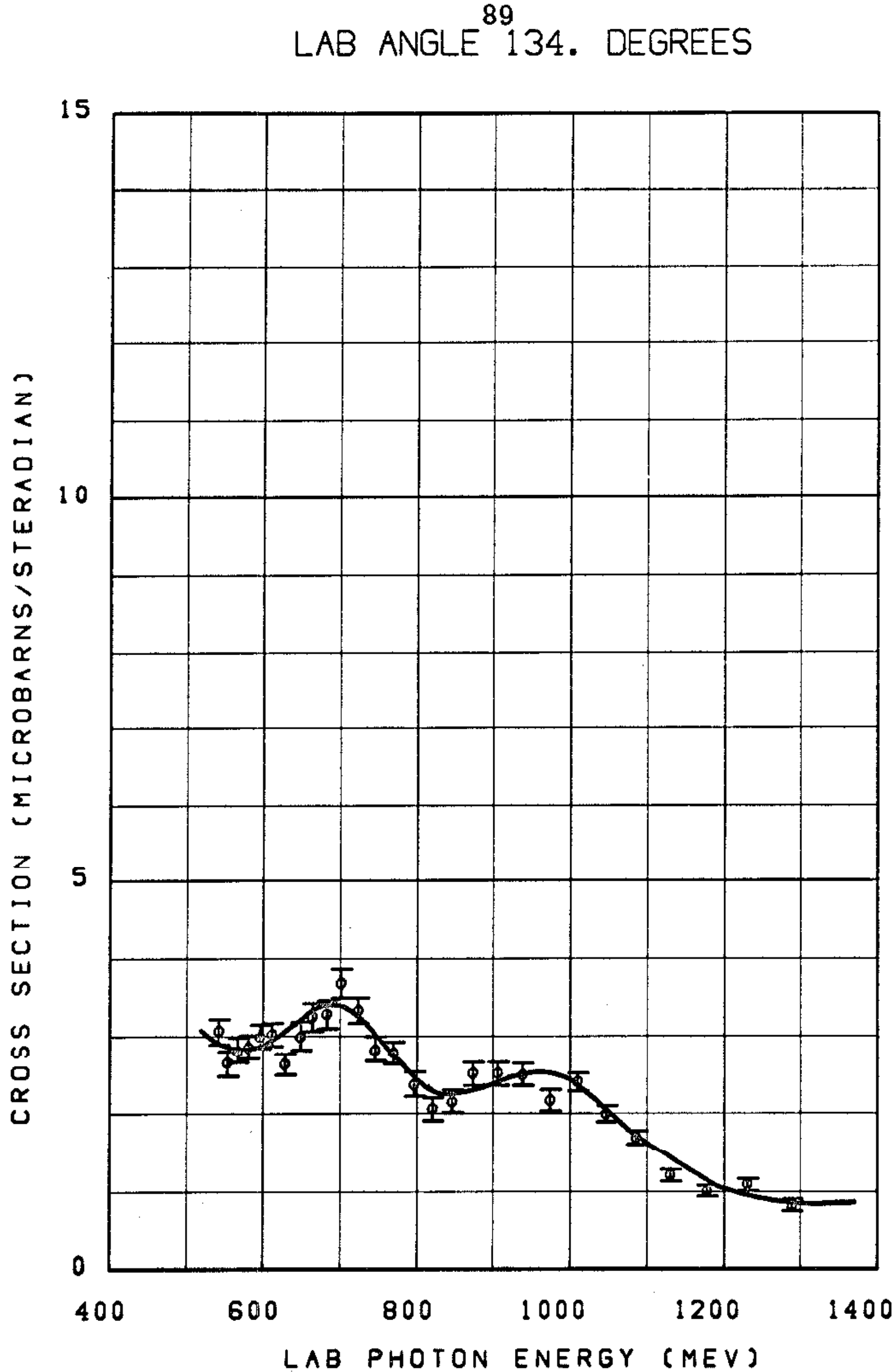
LAB ANGLE 134. DEGREES
15
10
5
0
CROSS SECTION (MICROBARNS/STERADIAN)
400
600
800
1000
1200
1400
LAB PHOTON ENERGY (MEV)

Figure 13k

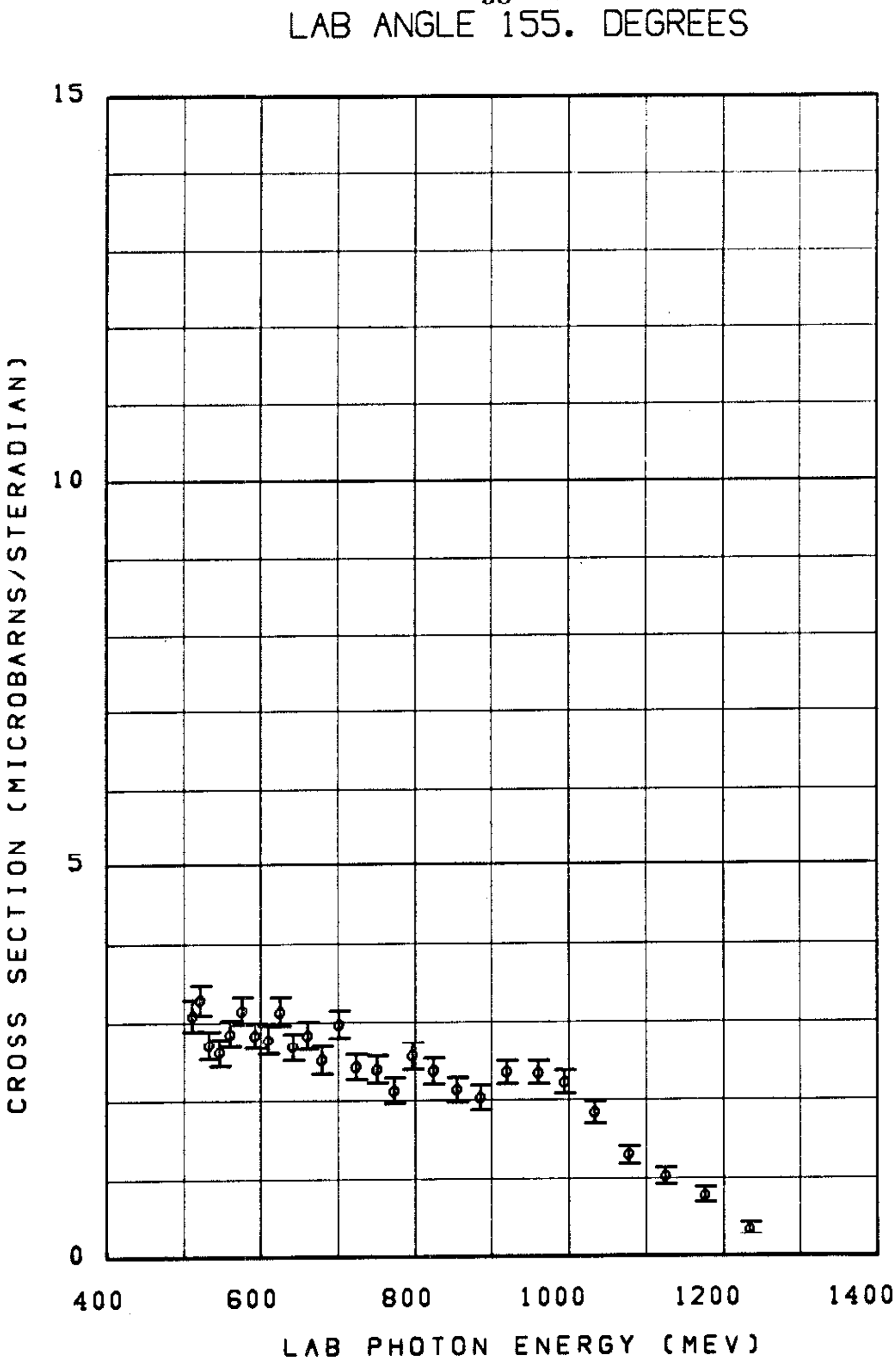
LAB ANGLE 155. DEGREES
15
10
5
0
400
600
800
1000
1200
1400
CROSS SECTION (MICROBARNS/STERADIAN)
LAB PHOTON ENERGY (MEV)

Figure 13 1

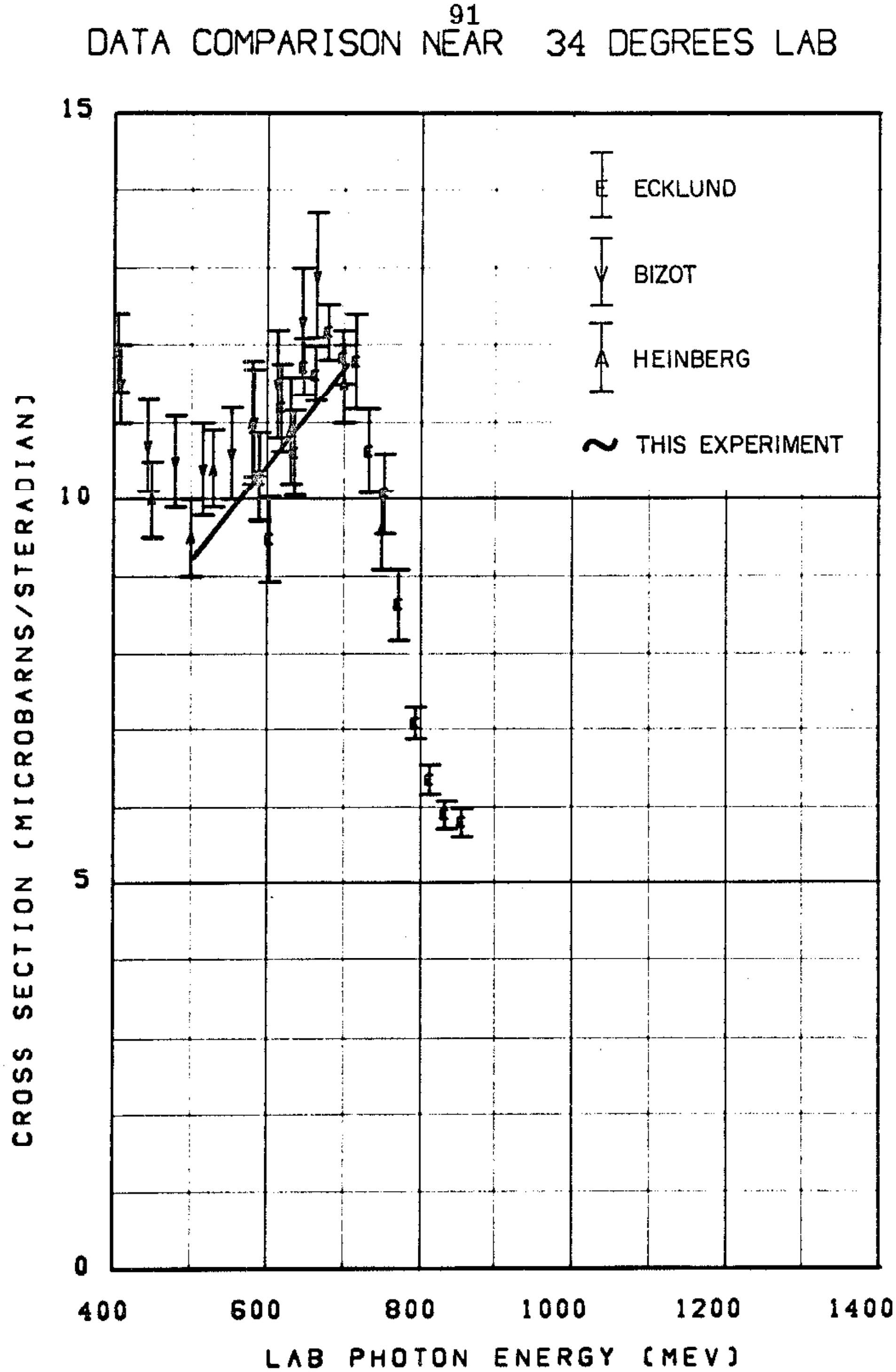
DATA COMPARISON NEAR 34 DEGREES LAB
15
10
5
0
400
600
800
1000
1200
1400
CROSS SECTION (MICROBARNS/STERADIAN)
LAB PHOTON ENERGY (MEV)
ECKLUND
BIZOT
HEINBERG
THIS EXPERIMENT

Figure 13m

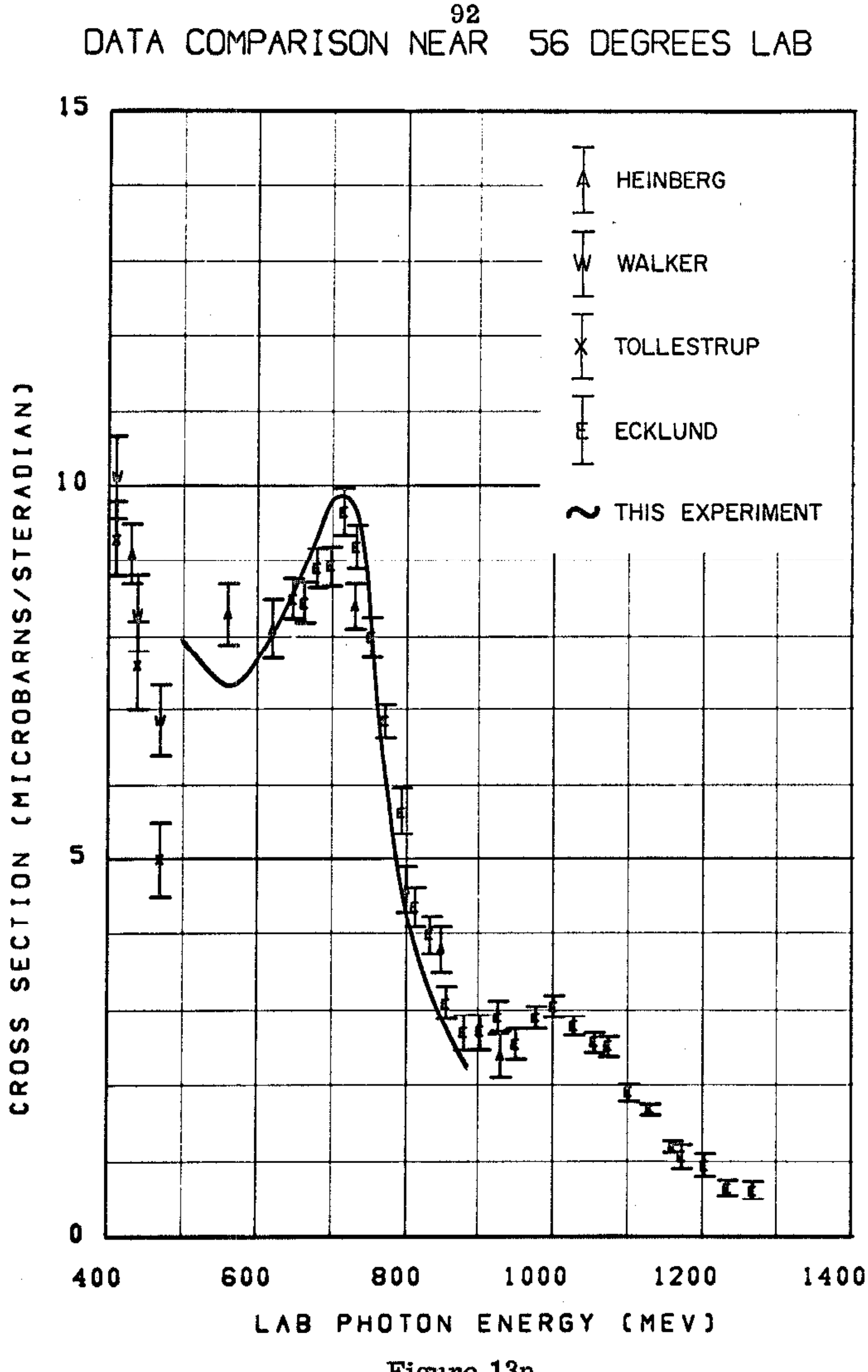
DATA COMPARISON NEAR 56 DEGREES LAB
HEINBERG
WALKER
TOLLESTRUP
ECKLUND
THIS EXPERIMENT
CROSS SECTION (MICROBARNS/STERADIAN)
LAB PHOTON ENERGY (MEV)
0
5
10
15
400
600
800
1000
1200
1400

Figure 13n

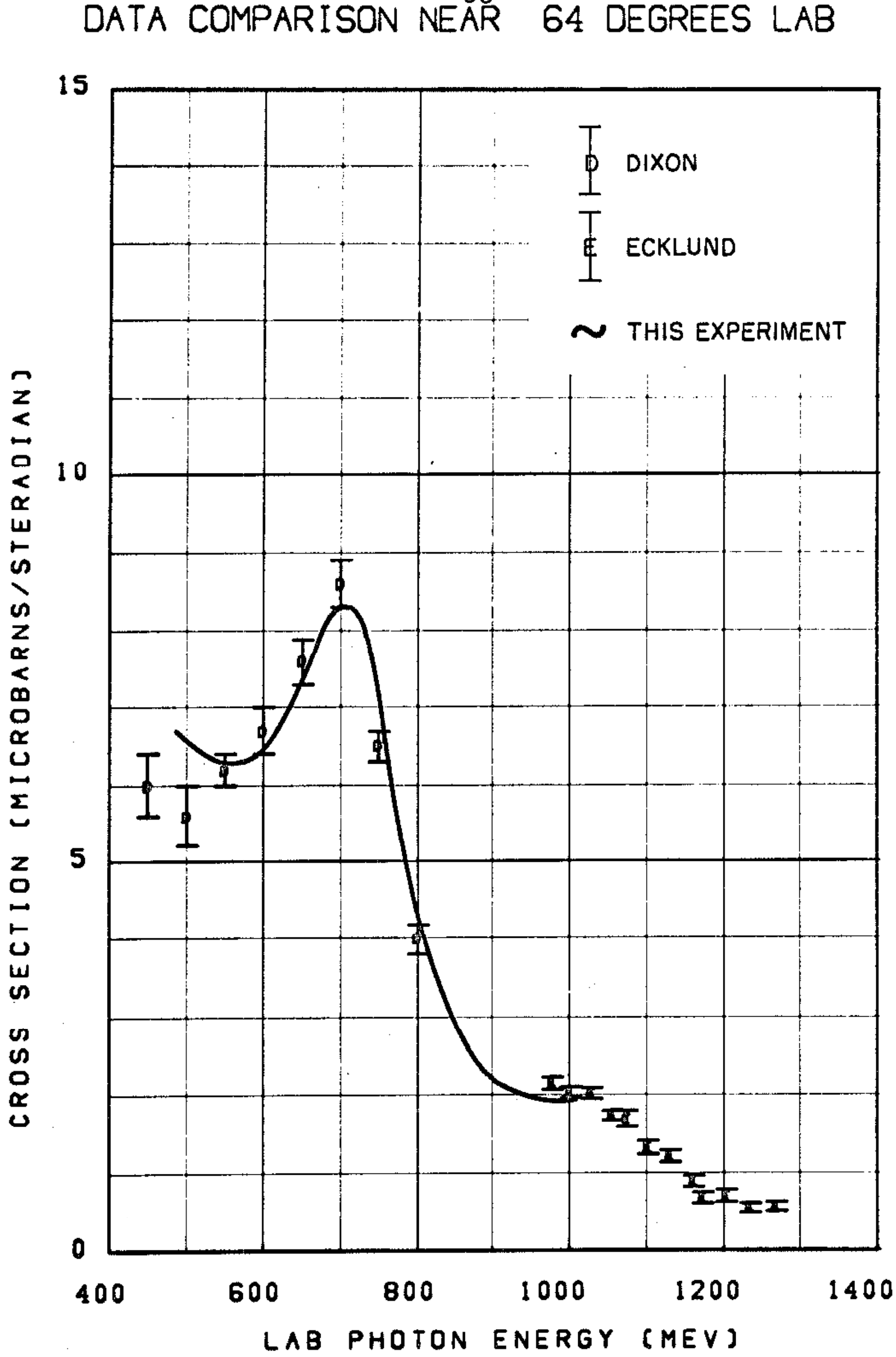
DATA COMPARISON NEAR 64 DEGREES LAB
DIXON
ECKLUND
THIS EXPERIMENT
CROSS SECTION (MICROBARNS/STERADIAN)
15
10
5
0
400
600
800
1000
1200
1400
LAB PHOTON ENERGY (MEV)

Figure 13 o

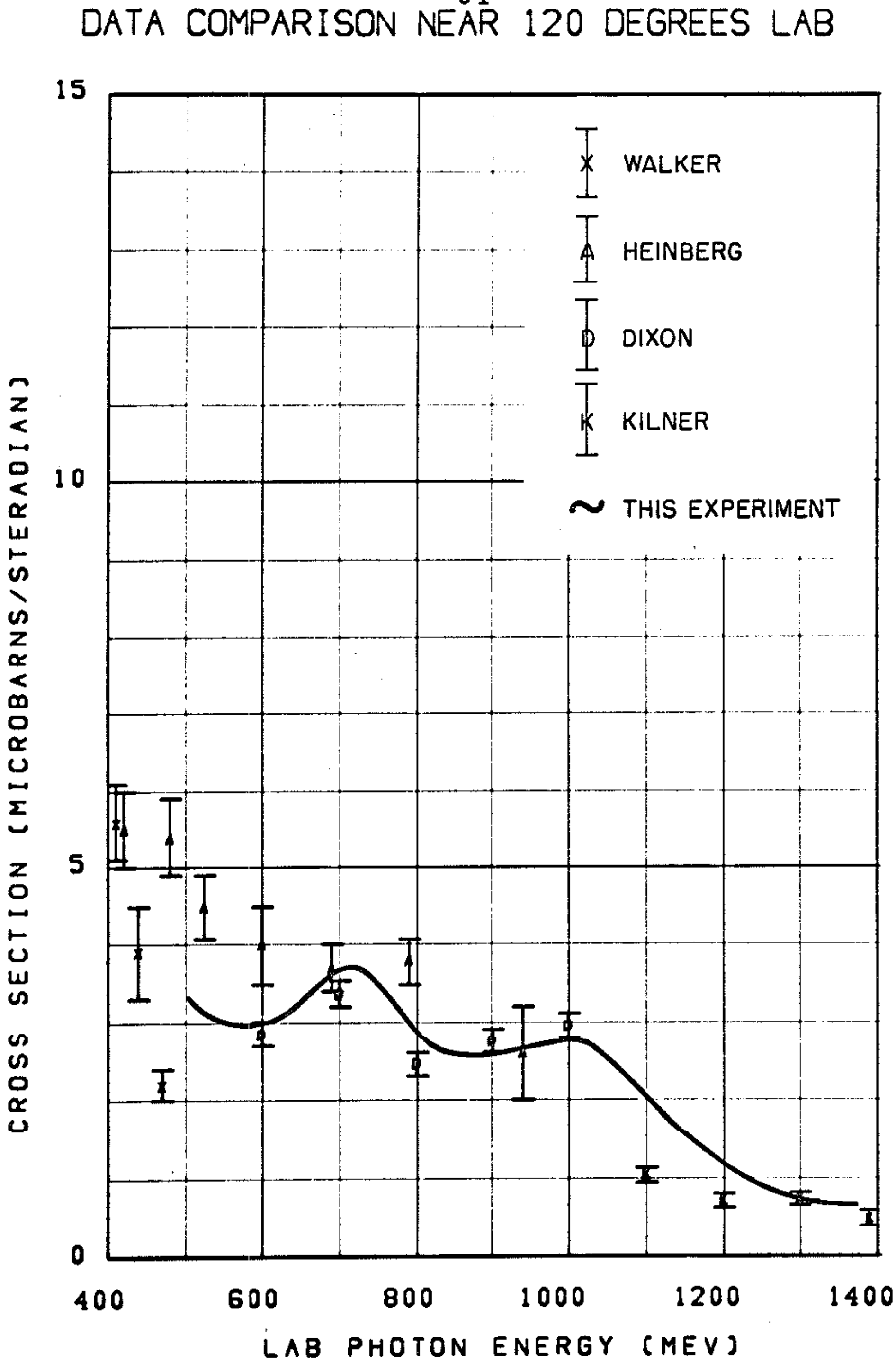
DATA COMPARISON NEAR 120 DEGREES LAB
15
10
5
0
CROSS SECTION (MICROBARNS/STERADIAN)
WALKER
HEINBERG
DIXON
KILNER
THIS EXPERIMENT
400
600
800
1000
1200
1400
LAB PHOTON ENERGY (MEV)

Figure 13p

DATA COMPARISON NEAR 134 DEGREES LAB

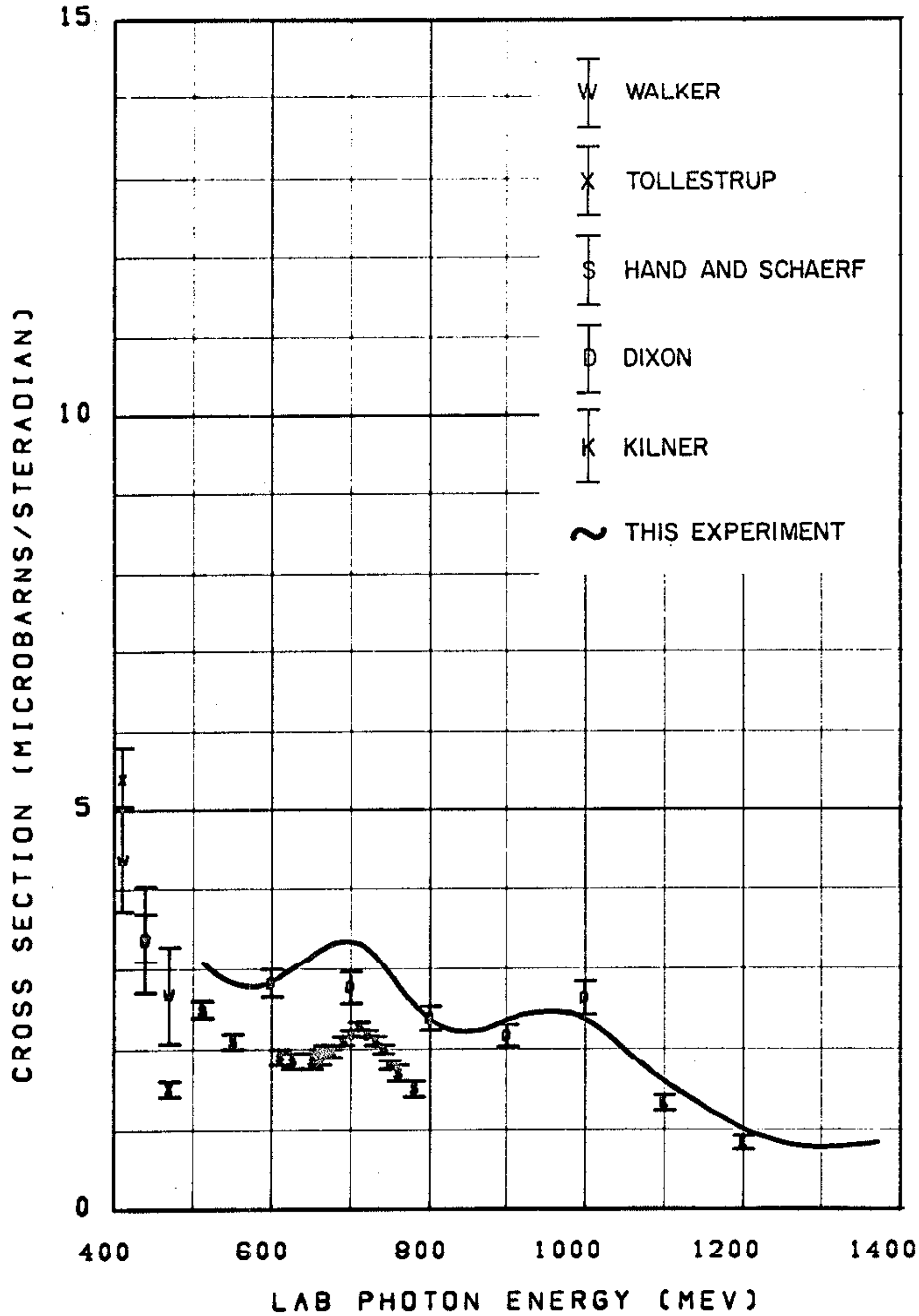

Figure 13q

In general, this experiment agrees with other experiments as well as can be expected. There is excellent agreement with the data of Ecklund and Walker.[9] A detailed comparison of the results in the region of overlap of the two experiments gives a difference of 2.5 ± 2.0%, where the cross sections of this experiment are smaller than those of Ecklund and Walker. This experiment also agrees very well with Dixon and Walker[12] after a small correction is made to interpolate their results to constant lab angle. This experiment is in good agreement with the results of Kilner[13] at 1300 and 1390 MeV, but his data seem to be systematically smaller than the data of this experiment at 1100 MeV and 1200 MeV, especially at 120 degrees in the lab. Since this experiment agrees with Dixon and Walker at 1000 MeV at the same angle and varies smoothly through the region of 1000 to 1350 MeV, it is hard to explain the 30-50% disagreement with Kilner.

An important experimental problem is the matching of this experiment with lower energy experiments near the first resonance. Only two experiments provide any data which overlap both the first and second resonance, namely, the experiments of Heinberg et al.[15] and Bizot et al.[37] The Heinberg data is in agreement with this experiment at 3^o and 58^o in the lab, but the 118^o data are significantly larger near 500 MeV. The data of Bizot et al. at 35^o are approximately 10% larger than the data of this experiment. On the other hand, the two previous experiments at 470 MeV, namely Walker et al.[35] and Tollestrup et al.,[36] gave cross sections systematically 20% to 50% smaller than those of this experiment at ~ 500 MeV. Both of those experiments agree to the order of 10% with other data at 400 MeV and lower. It is possible that their results at 470 MeV were in error because the synchrotron end point energy was very near the photon energy (the synchrotron end point energy was 500 ± 5 MeV for all data taken in both experiments). If the data of Walker and Tollestrup at 470 MeV are ignored, it is possible to draw a smooth curve which passes through the low energy data and the data of this experiment.

There is a serious disagreement between this experiment and the experiment of Hand and Schaerf.[16] This experiment reproduced the energy dependence of the cross section measured by Hand and Schaerf at 135° lab, but their data are systematically 30% smaller. Since these authors assumed that no muons were counted in their apparatus, a correct treatment of the decay correction is likely to make the discrepancy as large as 40% - 50%. Hand and Schaerf estimate their systematic errors to be less than 25%. A portion of the experiment was repeated by Schaerf.[17] The new results agreed with the old to the order of 5%, and again Schaerf estimated his systematic errors to be on the order of 20%. Because the results of this experiment are larger than those of Hand and Schaerf, the possibility exists that an undetected background is included in our data. However, the excitation curve measured at 134° indicates that the background is 1.0 ± 1.0% (see Section IV-D). Thus, we conclude that Hand and Schaerf made a beam monitoring or magnet calibration error, and that their data should be multiplied by the factor 1.5 to get an absolute cross section which agrees with this experiment.

E. Angular Distributions by Interpolation

For some purposes, angular distributions of the cross section are more useful than data in the form of energy distributions at constant angle. A set of angular distributions was obtained by linear interpolation in the data of Table 7a - 7e. The energies chosen were the nominal energies of Stan Ecklund's angular distributions[9], with a few additional energies below 589 MeV. For the lowest and highest energies, the interpolated data may represent an extrapolation of the measured data. However, no data were used which came from an extrapolation of more than 20 MeV. The error bars on the interpolated data were arbitrarily taken to be equal to the error bars on the nearest measured point. The interpolated angular distributions are presented in Tables 8a - 8d.

TABLE 8a - 8d

Interpolated Angular Distributions

THETA	is the c. m. pion angle in degrees
SIGMA	is the c. m. differential cross section in microbarns per steradian
DSIGMA	is the statistical error associated with SIGMA in microbarns per steradian
K	is the laboratory photon energy in MeV
W	is the total center of mass energy in MeV

TABLE 8a

INTERPOLATED ANGULAR DISTRIBUTIONS

K= 490.
W= 1342.

THETA*	SIGMA	DSIGMA
48.3	11.029	0.289
66.4	9.775	0.421
85.3	6.128	0.287
96.1	5.620	0.363
106.2	4.605	0.258
137.7	3.565	0.216
163.5	2.740	0.196

K= 510.
W= 1355.

THETA*	SIGMA	DSIGMA
48.7	9.609	0.289
56.7	9.935	0.445
66.9	8.706	0.395
76.6	8.584	0.357
85.8	6.673	0.284
96.6	5.841	0.346
106.7	4.431	0.237
126.7	3.756	0.228
138.0	3.477	0.200
163.6	3.088	0.196

K= 530.
W= 1369.

THETA*	SIGMA	DSIGMA
49.1	9.273	0.275
57.1	9.701	0.445
67.3	8.212	0.389
77.1	7.589	0.357
86.3	6.364	0.263
97.2	5.432	0.337
107.2	4.274	0.213
116.6	4.209	0.254
127.1	3.722	0.223
138.4	3.286	0.191
148.9	3.437	0.167
163.7	2.881	0.190

K= 550.
W= 1383.

THETA*	SIGMA	DSIGMA
49.5	9.909	0.271
57.5	8.884	0.408
67.8	7.935	0.406
77.6	7.139	0.339
86.8	6.319	0.260
97.7	5.285	0.270
107.7	4.305	0.202
117.1	3.745	0.248
127.5	3.136	0.206
138.7	2.853	0.178
149.1	2.768	0.167
163.9	2.674	0.172

K= 570.
W= 1396.

THETA*	SIGMA	DSIGMA
49.9	9.920	0.293
58.0	9.126	0.392
68.3	8.471	0.411
78.1	7.200	0.324
87.4	6.224	0.205
98.2	5.316	0.261
108.2	4.244	0.199
117.5	3.401	0.228
127.9	3.475	0.194
139.0	2.930	0.187
149.4	2.826	0.158
164.0	3.038	0.172

K= 589.
W= 1409.

THETA*	SIGMA	DSIGMA
50.2	10.690	0.287
58.4	9.358	0.438
68.7	8.233	0.404
78.6	7.369	0.317
87.8	6.689	0.198
98.6	5.225	0.250
108.7	4.295	0.185
118.0	4.159	0.236
128.3	3.419	0.209
139.4	2.605	0.192
149.6	2.938	0.158
164.2	2.888	0.172

K= 603.
W= 1418.

THETA*	SIGMA	DSIGMA
50.5	10.366	0.287
58.7	10.468	0.442
69.1	9.028	0.412
78.9	7.533	0.277
88.2	6.277	0.191
99.0	5.278	0.250
109.0	4.419	0.194
118.3	4.096	0.236
128.5	3.506	0.219
139.6	3.295	0.201
149.8	3.009	0.154
164.2	2.801	0.185

K= 618.
W= 1428.

THETA*	SIGMA	DSIGMA
50.8	10.448	0.382
59.0	9.439	0.415
69.4	8.896	0.482
79.3	8.144	0.283
88.5	6.705	0.188
99.3	5.525	0.244
109.3	4.662	0.194
118.6	4.142	0.232
128.8	3.410	0.219
139.8	2.962	0.201
150.0	2.872	0.151
164.3	2.980	0.185

K= 635.
W= 1439.

THETA*	SIGMA	DSIGMA
51.1	10.671	0.382
59.3	10.125	0.427
69.8	10.508	0.517
79.7	7.753	0.275
89.0	7.347	0.243
99.8	5.712	0.227
109.7	4.819	0.252
118.9	4.095	0.232
129.2	3.482	0.198
140.1	3.184	0.188
150.2	2.761	0.175
164.5	2.874	0.183

K= 647.
W= 1447.

THETA*	SIGMA	DSIGMA
51.3	10.439	0.379
59.6	9.944	0.407
70.1	9.710	0.496
80.0	8.270	0.275
89.2	7.117	0.243
100.0	5.868	0.226
110.0	5.348	0.261
119.2	4.322	0.234
129.4	3.736	0.204
140.3	3.030	0.188
150.3	2.986	0.175
164.5	2.732	0.176

K= 663.
W= 1458.

THETA*	SIGMA	DSIGMA
51.6	10.885	0.365
59.9	11.018	0.391
70.4	9.566	0.482
80.3	8.707	0.385
89.6	7.285	0.243
100.4	6.370	0.227
110.4	5.380	0.261
119.5	4.657	0.234
129.7	3.849	0.204
140.5	3.315	0.191
150.5	3.223	0.178
164.6	2.790	0.176

K= 680.
W= 1468.

THETA*	SIGMA	DSIGMA
52.0	11.948	0.370
60.3	11.389	0.382
70.8	10.572	0.489
80.7	9.065	0.395
90.0	7.947	0.243
100.8	6.894	0.231
110.7	5.662	0.256
119.9	4.982	0.245
130.0	3.958	0.208
140.8	3.565	0.210
150.7	3.279	0.182
164.7	2.517	0.176

INTERPOLATED ANGULAR DISTRIBUTIONS

K= 698.
W= 1480.

THETA*	SIGMA	DSIGMA
52.3	11.417	0.370
60.6	11.336	0.374
71.2	10.772	0.469
81.2	9.334	0.398
90.4	8.268	0.252
101.2	6.778	0.231
111.1	5.893	0.256
120.2	5.261	0.245
130.3	4.601	0.268
141.0	3.788	0.217
150.9	3.593	0.182
164.9	2.912	0.177

K= 715.
W= 1491.

THETA*	SIGMA	DSIGMA
61.0	11.353	0.377
71.6	10.155	0.300
81.5	9.095	0.398
90.8	8.318	0.252
101.6	7.652	0.225
111.5	6.315	0.259
120.6	5.235	0.263
130.6	4.885	0.268
141.3	3.894	0.217
151.1	3.463	0.177
165.0	2.641	0.177

K= 733.
W= 1502.

THETA*	SIGMA	DSIGMA
61.3	9.148	0.377
72.0	9.843	0.291
81.9	9.544	0.380
91.2	8.007	0.268
102.0	6.805	0.211
111.9	5.907	0.259
120.9	5.467	0.263
130.9	4.589	0.262
141.5	3.709	0.205
151.3	3.107	0.168
165.1	2.419	0.173

K= 752.
W= 1514.

THETA*	SIGMA	DSIGMA
72.4	7.721	0.271
82.4	7.312	0.323
91.7	6.813	0.251
102.4	6.057	0.198
112.2	5.714	0.242
121.3	4.430	0.242
131.2	4.101	0.249
141.8	3.536	0.193
151.5	2.817	0.160
165.2	2.376	0.173

K= 772.
W= 1526.

THETA*	SIGMA	DSIGMA
72.8	6.831	0.235
82.8	6.282	0.258
92.1	5.659	0.237
102.8	5.325	0.186
112.7	5.110	0.241
121.7	4.180	0.229
131.5	3.636	0.223
142.0	3.287	0.182
151.7	2.741	0.156
165.3	2.141	0.173

K= 793.
W= 1539.

THETA*	SIGMA	DSIGMA
73.3	5.096	0.235
83.3	4.898	0.233
92.6	4.513	0.192
103.3	4.755	0.170
113.1	4.187	0.200
122.0	3.869	0.220
131.9	3.549	0.223
142.3	2.485	0.173
151.9	2.425	0.156
165.4	2.486	0.167

K= 813.
W= 1551.

THETA*	SIGMA	DSIGMA
83.7	3.764	0.184
93.0	3.956	0.185
103.7	3.879	0.164
113.5	3.657	0.191
122.4	3.442	0.203
132.2	2.865	0.208
142.6	2.565	0.173
152.1	2.158	0.156
165.5	2.458	0.167

K= 834.
W= 1564.

THETA*	SIGMA	DSIGMA
84.1	3.160	0.167
93.4	3.262	0.169
104.1	3.308	0.166
113.9	3.356	0.175
122.8	3.076	0.194
132.5	2.511	0.189
142.9	2.449	0.198
152.3	2.115	0.146
165.6	2.300	0.157

K= 857.
W= 1577.

THETA*	SIGMA	DSIGMA
84.6	2.430	0.158
93.9	2.656	0.120
104.6	2.740	0.165
114.3	2.906	0.171
123.2	2.886	0.178
132.9	2.706	0.189
143.1	2.534	0.198
152.5	2.294	0.146
165.7	2.131	0.153

K= 880.
W= 1591.

THETA*	SIGMA	DSIGMA
94.4	2.330	0.114
105.1	2.493	0.146
114.7	2.850	0.166
123.6	2.938	0.178
133.2	2.673	0.190
143.4	2.604	0.196
152.8	2.509	0.146
165.8	2.058	0.153

K= 902.
W= 1604.

THETA*	SIGMA	DSIGMA
94.8	2.106	0.101
105.5	2.616	0.146
115.1	2.843	0.172
124.0	3.022	0.178
133.6	2.637	0.190
143.7	2.551	0.186
153.0	2.511	0.146
165.9	2.191	0.153

K= 926.
W= 1618.

THETA*	SIGMA	DSIGMA
95.3	2.088	0.100
105.9	2.598	0.141
115.6	2.939	0.172
124.3	2.988	0.173
133.9	2.811	0.178
144.0	2.576	0.187
153.2	2.504	0.142
166.1	2.361	0.147

TABLE 8c

INTERPOLATED ANGULAR DISTRIBUTIONS

K= 951.
W= 1632.

THETA*	SIGMA	DSIGMA
95.8	2.222	0.100
106.4	2.544	0.141
116.0	2.980	0.164
124.7	2.904	0.174
134.2	2.916	0.178
144.3	2.597	0.187
153.4	2.383	0.142
166.2	2.355	0.147

K= 977.
W= 1647.

THETA*	SIGMA	DSIGMA
96.3	1.904	0.100
106.9	2.703	0.169
116.5	3.076	0.164
125.2	3.619	0.174
134.6	2.859	0.179
144.6	2.668	0.190
153.6	2.193	0.136
166.3	2.295	0.147

K= 1002.
W= 1661.

THETA*	SIGMA	DSIGMA
107.3	2.643	0.169
116.9	3.050	0.162
125.5	3.359	0.174
134.9	2.863	0.180
144.8	2.750	0.190
153.8	2.353	0.136
166.4	2.165	0.147

K= 1028.
W= 1676.

THETA*	SIGMA	DSIGMA
107.8	2.248	0.159
117.3	2.880	0.162
125.9	2.984	0.169
135.3	3.034	0.180
145.1	2.817	0.183
154.0	2.212	0.105
166.5	1.906	0.147

K= 1056.
W= 1692.

THETA*	SIGMA	DSIGMA
108.3	1.840	0.142
117.8	2.306	0.143
126.4	2.485	0.155
135.6	2.705	0.180
145.4	2.449	0.183
154.3	1.931	0.096
166.6	1.565	0.134

K= 1074.
W= 1702.

THETA*	SIGMA	DSIGMA
108.6	1.569	0.131
118.1	1.877	0.143
126.6	2.149	0.120
135.9	2.386	0.180
145.6	2.213	0.155
154.4	1.791	0.096
166.7	1.334	0.134

K= 1102.
W= 1717.

THETA*	SIGMA	DSIGMA
109.1	1.138	0.118
118.5	1.265	0.094
127.0	1.650	0.107
136.2	1.713	0.133
145.9	1.862	0.155
154.6	1.524	0.089
166.8	1.156	0.115

K= 1131.
W= 1733.

THETA*	SIGMA	DSIGMA
109.6	0.704	0.122
119.0	0.881	0.082
127.4	1.041	0.107
136.6	1.252	0.113
146.1	1.640	0.146
154.8	1.207	0.077
166.9	1.002	0.100

K= 1162.
W= 1749.

THETA*	SIGMA	DSIGMA
110.1	0.641	0.122
119.4	0.610	0.073
127.8	0.775	0.092
136.9	1.029	0.098
146.4	1.434	0.133
155.1	1.079	0.077
167.1	0.863	0.100

K= 1174.
W= 1756.

THETA*	SIGMA	DSIGMA
110.3	0.617	0.122
119.6	0.496	0.073
128.0	0.702	0.079
137.1	1.017	0.098
146.6	1.327	0.133
155.1	1.029	0.077
167.1	0.809	0.100

K= 1204.
W= 1772.

THETA*	SIGMA	DSIGMA
120.0	0.419	0.065
128.4	0.615	0.079
137.4	1.012	0.093
146.8	1.069	0.114
155.3	1.046	0.073
167.2	0.592	0.090

K= 1235.
W= 1788.

THETA*	SIGMA	DSIGMA
120.5	0.392	0.062
128.8	0.578	0.075
137.8	1.020	0.090
147.1	0.829	0.114
155.6	1.074	0.073
167.3	0.359	0.090

TABLE 8d

INTERPOLATED ANGULAR DISTRIBUTIONS

THETA*	SIGMA	DSIGMA	THETA*	SIGMA	DSIGMA	THETA*	SIGMA	DSIGMA
K= 1269.								
W= 1806.								
120.9	0.372	0.062						
129.2	0.550	0.077						
138.1	0.834	0.090						
147.4	0.777	0.117						
155.8	0.923	0.073						

F. Summary of Experimental Errors

The random and rapidly fluctuating errors which have been included in the error bars of all cross sections are as follows:

Counting Statistics	3-5%
Irreproducibility of Runs (see Appendix VI)	1.65%
Negative Field Background	0-5%
Unfolding Process	1%

The systematic errors are estimated in the table below (errors of less than ± 0.5% have been ignored). These errors are to be interpreted in the sense of standard deviations.

Quantameter Calibration[21]	3%
Nuclear Absorption	1.5-3%
Bremsstrahlung Spectrum[30]	2%
Pi-Mu Decay Correction	1%
Liquid Hydrogen Target	1%
Electronic Efficiency	1%
Total Energy Per BIP	0.6%
Total	4-5%

G. Data Fitting

The most important problem to be solved in data fitting is the multipole and isotopic spin decomposition of the photoproduction amplitudes. Stan Ecklund and Carl Clinesmith are presently working on this problem and are using independent methods. Stan Ecklund is using only π^+ cross section data and has fit the angular distributions with a Moravcsik type formula. Then he is attempting to explain the coefficients of the Moravcsik fits with simple functions of energy.[9] Carl Clinesmith is attempting to fit all the data available for all the isotopic spin channels by assuming that the multipole coefficients are either Breit-Wigner forms or slowly varying functions of energy.[10] Since both of these projects are near completion, it is difficult to make a direct contribution to the fitting without also duplicating a large part of the effort.

Rather than work directly on the overall fitting project, an effort was made to explain a striking feature of the π^+ cross section at 180° which was observed by Hand and Schaerf[16] and later repeated by Schaerf.[17] The important characteristic of this cross section is that there is a very narrow bump at a photon energy of approximately 710 MeV (W = 1490 MeV). On the basis of evidence from the forward π^0 photoproduction cross section, D. Beder[38] concluded that the ratio $E_{2-}/M_{2-} \approx 3$ in the vicinity of the second resonance (N**(1512), k_γ = 750 MeV) which causes the contribution of the second resonance to the photoproduction amplitudes to be small at 0° and 180°. An extrapolation of the π^+ data of Ecklund and Walker to 0° gives the same conclusion.[9] Theoretically Bietti[1] has used saturated sum rules to derive the same result. Thus we expect that the second resonance does not contribute to the bump at 180° in the π^+ cross section.

Sakurai[39] suggested that the bump might be a cusp effect at the threshold for production of the eta meson (W = 1487 MeV, k_γ = 708 MeV). Since the differential cross section for single π^+ photoproduction is smallest at 180^o for energies near 700 MeV, it is possible that a small cusp in the S_{11} or P_{11} (first index = 2T, second index = 2J) part of the photoproduction amplitude would show up most at 180^o.

The most extensive measurements of the eta production reaction come from the experiments of Bulos et al. [40] and Richards et al. [41] These experiments show that the eta production angular distribution is isotropic near threshold, which indicates that either the S_{11} or the P_{11} states dominate. When the total cross section is plotted as a function of energy, the first three points fall on a straight line which also passes through the threshold. From this fact, Richards et al. conclude that the S_{11} state is dominant.

An examination of the results of several recent partial wave analyses[4, 6, 7, 8] of π-N elastic scattering shows that the S_{11} absorption parameter, η_{11}, is consistent with 1.0 (no absorption) below the eta threshold, but that it drops rapidly to approximately 0.5 shortly above threshold. The reaction cross section computed from the S_{11} absorption parameter is consistent with the total cross section for eta production. [41] In addition, at least two authors show a cusp behavior in the S_{11} phase shift. [4, 8] On the basis of this evidence, we may conclude that a cusp at the eta threshold has been observed in S-wave π-N scattering and that the photoproduction data should be analyzed in terms of the same phenomenon.

The R matrix formalism of Wigner[42] has been applied to the production of strange particles in π-N and γ-N interactions by Adair. [43] With only negligible changes, this formalism may be used for the production of eta mesons in the same interactions. If we assume that the absorption in the S_{11} π-N state is due to eta production (and a small contribution from inverse photoproduction), we may use a three channel S matrix for total angular momentum 1/2, I spin 1/2, odd parity scattering where the three channels are π-N, η-N, and γ-N. Since a nucleon appears in each channel, we may simplify the notation by labelling the three channels, π, η, and γ. Near the eta threshold the S matrix may be written in the form

$$S_{if} = e^{+i\,k_i a_i} (\delta_{if} - N_{if}/D)\, e^{+i\,k_f a_f}$$

where

$$N_{if} = -2i \sqrt{k_i\, P_i\, R_{ii}\, R_{ff}\, P_f\, k_f}$$

$$D = 1 - i\,k_\pi R_{\pi\pi} - i\,k_\eta R_{\eta\eta} - i\,k_\gamma R_{\gamma\gamma}$$

k_i = center of mass momentum of i^{th} channel with the convention that k is positive imaginary below threshold

a_i = the channel radius for channel i

$$P_i = \begin{Bmatrix} 1 & \text{above threshold in channel } i \\ 0 & \text{below threshold in channel } i \end{Bmatrix}$$

and we may take the elements of the R matrix to be independent of energy. The total cross section may be written in the form

$$\sigma_{\pi f} = \frac{\pi}{k_\pi^{\,2}} \left| \delta_{\pi f} - S_{\pi f} \right|^2$$

and

$$\sigma_{\gamma f} = \frac{\pi}{3k_{\gamma}^{2}} \left| \delta_{\gamma f} - S_{\gamma f} \right|^{2}$$

The parameters of this formalism may be adjusted to fit the S_{11} phase shift and absorption parameter, and the eta photoproduction reaction cross section. Because of the inconsistencies of the phase shifts and absorption parameters determined by different authors, the high accuracy of a computer fit to the data is not worthwhile at the present time. However, a hand fit was made. For the purposes of this fit, the absorption parameter was assumed to be 0.5 at a pion kinetic energy (lab) of 660 MeV. The parameters were adjusted to satisfy this condition and to give a reasonable fit to the S_{11} phase shift data of Cence[(8)] and the eta photoproduction data from Stanford.[(44)] The resulting parameters were ($\hbar = c = 1$)

$$R_{\pi\pi} = 2.096 \quad GeV^{-1}$$

$$R_{nn} = 3.699 \quad GeV^{-1}$$

$$R_{\gamma\gamma} = 0.019 \quad GeV^{-1}$$

$$a_{\pi} = 0.200 \quad GeV^{-1}$$

$$a_{\gamma} = 0.000 \quad GeV^{-1}$$

In order to fit the π^{+} photoproduction data at 180^{o}, it was necessary to make some assumption about the other contributions to the photoproduction amplitude. The simplest assumption was that this background was pure imaginary (pure real in the usual convention of perturbation theory). A constant background of + 0.66(μ barn)$^{1/2}$ gives the best fit to the corrected Schaerf data[17] in the region of the cusp (see Section V-D for the correction to the Schaerf data). The fit and the data for the several reactions are presented in Figures 14a and 14b. The branching ratio for $\eta \rightarrow 2\gamma$ was assumed to be 0.35 in drawing these figures.

The fit to the eta production and eta photoproduction data has the difficulty that it rises too rapidly near threshold. This problem appears to be common to several theories which neglect other open channels.[45, 46, 47] Moorhouse and Hendry[48] have shown that it is possible to correct this problem by including approximately the multiple pion production channels. However, the fit to the 180 degree π^+ photoproduction differential cross section has the property that it gives a good fit to the shape of the cusp for photon energies within $\pm$ 50 MeV of the eta threshold.

The conclusion derived from this fit is that it is possible to explain the π^+ photoproduction differential cross section at 180 degrees in terms of a cusp at the eta threshold, and that this interpretation is consistent with present data on pion scattering, eta production, and eta photoproduction. This interpretation removes a possible difficulty with the assumption that $E_{2-}/M_{2-} = 3$ in the vicinity of the second resonance.

On the basis of pion scattering and eta production data, several authors have made conclusions about the source of the cusp.[46, 47, 48] These authors conclude that there is an eta-nucleon state at approximately the eta nucleon threshold (1487 MeV). This state should be called a resonance if the mass of the "particle" is greater than the threshold, or a virtual bound state if the mass is

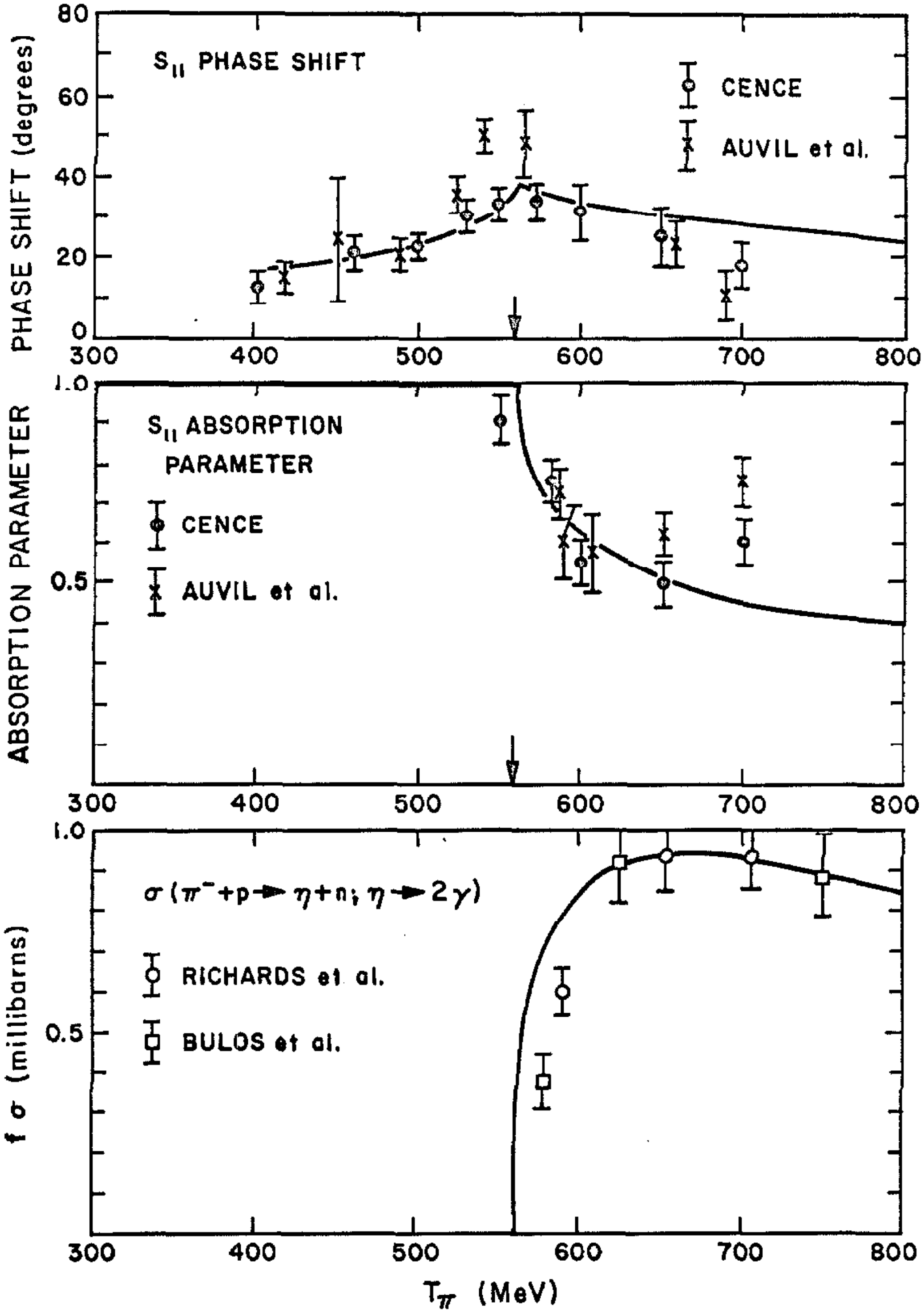

Figure 14a. Cusp Fit to π-N Channel

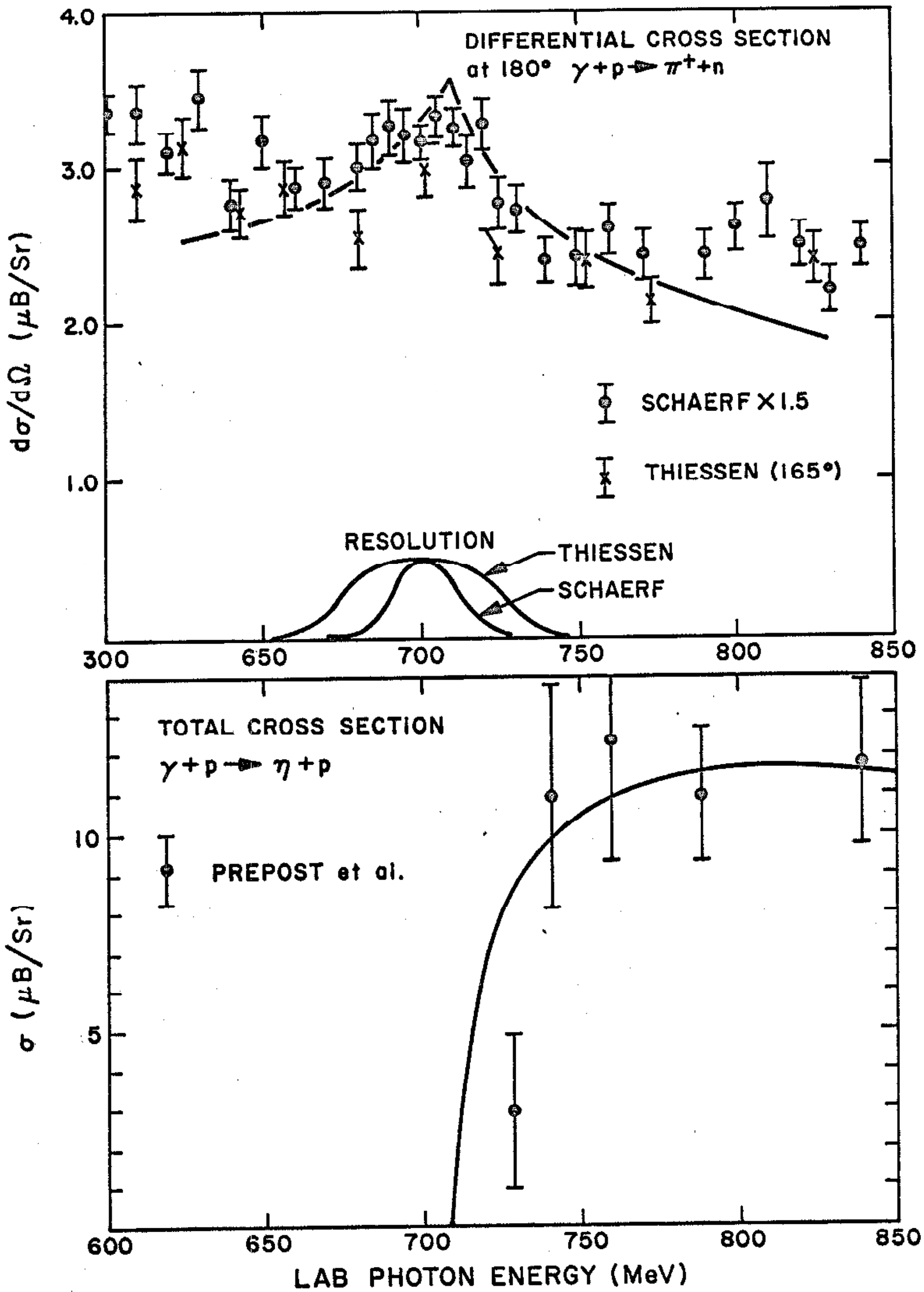

Figure 14b. Cusp Fit to Photoproduction

less than threshold. This particle has been speculatively identified[48] with the $\tilde{N}$ particle of the η-baryon octet $B = (\tilde{N}, \tilde{\Lambda}, \tilde{\Sigma}, \tilde{\Xi})$ postulated by Gyuk and Tuan.[49] Further data on π-N scattering and eta production are required before the mass of this state can be determined accurately.

VI. CONCLUSIONS AND SUGGESTIONS

A large number of points of the differential cross section for π^+ photoproduction at backward angles were measured in this experiment. When combined with the data of Ecklund and Walker[9], reasonably complete angular distributions are available for all energies between 589 MeV and 1269 MeV. These data can be used to make a considerable improvement in the precision of the phenomenological analysis of pion photoproduction in the region of the second and third π-N resonances. Because of operational difficulties with the synchrotron, it was not possible to continue the experiment into the region of the first resonance which has been measured carefully. Thus a similar experiment should be performed covering the energy region from approximately 350 MeV to 650 MeV. It may be necessary to do this experiment at a different accelerator: the Mark III Linac at Stanford University is a logical choice.

In order to obtain a unique multipole and isotopic spin decomposition of the photoproduction amplitudes, it will be necessary to take cross section and polarization data on the other pion photoproduction reactions. The most direct way to start on this program would be to measure the differential cross section for the reaction $\gamma + n \rightarrow \pi^- + p$ using a deuterium target. A synchrotron subtraction might be used to separate the events coming from free neutrons. With careful planning, it would be possible to take data with both magnets simultaneously. It should be emphasized that absolutely no apparatus changes are required to perform this experiment! Later, a carbon plate spark chamber might be added to measure the recoil proton polarization as an extension of the same experiment.

If a polarized proton target with the order of 20% polarized, free protons can be developed, it would be possible to measure the polarized target asymmetry in the reaction $\gamma + p \rightarrow \pi^+ + n$. A synchrotron subtraction would be required to separate the events due to free protons.

Another interesting experiment would be to extend the π^+ differential cross section measurements to exactly 180°. However, this experiment would require significant changes in the magnet and beam line geometry. Since some data are already available, this experiment should be assigned a lower priority than the previously suggested experiments.

Two improvements in the apparatus would prove to be useful. First, an electron counter could be installed. Such a counter might reduce the field reversed background which was as much as 10% at high energies. Second, the paper tape punch might be replaced with an on-line link to the campus IBM 360 series computers. Including the price of a remote console (with typewriter input-output), the design and construction cost of the required hardware would be on the order of $4000. Such a data link would reduce the turn around time for data processing from several days to a few minutes, and experimental errors would be more easily detected. In addition, the reliability of the system would be significantly improved by eliminating the mechanical tape punch and the paper tape to magnetic tape conversion system.

APPENDIX I. BEAM MONITORING AND HYDROGEN TARGET DETAILS

The several beam monitors used during this experiment include the quantameter, the beam catcher thick ion chamber, two thin ion chambers, a counter telescope mounted at 90^{0} from the beam line under the hydrogen target, and the "40 mc. probe" which monitored the intensity of the circulating beam. The locations of these monitors are shown in Figure 1.

The charge produced by each ion chamber was measured with the standard electronic integrators used in this laboratory for many years. Each time a specified amount of charge has been collected, these integrators put out a pulse called a BIP (beam integrator pulse) and this pulse is usually used to operate a Sodeco mechanical counter. Unfortunately, the generation of the output pulse and the determination of the amount of charge per BIP depend on two relays. If either of these relays chatter or the contacts get dirty, it is possible to get a wrong charge/BIP ratio. For this reason, it is important to use several beam monitors even if the beam monitors themselves are stable. The output of the 40 mc. probe is monitored by a voltage-to-frequency converter and the result is counted on an electronic scaler. The counter telescope output is also counted on an electronic scaler. No difficulties with the readout mechanism for either of these beam monitors was observed.

The normalization of this experiment depends on the quantameter charge output. However, the quantameter cannot be left in the beam line during a data taking run as it absorbs all the energy in the beam. It is not possible to place the quantameter in the beam catcher since the beam spot is too large at that location. Thus this experiment also depends on an intercalibration with secondary monitors.

The beam monitors which can be directly intercalibrated with the quantameter are the 40 mc. probe and the two thin ion chambers. Unfortunately, the charge collected by thin chamber No. 2 was strongly dependent on the status of the UCLA hydrogen target. In addition, the integrator used with this ion chamber was found to be very unstable. After a short trial period, the use of this ion chamber was discontinued. The two remaining monitors, TC-1 and the 40 mc. probe, were intercalibrated against the quantameter in a short run before and after each data taking run.

The monitors which are available only during a data taking run are the monitor telescope and the beam catcher ion chamber. The beam catcher ion chamber should be as good as the quantameter, except that its calibration depends on the energy of the synchrotron. In addition, the beam catcher ion chamber is not available when the yoke of the High Energy Magnet is in the beam line. Since the beam catcher ion chamber and the quantameter are never available simultaneously, the same integrator was used for both. Thus the ratio Q/BC is independent of slow drifts in the integrator. The monitor telescope has also been demonstrated to be stable. Unfortunately, the monitor telescope was operated from the High Energy Magnet Electronics. Since Mr. F. Wolverton was constantly testing and changing the electronics and turning the power supplies on and off, keeping the monitor telescope calibrated proved to be a tedious chore and its use was eventually discontinued. The monitor telescope probably should be set up as a lab instrument and made to be independent of the transistor power supplies for either magnet.

The procedure used to calculate the number of quantameter BIPs was to calibrate the 40 mc. probe and TC-1 against the quantameter in a short run before and after each data taking run. The average ratios $\langle Q/40\ \text{mc.}\rangle$ and $\langle Q/TC\text{-}1\rangle$ were calculated from these short calibration runs. The number of quantameter BIPs based on each of these intermediate monitors was calculated from these average ratios and the number of TC-1 and 40 mc. BIPs obtained in the data run, i. e.

$$Q40 = 40\ \text{mc.} \times \langle Q/40\ \text{mc.}\rangle$$

$$QTC = TC\text{-}1 \times \langle Q/TC\text{-}1\rangle$$

The beam catcher ion chamber could be intercalibrated against the quantameter only by comparing BC with Q40 and QTC. This intercalibration was done for each night's running by comparing the total BC for a night with the average of Q40 and QTC. The formula used was

$$\langle Q/BC\rangle = \frac{\Sigma(Q40 + QTC)}{2\Sigma\ BC}$$

where the sum represents the normal data runs taken during one night. Then the number of quantameter BIPs for each run was computed using BC and the average ratio given above, namely

$$QBC = BC \times \langle Q/BC\rangle$$

Finally, the number of quantameter BIPs for a given run was calculated from the average of Q40, QTC, and QBC. This final value, QAVG, was used for all cross section calculations.

This complicated averaging procedure had the advantage that a gross error in one of the monitors was easily detected. When an error of more than ~ 2% was detected, the suspected number was ignored and QAVG was recomputed using all the remaining information. Similarly, QBC was ignored when the High Energy Magnet was in the beam line. By using this technique, the r. m. s. deviations of the individual monitors from QAVG were ± 0.5%, except at E_o = 1350 MeV where ± 1.0% was observed. These errors are presumably already included in the random error deduced from a series of plexiglass target runs (see Appendix VI), and this error was included in the error bars on all cross sections measured in this experiment.

The ratio of Q/BC observed at several energies in this experiment may be of use to future experiments. These ratios are given in the following table:

E_o (meter)	Q/BC
660	11.32 ± 0.07
750	11.18 ± 0.07
850	11.35 ± 0.07
950	11.67 ± 0.07
1050	11.64 ± 0.07
1150	11.79 ± 0.07
1350	12.07 ± 0.12

The quantameter calibration constant, U_Q, is given by the relation

$$U_Q = (4.80 \pm 0.14) \times \frac{2.730}{P/T} \times 10^{18} \text{ MeV/coulomb}^{(21)}$$

where P and T are the absolute pressure and absolute temperature of the quantameter gas in mm. Hg. and ^{0}K respectively. The P/T ratio appears to fluctuate by $\pm$ 0.5% r. m. s. and, in addition, a gradual drop was observed. The random fluctuation may be due to non-equilibrium thermal effects (see separate report).[(50)] The typical quantameter gas pressure was 715 mm. Hg. which was well below atmospheric pressure. Thus the gradual drop must be due to an absorption or selective leakage process which has never been understood. In any case, the P/T value for the first period of data taking (run no. $\leq$ 700) was 2.445 $\pm$ 0.010, while during the second period of data taking (run no. $\geq$ 701) the ratio of P/T was 2.413 $\pm$ 0.010. Integrator No. 0628 was always used with the quantameter. For some early data (run no. $\leq$ 407), the integrator was used on scale 3 with a charge/BIP ratio of $2.225 \pm 0.005 \times 10^{-7}$ coulomb/BIP. For all later data, the integrator was operated on scale 4 with a charge/BIP ratio of $2.235 \pm 0.005 \times 10^{-6}$ coulomb/BIP. The resulting values for the total energy per QBIP are given in the following table.

Run Number	Total Energy/QBIP
000-407	$(0.1192 \pm 0.0007) \times 10^{13}$ MeV/QBIP
408-700	$(1.198 \pm 0.007) \times 10^{13}$ MeV/QBIP
701-1348	$(1.214 \pm 0.007) \times 10^{13}$ MeV/QBIP

The liquid hydrogen is contained within an 0.005" wall Mylar cylinder approximately 3" in diameter. On September 24, 1965, this cup was accidentally broken during the normal cleaning process (no liquid hydrogen was in the target at the time). The Mylar cup was replaced by a new one which was approximately the same diameter. The cup diameter was measured by Mr. Earl Emery at room temperature with a 15 psi pressure on the inside of the cup. The results for the two cups are:

run number $\leq$ 700	3.003 $\pm$ 0.005" diameter
run number $>$ 700	2.980 $\pm$ 0.005" diameter

The diameter of the cup must be reduced by 0.4% to correct for the contraction of the Mylar at liquid hydrogen temperature.[51]

The liquid hydrogen in the cup is operated at the boiling point and a pressure of 0.5 psi is maintained by a safety check valve. Under these conditions, the hydrogen temperature is 20.30°K[52] and its density is 0.0711 gm/cm^3.[53] Since the "empty" target runs were taken with hydrogen gas at the same temperature and pressure, the gas density of 0.0014 gm/cm^3 [52] must be subtracted from the liquid hydrogen density to give an effective density of 0.0697 gm/cm^3.

The number which is used in the cross section calculation is N_H, the number of protons per cm^2 in one diameter of the hydrogen target. Taking Avogadro's number to be 6.025×10^{23} the atomic weight of hydrogen to be 1.008 (which assumes that the deuterium contamination in the liquid hydrogen is small), and the target parameters discussed above, we find that N_H is

$$N_H = \begin{cases} 3.162 \pm 0.030 \times 10^{23} & \text{for run number} \leq 700 \\ 3.138 \pm 0.030 \times 10^{23} & \text{for run number} > 700 \end{cases}$$

The error associated with N_H is arbitrarily taken to be $\pm$ 1% which includes the errors in geometry and the hydrogen density.

APPENDIX II. NUCLEAR ABSORPTION

All of the pions detected in this experiment had to pass through matter including the hydrogen target vacuum jacket, air, and several counters. Some of the pions incident upon the system interacted with this matter and were lost. For the purposes of this experiment, any interaction other than multiple scattering was defined as nuclear absorption.

The nuclear absorption for several locations of absorbers was measured. The technique consisted of placing an additional piece of matter in the path of the pions and noting the difference in counting rate with the additional absorber in or out of the path. In order to get sufficient statistics, a plexiglass target was used, and several runs were taken with absorber in and out. The normal reproducibility of runs over short times precludes any measurement to an accuracy better than ± 1% of the no absorber rate. The data taken by this direct technique appear in Table 9.

An improved method of measuring the nuclear absorption was used for measuring the effects of nuclear absorption in the counter telescope at the rear of the magnet. For these measurements, a pion was defined by all the counters but the last. A certain fraction of the pions defined in this way did not count in the last counter. This fraction increased when an additional absorber was placed just ahead of the last counter. The difference between the fractional miss rate with and without the additional absorber was defined as the absorption in the additional absorber. In order to measure the effect of an absorber placed a long distance from the last counter, it was necessary to move the last counter further from counter p^i than the normal configuration. Thus some data were

TABLE 9. Absorption Measurements by Direct Method

Location	Absorber	Momentum	Absorption
At counter S1			
26 1/2" ahead of S2	1" plexiglass	300	0.073 ± 0.010
		400	0.044 ± 0.010
		570	0.038 ± 0.010
At counter A			
87" ahead of S2	1/2" plexiglass	570	0.032 ± 0.010
At hydrogen target			
	3/8" aluminum	570	0.039 ± 0.010

TABLE 10. Absorption Measurements by Improved Method

Distance Absorber to S2	Configuration	Absorber	Momentum	Absorption
18"	long	1" plexiglass	500 MeV/c	0.0350 ± 0.0048
12"	long	1" plexiglass	500 MeV/c	0.0227 ± 0.0044
8 1/2"	long	1" plexiglass	500 MeV/c	0.0133 ± 0.0042
8 1/2"	normal	1" plexiglass	500 MeV/c	0.0217 ± 0.0024
6"	normal	1" plexiglass	500 MeV/c	0.0167 ± 0.0024
2 1/2"	normal	2" plexiglass	500 MeV/c	0.0359 ± 0.0026
18"	long	1" plexiglass	300 MeV/c	0.0590 ± 0.0050
14"	long	1" plexiglass	300 MeV/c	0.0519 ± 0.0032
9 1/4"	normal	1" plexiglass	300 MeV/c	0.0494 ± 0.0034
6"	normal	1" plexiglass	300 MeV/c	0.0390 ± 0.0041
2 1/2"	normal	1" plexiglass	300 MeV/c	0.0250 ± 0.0044

taken with two different geometries: one with the last counter in its normal position 12" behind S1, and one with the last counter mounted 24" behind counter p^i. The statistical accuracy of the data taken with this technique is greater than for the data taken by the direct method, however unknown systematic errors may have entered because of the different geometry and the different event definition. The data taken by this method in both configurations is presented in Table 10.

Some data on the interaction of pions with light nuclei exist in the literature.[54, 55, 56, 57, 58] The main data for pion momenta comparable to those used in this experiment comes from bubble chamber studies. These studies indicate that the $\sigma \alpha A^{2/3}$ law is verified, but that the constant of proportionality varies with the incident pion momentum. In addition, the majority of the events are inelastic. This is to be contrasted with the $\pi^+ p$ interaction which is almost entirely elastic at low momenta. The number obtained from the bubble chamber experiments is called the total absorption cross section. This cross section includes all events with a scattering angle greater than a specified cutoff, but it does not include diffraction scattering.

The dependence of the nuclear absorption on the distance from the last counter is explained by the fact that the solid angle for detecting a secondary from an absorption event depends on this distance. For an absorber at counter S1, the counter system will accept only those events which scatter less than about 30^o. This cutoff is approximately the same as the one used for the total absorption cross section in the bubble chamber measurements. Thus the nuclear absorption measurement for absorber placed 26" from counter S2 can be used to calculate a number for the total

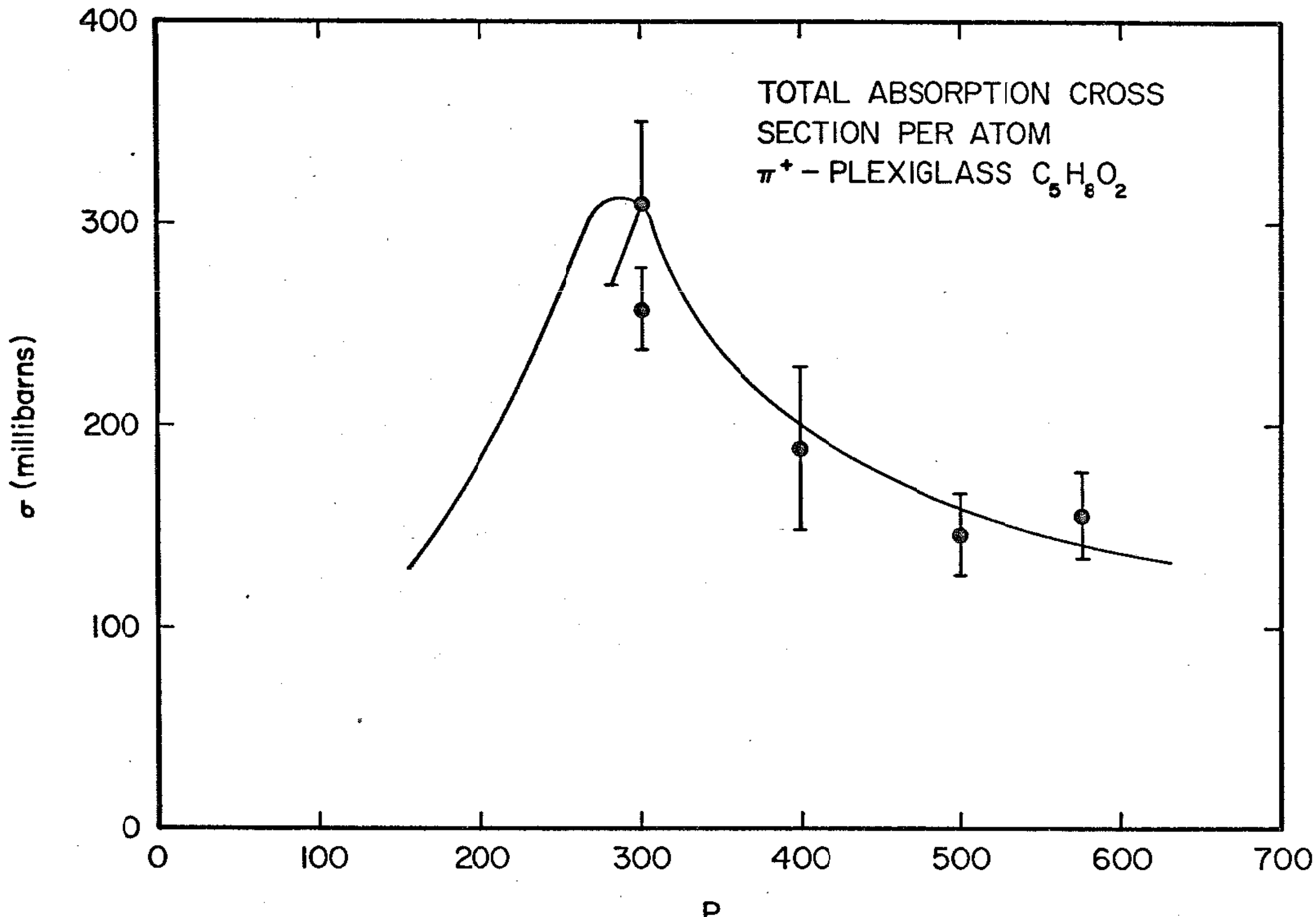
TOTAL ABSORPTION CROSS
SECTION PER ATOM
π^+ – PLEXIGLASS $C_5H_8O_2$
σ (millibarns)
400
300
200
100
0
0
100
200
300
400
500
600
700
P_π

Figure 15

absorption cross section for pions on plexiglass. The cross section must be divided by f, the fraction of events due to pions, for the muons in the beam defined at the rear of the magnet have a much smaller total cross section. The details of calculation are presented in Table 11.

In order to calculate the total absorption cross section per atom for pions on plexiglass ($C_5 H_8 O_2$), the cross section from each of the three constituent elements was calculated. The total cross section for hydrogen was taken from the well known π^+ p total cross section.[59] The carbon and oxygen cross sections were computed from the $A^{2/3}$ law and the bubble chamber measurement of σ/σ_{geom}.[55] The measured and expected values of this total absorption cross section are presented in Figure 15. The data and the calculation agree very well.

The absorption correction which was used for the cross sections of this experiment was calculated in a similar manner. First, each piece of matter through which the pions must pass was reduced to a mass of hydrogen and an equivalent mass of carbon using the $A^{2/3}$ law. In order to correct for the fact that some of the secondaries from an absorption event may be counted, an empirical factor, η, was defined as the ratio of the measured absorption (from Tables 9 and 10) to the absorption calculated from the total cross section. Then the effective mass of each absorber was defined as the product of η and the equivalent mass of each absorber, and the absorption resulting from the total effective mass of carbon and hydrogen was computed from the total cross sections. Finally, the absorption was multiplied by the fraction of the events which are due to pions, assuming that the muons have negligible total cross section.

TABLE 11. Calculation of Total Absorption Cross Section per Atom for Pions Incident on Plexiglass ($C_5H_8O_2$)

P (MeV/c)	Measured Absorption in 1" Plexiglass	σ_T per atom (mb.)	Fraction of Pions in Beam	Corrected σ_T per atom (mb.)
300	0.070 ± 0.010	259 ± 37	0.84	310 ± 45
300	0.059 ± 0.005	209 ± 17	0.84	250 ± 20
400	0.044 ± 0.010	162 ± 35	0.87	187 ± 40
500	0.035 ± 0.005	129 ± 18	0.89	146 ± 20
570	0.038 ± 0.010	140 ± 36	0.90	156 ± 40

In Table 12 is presented a list of the various absorbers in the system, the mass of each absorber, the factor η for each absorber, and the effective mass of each absorber. The fact that η is statistically consistent with 1.0 for most of the matter of the system is evidence that the calculation is correct. Some intermediate results and the final numerical values for the absorption as a function of momentum are presented in Table 13. The absorption correction used for the cross section calculation was obtained by linear interpolation in this table. Some additional absorption was added because the pions must pass through a thicker part of the hydrogen target structure at certain angles. This additional absorption was $3.0 \pm 0.8\%$ at 34° lab and $0.9 \pm 0.2\%$ at 40° lab. Since only three momenta near 500 MeV/c were used at these angles, the momentum dependence of the additional absorption was ignored.

The error of the absorption correction depends directly on the statistical errors of the absorption measurements. Considering the fact that measurements were made at a very limited number of momenta, it is expected that the error in the absorption correction is $\pm$ 25% of the correction. This results in a 1.5 - 3.0% normalization error in the cross sections.

TABLE 12. Material Through Which Pions Pass

Material		Composition	gm/cm^2	gm/cm^2 C equivalent	gm/cm^2 H	η	Effective Mass gm/cm^2 C equiv.	Effective Mass gm/cm^2 H
Target	Liquid Hydrogen	H	0.23	0.00	0.23	1.0*	0	0.230
	Mylar	CH	0.02	0.02	0		0.03	0
	Heat Shield	Cu	0.04	0.02	0	1.5 ± 0.4	0.03	0
	Outer Shield	Al	0.43	0.33	0		0.50	0
Air	Target to Counter A	N_8O_2	0.25	0.23	0	1.0*	0.23	0
Counter A	Ne 102 Scintillator	$C_{10}H_{11}$	0.47	0.44	0.03	1.2 ± 0.3	0.53	0.036
Air	Counter A to Counter S2	N_8O_2	0.25	0.23	0.00	1.0*	0.23	0
Counter S1	Ne 102 Scintillator	$C_{10}H_{11}$	0.69	0.65	0.044	0.95 ± 0.05	0.64	0.042
	Wrapping	Al	0.07	0.05	0		0.05	0
Counter P^i	Ne 102 Scintillator	$C_{10}H_{11}$	1.06	1.00	0.067	0.64 ± 0.05	0.64	0.043
	Wrapping	Al	0.07	0.05	0		0.03	0
Counter LC	Plexiglass	$C_5H_8O_2$	2.98	2.66	0.24	0.40 ± 0.05	1.06	0.096
	Wrapping	Al	0.07	0.05	0		0.02	0
Counter S2	Ne 102 Scintillator	$C_{10}H_{11}$	0.37	0.35	0.02	0.30 ± 0.05	0.11	0.011
	Wrapping	Al	0.04	0.02	0		0.00	0
						Total	4.16	0.458

* Assumed

TABLE 13. Calculation of Nuclear Absorption Vs. Pion Momentum

p_π (MeV/c)	σ_{geom} carbon (mb.)	σ/σ_{geom}	Absorp-tion π-C (%)	$\sigma_{\pi-p}$ (mb.)[4]	Absorp-tion π-p (%)	π-p+ π-C Absorp-tion (%)	fraction of events due to pions	Total Absorp-tion (%)
198	330	0.86[1]	5.92	70	1.93	7.85	0.79	6.2
233	330	1.08[1]	7.43	110	3.02	10.45	0.80	8.3
259	330	1.17[1]	8.13	162	4.45	12.58	0.82	10.3
282	330	1.17[1]	9.13	205	5.63	13.76	0.83	11.4
305	330	1.18[1]	8.20	190	5.25	13.45	0.84	11.3
332	330	1.04[1]	7.17	158	4.35	11.52	0.85	9.8
354	330	0.96[1]	6.61	135	3.71	10.32	0.85	8.8
376	330	0.95[1]	6.55	105	2.88	9.43	0.86	8.1
398	330	0.91[1]	6.21	90	2.47	8.68	0.87	7.7
522	330	0.82[2]	5.66	25	0.69	6.35	0.89	5.7
625	330	0.74[2]	5.10	20	0.50	5.60	0.90	5.0
727	330	0.66[3]	4.56	17	0.47	5.03	0.91	4.5

computed for

0.458 grams hydrogen
4.16 grams carbon equivalent

1. Meshkovskii et al. (55)
2. Interpolated
3. Cronin et al. (58)
4. Jacob and Chew (59)

APPENDIX III. MULTIPLE SCATTERING

Multiple scattering in the matter through which pions pass affects the results of the experiment in two ways. First, some events may be scattered out of the apertures and lost. In addition, multiple scattering causes a degrading of the momentum resolution and angular resolution of the spectrometer.

The loss of events due to scattering out of the apertures was investigated under the assumption that the spectrum of pions incident on the spectrometer is independent of angle and momentum. An analytic calculation verified that these losses are less than 0.5% for pion momenta greater than 200 MeV/c. A similar, but less accurate, result was obtained in a Monte Carlo calculation of multiple scattering losses in the High Energy Magnet by J. Kilner.[13]

In the 600 MeV/c spectrometer, the momentum of a particle is defined by the intercept of the particle trajectory and the momentum counter. Multiple scattering ahead of the plane of the momentum counter causes a smearing of this intercept and results in a wider momentum resolution function. The effects of multiple scattering in an optical system can be calculated analytically if first-order optics and Gaussian multiple scattering are assumed. Under these assumptions, we may calculate the contribution of a scatterer of thickness ds at the point s along the central ray of the spectrometer

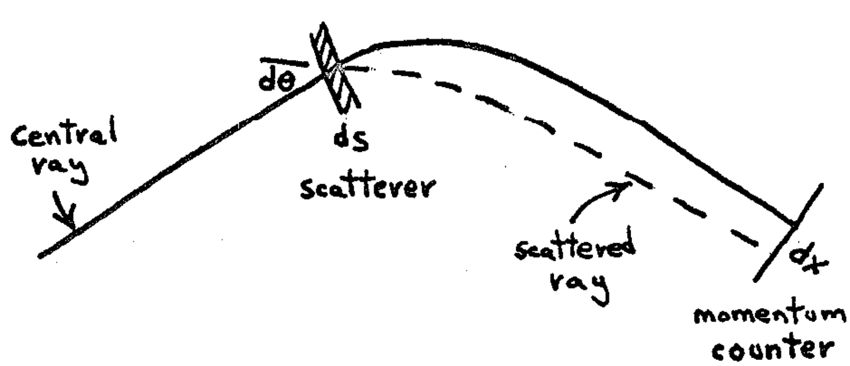

to the uncertainty, dx, in the intercept of the ray with the momentum counter. The mean square projected scattering angle resulting from multiple scattering in thickness ds is given by the relation

$$\langle d\,\theta^2 \rangle = \left(\frac{E_{ps}}{p\,\beta}\right) \frac{ds}{x_o(s)}$$

where $x_o(s)$ is the radiation length of the scatterer at point s, p and β are the momentum and velocity of the particle, respectively, and E_{ps} is the multiple scattering constant for the projected distribution. E_{ps} is related to the constant, E_s, defined by Rossi[60], by the relation

$$E_{ps} = E_s/\sqrt{2} = 14.9 \text{ MeV}$$

Since, in the first order approximation, dx and ds are linearly related, we may write

$$\langle d\,x^2 \rangle = L^2(s) \langle d\,\theta^2 \rangle$$

where L(s) is given by the first order magnet theory. Since the scattering at each point along the trajectory is independent of the scattering at any other point, we may write the relation for the total mean square displacement as

$$\langle d\,x^2 \rangle = \frac{E_{ps}}{p\,\beta} \int_{\substack{\text{hydrogen}\\\text{target}}}^{\substack{\text{momentum}\\\text{counter}}} \frac{L^2(s)}{x_o(s)}\, d\,s$$

The contributions of the various scatterers to this integral are given in the table below

Scatterer	$\int \frac{L^2(s)\,ds}{x_o(s)}$
liquid hydrogen	0.05
hydrogen target structure	4.05
air front	6.25
center	10.92
rear	9.60
counter A	54.40
counter S1	2.22
Total	87.57 in^2

To relate the root mean square displacement, $\langle dx^2 \rangle^{1/2}$, to a root mean square uncertainty in momentum, $\langle (\frac{dp}{p})^2 \rangle^{1/2}$, we must divide by the dispersion of the spectrometer, D = 51.7 inches,

$$\langle (\frac{dp}{p})^2 \rangle^{1/2} = \frac{\langle dx^2 \rangle^{1/2}}{D} = 0.181\ \frac{E_{ps}}{p\beta}$$

When the multiple scattering is folded into the natural resolution of the spectrometer, the momentum resolution becomes a function of the central momentum of the spectrometer. The r.m.s. width of the momentum resolution at several momenta is given in the table below

P (MeV/c)	$\langle (\frac{dp}{p})^2 \rangle^{1/2}$ natural	$\langle (\frac{dp}{p})^2 \rangle^{1/2}$ multiple scattering	$\langle (\frac{dp}{p})^2 \rangle^{1/2}$ total
200	1.10×10^{-2}	1.63×10^{-2}	1.94×10^{-2}
300	1.10	0.94	1.45
400	1.10	0.71	1.31
500	1.10	0.56	1.23
600	1.10	0.46	1.19

A similar method has been used to calculate the r. m. s. angular resolution due to multiple scattering. The result is:

$$\langle d\,\theta^2 \rangle^{1/2} = 0.194\ \frac{E_{ps}}{p\,\beta}$$

APPENDIX IV. π-μ DECAY CORRECTIONS

The decay of the π^+, namely, $\pi^+ \rightarrow \mu + \nu$ is a problem in any experiment with a long flight path. In this experiment, as many as 30% of the pions decay in the 421 cm. distance from the hydrogen target to counter p^i. If the counter system of the spectrometer were able to distinguish pions from muons, then the decay would simply reduce the number of events observed. However, since pions and muons were indistinguishable, some of the muons from the decay of pions were counted. In general, the muons counted did not come from pions which had the same momentum that the spectrometer was set for. Thus the momentum resolution functions of the spectrometer had long tails due to pions counted indirectly by the decay process.

The analytic calculation of the number of muons accepted by the spectrometer is a formidable problem involving multiple integrals with variable limits. A calculation of this type was performed by Dixon and Walker.[12] The same calculation can be easily coded for a digital computer if the Monte Carlo method is used. Such programs have been coded by Boyden[18] and Kilner.[13]

The Monte Carlo method was very inefficient and used large amounts of computer time. In order to obtain accurate resolution functions, it was necessary to run the Monte Carlo program for a few points and parameterize the output in such a way that the decay corrections could be used under a wide variety of kinematic conditions. In order to make this parameterization, it was assumed that a resolution function for the central momentum channel could be written as a function of P and P_o only. This resolution function gives the solid angle for accepting the decay muon from a pion with momentum between P and P + dP and with the magnet set at momentum P_o. A table of values of the solid angle for several values of P_o and $\frac{P-P_o}{P_o}$ was computed by the Monte Carlo program. Then at fixed $(P-P_o)/P_o$, the solid angle was fit with a quadratic in P_o. The coefficients of this fit are presented in Table 14. The raw data were computed for P_o = 200, 300, 400, 500 and 600 MeV. These data, and the value of $\Delta\Omega$ computed from the fit, are presented in Figures 16-a - 16-e. The points computed from the fit are connected by straight lines in these figures, since the trapezoid rule has been used for doing integrals with these functions.

The Monte Carlo program which was used to calculate the results of Table 14 was originally written by J. Kilner in FORTRAN II.[13] This program is described in his thesis. The program was converted to FORTRAN IV by the program SIFT, then it was modified to be able to compute results for a nearly vertical rear aperture counter. Finally, a modification was made to correctly compute the off-symmetry plane magnet optics in the first order model.[61]

Three approximations are involved in the use of the resolution functions presented in Table 14. The first is that the effect of the lab angle of the spectrometer is negligible. The only place that this angle enters is in the projection of the length of the illuminated region of the hydrogen target on a plane perpendicular to the central ray. All the computations were done for $\theta_{lab} = 45^o$. The second approximation is that the resolution function for the i^{th} channel can be simply computed from the Monte Carlo results for the central channel. Under the assumption that the fraction of the observed events due to muons in the i^{th} channel with momentum $\bar{p}_i$ is the same as the fraction of events due to muons

TABLE 14. Resolution Function for Pions Counted by π-μ Decay Process*

$$\Delta\Omega\left(\frac{P-P_o}{P_o}\right) = A\left(\frac{P-P_o}{P_o}\right) + P_o B\left(\frac{P-P_o}{P_o}\right) + P_o^2\, C\left(\frac{P-P_o}{P_o}\right)$$

$\frac{P-P_o}{P_o}$	$A\left(\frac{P-P_o}{P_o}\right)$	$B\left(\frac{P-P_o}{P_o}\right)$	$C\left(\frac{P-P_o}{P_o}\right)$
-0.210	0.3789×10^{-5}	-0.1696×10^{-7}	0.1804×10^{-10}
-0.180	0.3684×10^{-5}	-0.1649×10^{-7}	0.1754×10^{-10}
-0.150	0.2177×10^{-4}	-0.8289×10^{-7}	0.7780×10^{-10}
-0.120	0.2709×10^{-4}	-0.9321×10^{-7}	0.8075×10^{-10}
-0.090	0.3332×10^{-4}	-0.9218×10^{-7}	0.7159×10^{-10}
-0.060	0.1761×10^{-4}	0.3500×10^{-7}	-0.8357×10^{-10}
-0.045	0.1279×10^{-4}	0.8415×10^{-7}	-0.1355×10^{-9}
-0.030	0.5264×10^{-4}	-0.4960×10^{-7}	0.3000×10^{-11}
-0.015	0.9100×10^{-4}	-0.1454×10^{-6}	0.1335×10^{-9}
0.000	0.4559×10^{-4}	0.5426×10^{-7}	-0.1024×10^{-9}
0.015	0.3506×10^{-4}	0.1964×10^{-7}	-0.4764×10^{-10}
0.030	0.4990×10^{-4}	-0.3524×10^{-7}	-0.3221×10^{-10}
0.045	-0.1481×10^{-4}	0.2197×10^{-6}	-0.2860×10^{-9}
0.060	0.3823×10^{-4}	-0.5499×10^{-7}	0.2571×10^{-10}
0.090	0.5439×10^{-4}	-0.1595×10^{-6}	0.1382×10^{-9}
0.120	-0.5887×10^{-5}	0.1173×10^{-6}	-0.1611×10^{-9}
0.150	0.2993×10^{-4}	-0.7438×10^{-7}	0.5571×10^{-10}
0.180	0.1329×10^{-4}	-0.2618×10^{-7}	0.2187×10^{-10}
0.210	0.2091×10^{-4}	-0.7228×10^{-7}	0.7999×10^{-10}
0.240	0.9166×10^{-6}	0.5345×10^{-7}	-0.8128×10^{-10}
0.270	0.3046×10^{-4}	-0.1173×10^{-6}	0.1285×10^{-9}

* computed for 3.0" x 9.50" aperture counter

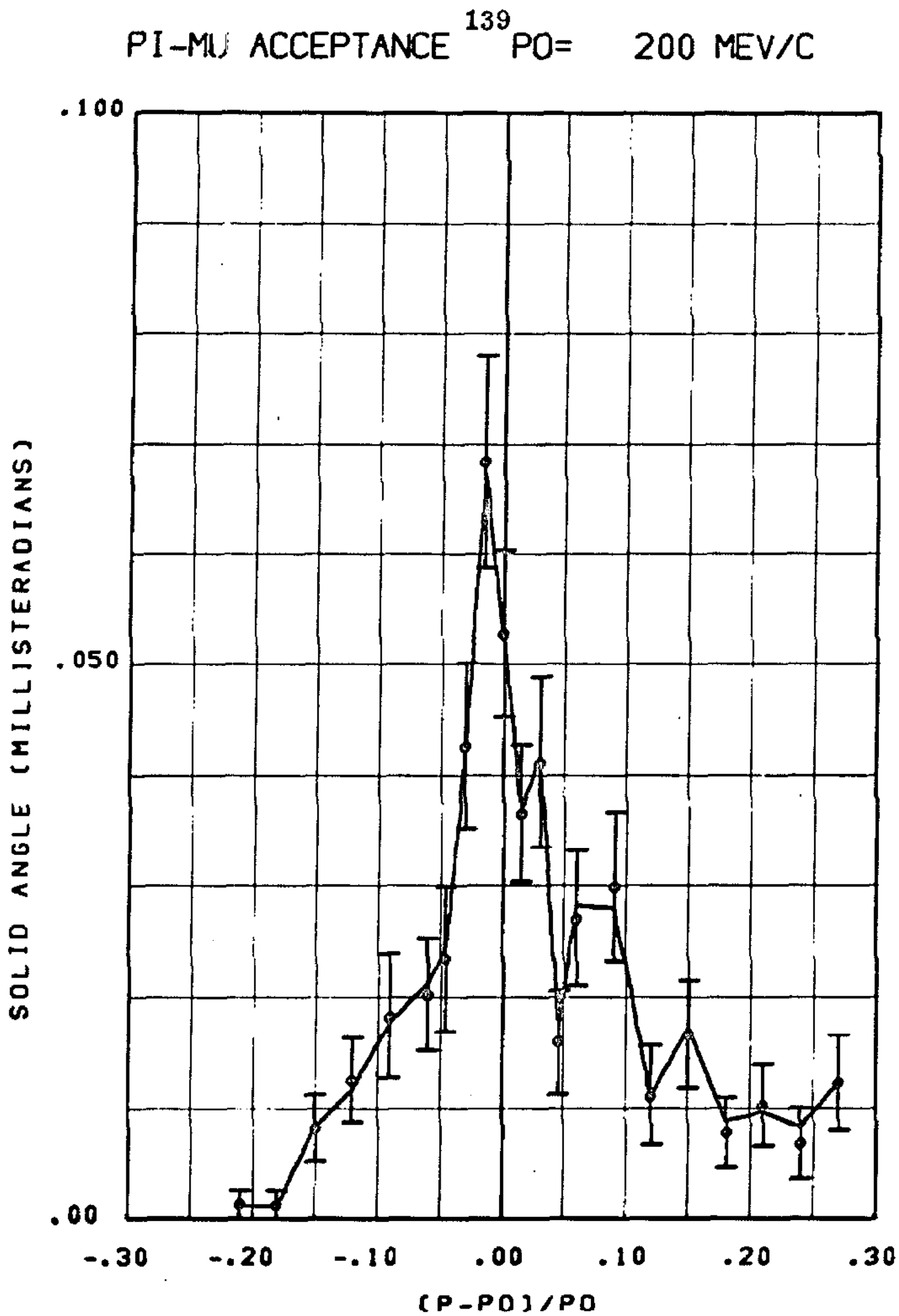
PI-MU ACCEPTANCE 139 PO= 200 MEV/C
.100
.050
.00
SOLID ANGLE (MILLISTERADIANS)
-.30
-.20
-.10
.00
.10
.20
.30
(P-PO)/PO

Figure 16a

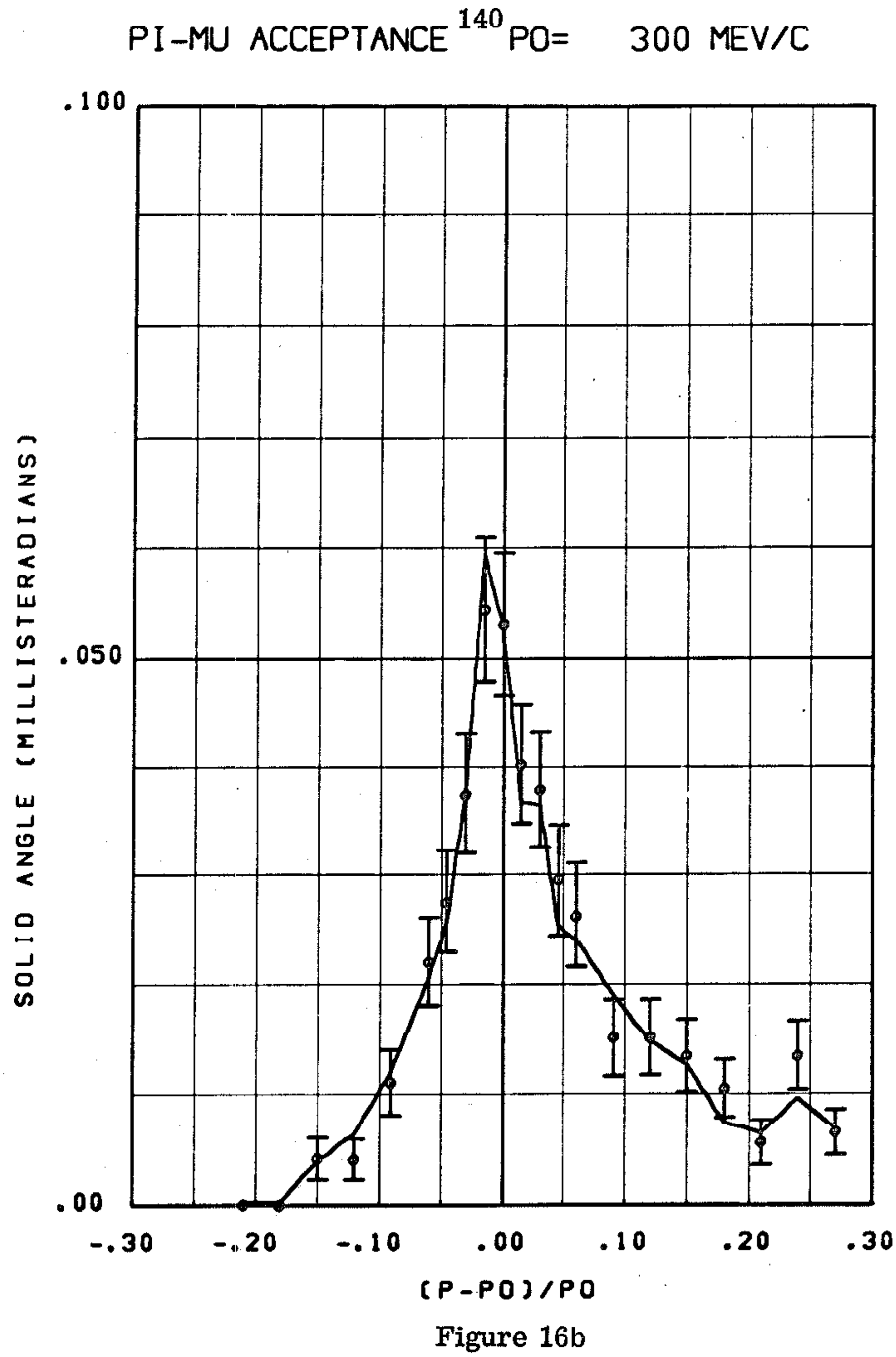
PI-MU ACCEPTANCE 140 PO= 300 MEV/C
.100
.050
.00
SOLID ANGLE (MILLISTERADIANS)
-.30
-.20
-.10
.00
.10
.20
.30
(P-PO)/PO
Figure 16b

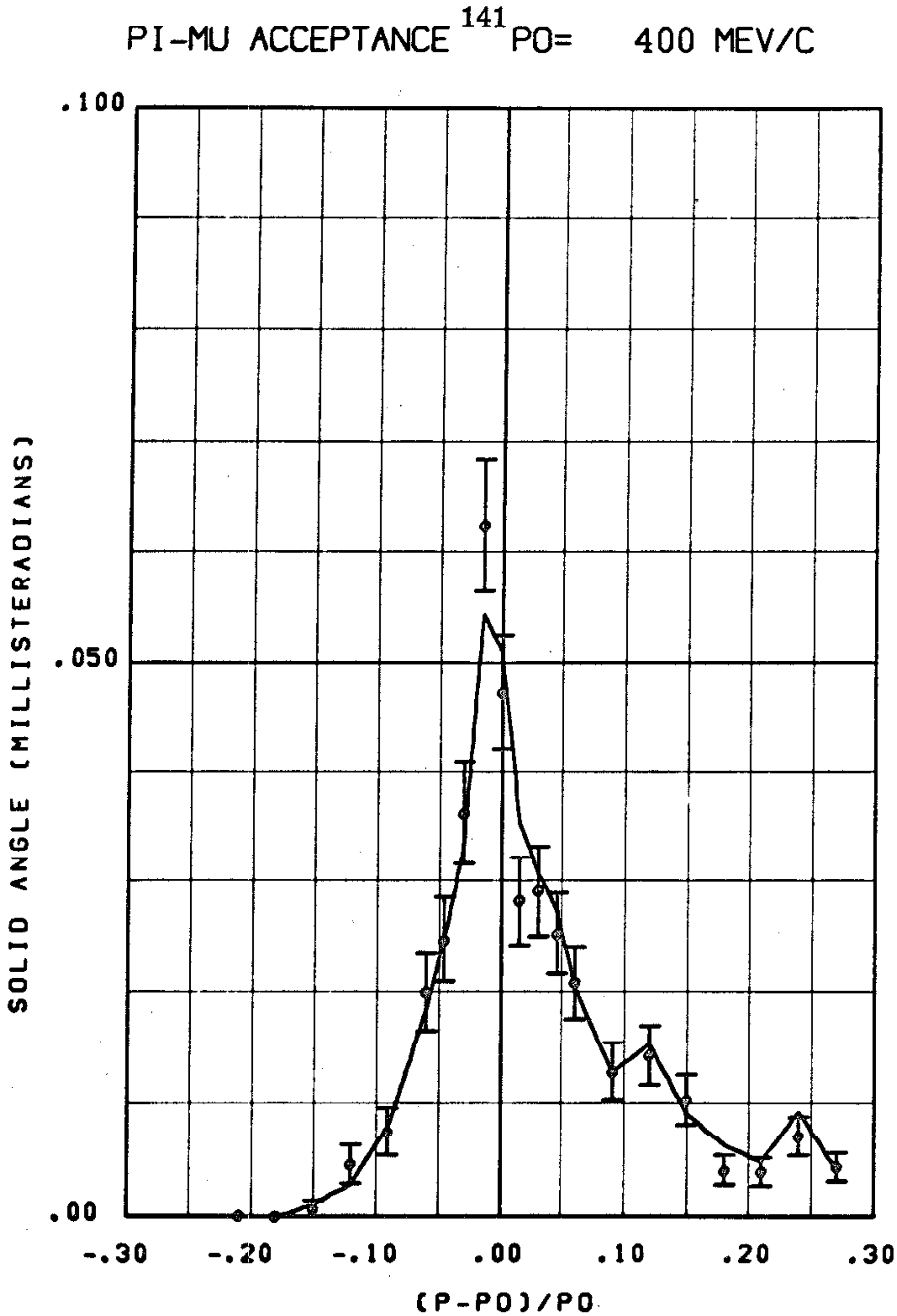
PI-MU ACCEPTANCE 141 PO= 400 MEV/C
.100
.050
.00
SOLID ANGLE (MILLISTERADIANS)
-.30
-.20
-.10
.00
.10
.20
.30
(P-PO)/PO

Figure 16c

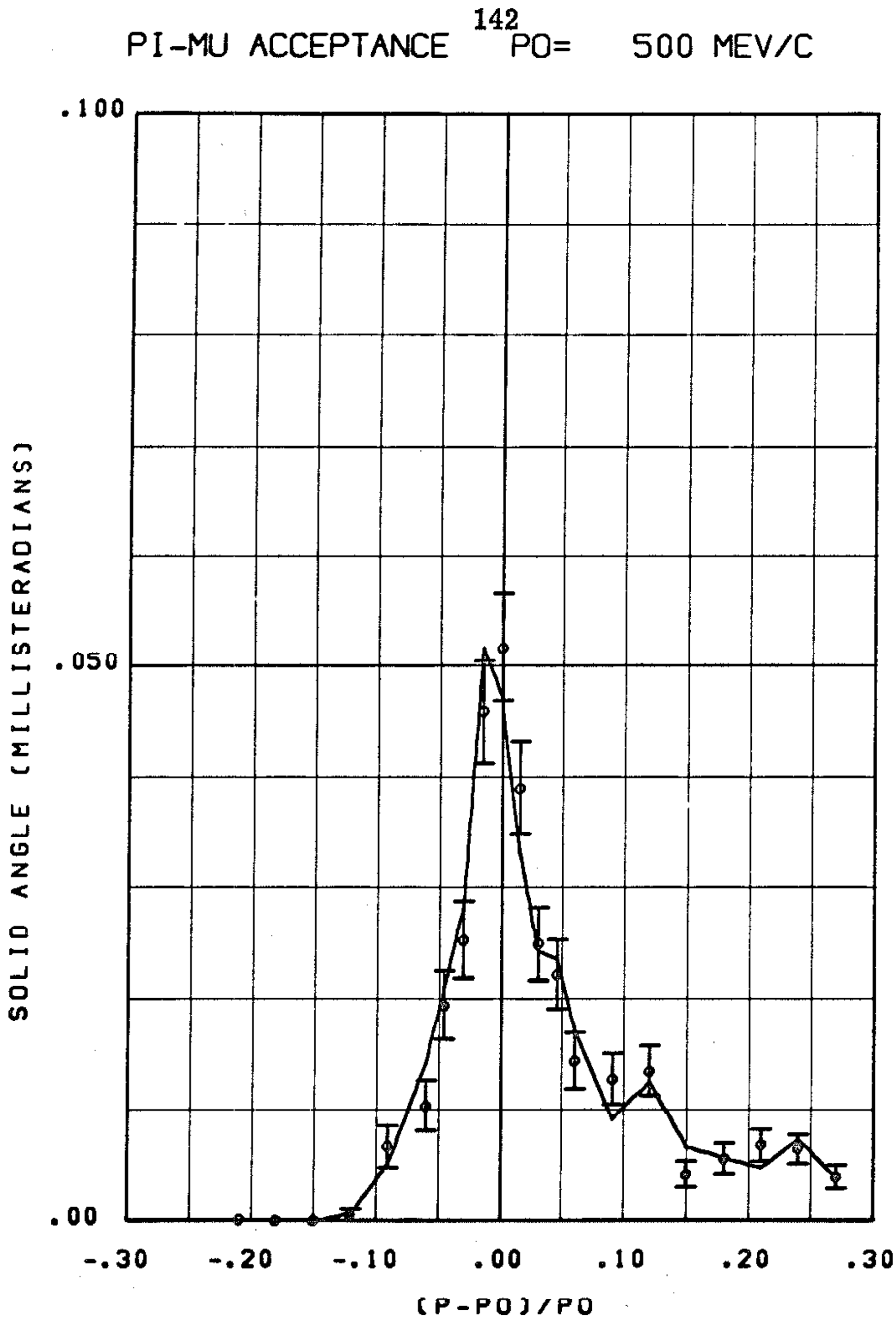

142
PI-MU ACCEPTANCE PO= 500 MEV/C
.100
.050
.00
SOLID ANGLE (MILLISTERADIANS)
-.30
-.20
-.10
.00
.10
.20
.30
(P-PO)/PO

Figure 16d

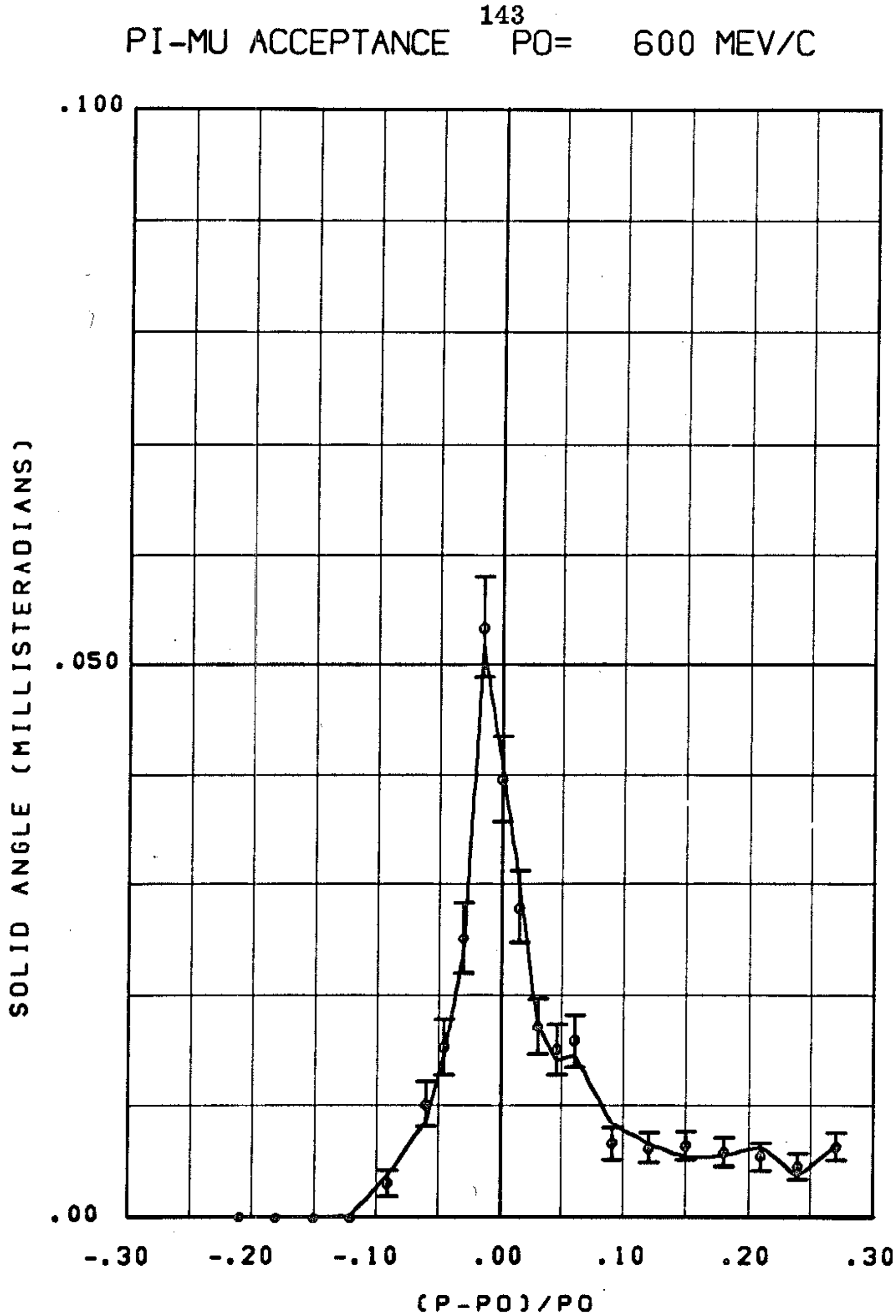
143
PI-MU ACCEPTANCE PO= 600 MEV/C
.100
.050
.00
SOLID ANGLE (MILLISTERADIANS)
-.30
-.20
-.10
.00
.10
.20
.30
(P-PO)/PO

Figure 16e

in the central channel if the central momentum were set to $\overline{p}_i$, we find that the decay part of the resolution function for the i^{th} channel may be written as

$$\Delta\Omega\left(\frac{p-\overline{p}_i}{p_o}\right) = \frac{(\Delta\Omega\Delta p/p_o)i}{(\Delta\Omega\Delta p/p_o)_{central}} \left[A\left(\frac{p-\overline{p}_i}{p_o}\right) + \overline{p}_i\, B\left(\frac{p-\overline{p}_i}{p_o}\right) + (\overline{p}_i)^2\, C\left(\frac{p-\overline{p}_i}{p_o}\right)\right]$$

where $\overline{p}_i$ is the mean momentum of the i^{th} channel, p_o is the central momentum of the spectrometer, the coefficients $A\left(\frac{p-\overline{p}_i}{p_o}\right)$, $B\left(\frac{p-\overline{p}_i}{p_o}\right)$, and $C\left(\frac{p-\overline{p}_i}{p_o}\right)$ are defined in Table 14, and the values of $(\Delta\Omega\,\Delta p/p_o)$ for the various channels are given in Table 2. The final approximation is that the resolution functions are proportional to the area of the aperture counter. This approximation is necessary because the resolution functions were computed for a 3.0" x 9.50" aperture counter in the early days of the experiment. The size of this counter was changed to 2.75" x 9.50" before any final data was taken. The correction factor $\frac{2.75}{3.0} = 0.9167$ has been used to correct the coefficients of Table 14 for all the cross sections computed in this experiment.

To compute total resolution functions from the resolution functions calculated for particles which do not decay, we first multiply the no decay resolution functions by a factor which gives the fraction of the pions which do not decay in the magnet. Then we add the resolution function calculated from the coefficients of Table 14. Some summarized results of this calculation are presented in Figure 17. The fraction of pions counted by the process $\pi \to \mu + \nu$ is computed from the trapezoid rule area of the resolution functions of Table 15. A constant cutoff at $(P-P_o)/P_o = +0.27$ has been used

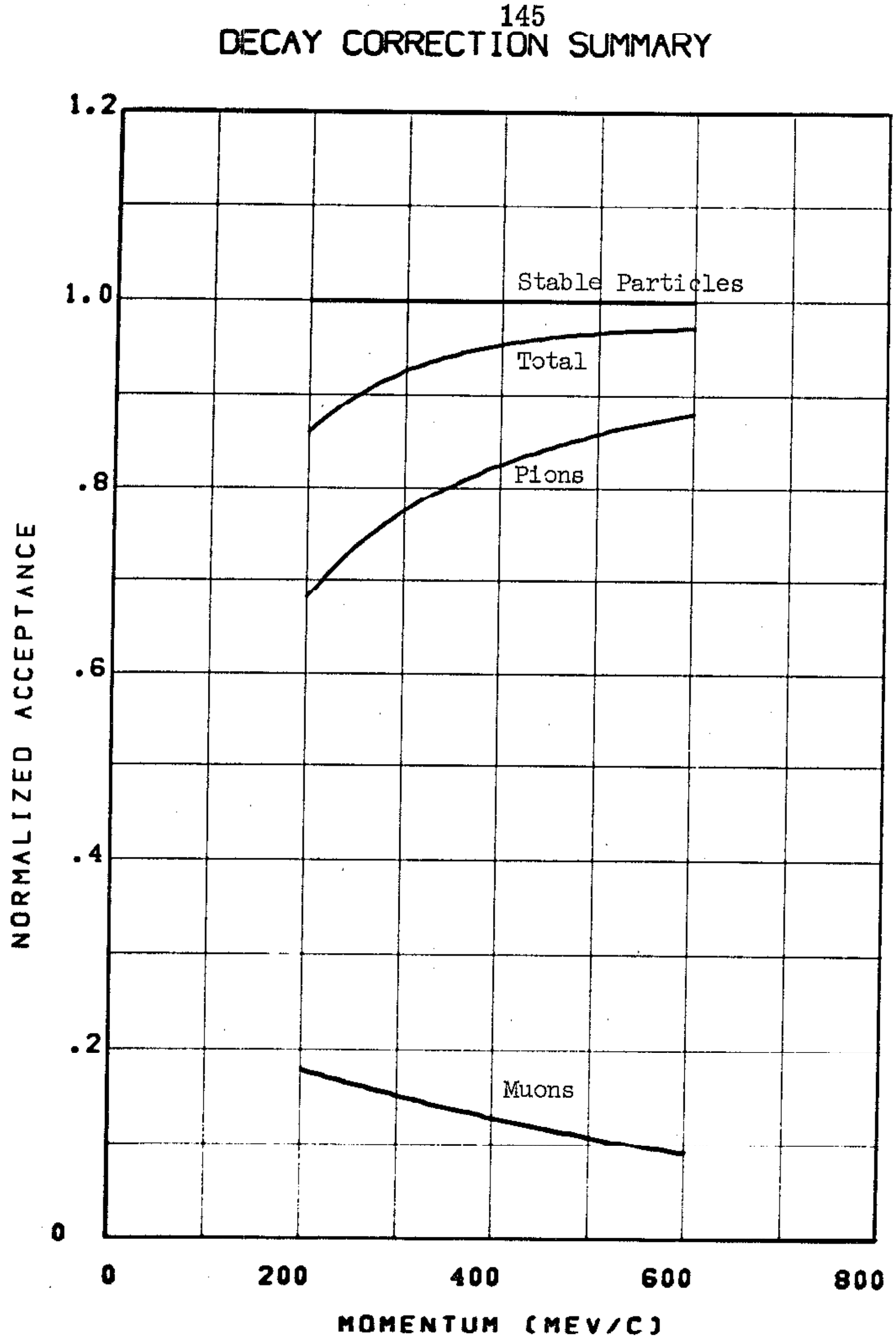

Acceptance for events originating as pions in hydrogen target which reach momentum counter in state indicated. Top curve is acceptance for stable particles originating in hydrogen target.

Figure 17

as well as the correction for the smaller aperture counter. The statistical error in the area of the resolution function is ± 0.3% of the total resolution function. Including the various approximations used, the decay calculation introduces a ± 1% error into the area of the total resolution functions. The decay resolution function also adds a "long tail" to the total resolution function which causes significant errors when the effects of finite resolution are considered. These effects are discussed separately in Section V-B.

APPENDIX V. RESOLUTION CALCULATIONS

The angular resolution of the 600 MeV/c spectrometer depends on the size of the hydrogen target cup, the size of the beam spot, the size of the aperture counter, the lab angle of the spectrometer, the central momentum of the spectrometer, and the spectrometer optical properties. The angular resolution functions were computed assuming a uniform beam spot and ignoring effects of pion decay and nuclear scattering. The results of this computation for two typical cases are shown in Figure 18. The effects of multiple scattering discussed in Appendix III have been included.

The momentum resolution functions were calculated for the parameters of each data point. For this calculation the resolution functions of Figure 3 were used as input data and the effects of pion decay and multiple scattering were included. Since, in the cross section computation, the angular resolution in θ^* was assumed to be a delta function, whereas the k resolution was treated correctly, a correction was made to the momentum resolution functions to include the effect of finite angular resolution on the photon energy resolution. This correction was made by converting the angular resolution functions discussed above into effective momentum resolution functions by the relation

$$\frac{P - P_o}{P_o} = \frac{1}{P_o} \frac{\partial k/\partial \theta}{\partial k/\partial P} (\theta - \theta_o)$$

Then these effective momentum resolution functions were folded into the momentum resolution functions for the spectrometer after

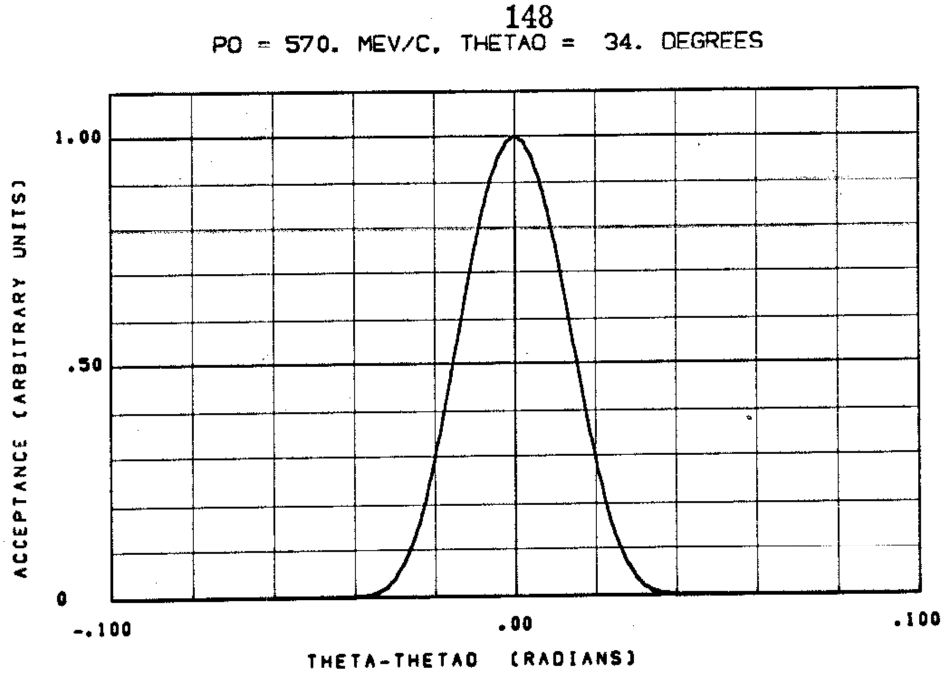

Figure 18. Laboratory Angular Resolution Functions, 600 MeV/c Magnet.

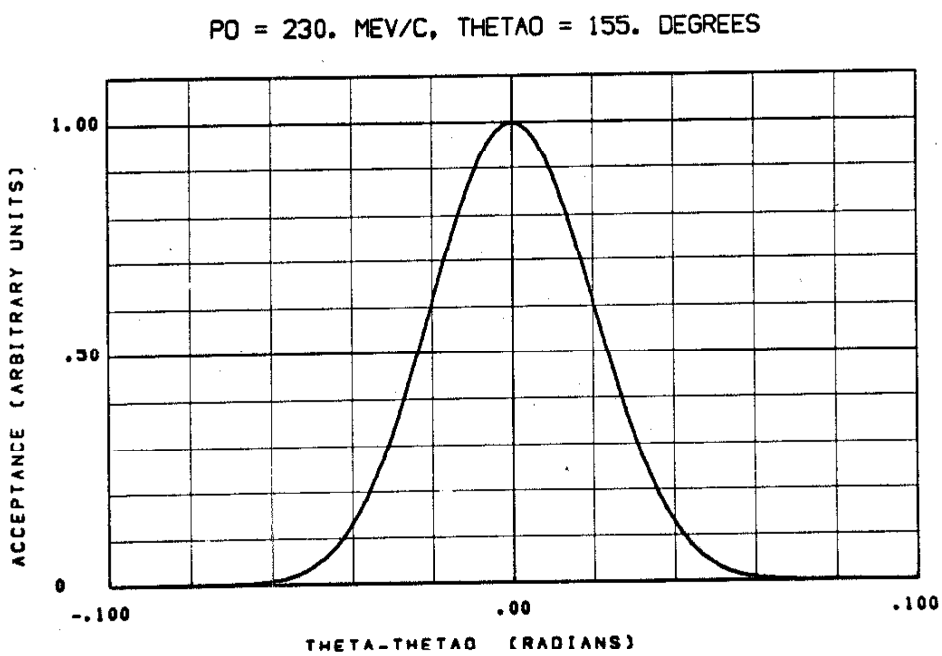

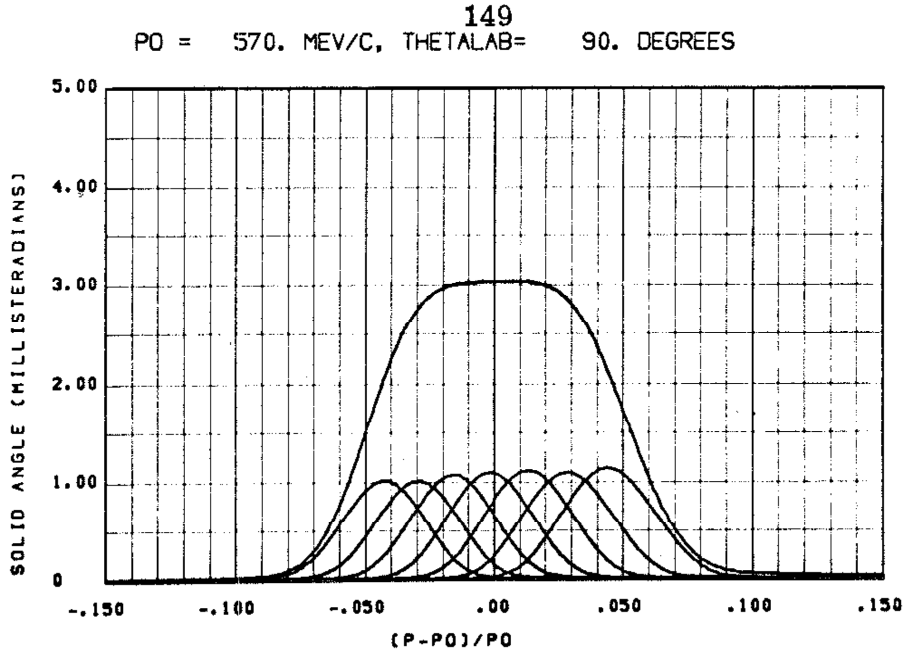

Figure 19. Total Momentum Resolution Functions, 600 MeV/c Magnet

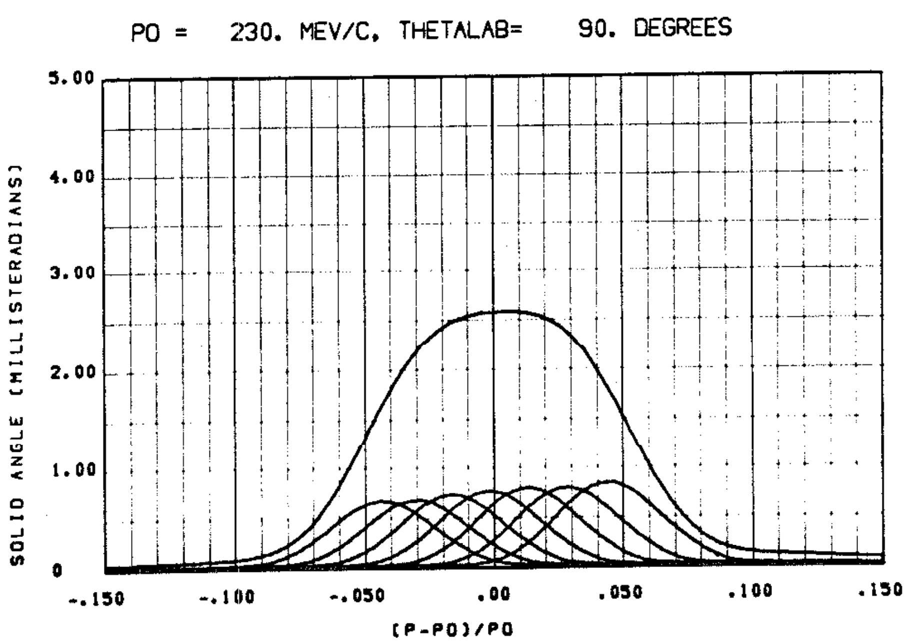

the multiple scattering and decay effects were calculated. Two examples of the total resolution functions are given in Figure 19. Typically, the angular resolution correction increased the width of the total resolution functions by 10 - 20%.

The r. m. s. resolution in photon energy, $\Delta k_{r.m.s.}$, was computed from the total momentum resolution functions for each point. Since the effects of the long tails which result from pion decay were corrected by the unfolding process (see Section V-B), the pion decay part of the momentum resolution functions was ignored for the calculation of the photon energy resolution. The values of the r. m. s. resolution obtained are presented in Figure 20. For comparison purposes, the values of the resolution obtained by S. Ecklund[9] are also shown.

The reasons for calculating the momentum resolution function in great detail while ignoring effects of resolution in θ^* were threefold. First, the momentum resolution function is weighted by $\bar{B}(k, E_0)$ in the cross section calculation and for a few measurements where k was very close to E_0, a delta function approximation to the momentum resolution function was not accurate enough. Second, the excitation curves of Section IV-D would not be expected to fit the data unless the photon energy resolution was accurately computed. Finally, at the start of the experiment, it was hoped that a successful method for unfolding the photon energy resolution could be found and it was assumed that accurate resolution functions would be required for this purpose. This final reason did not work out in practice (see Section V-B).

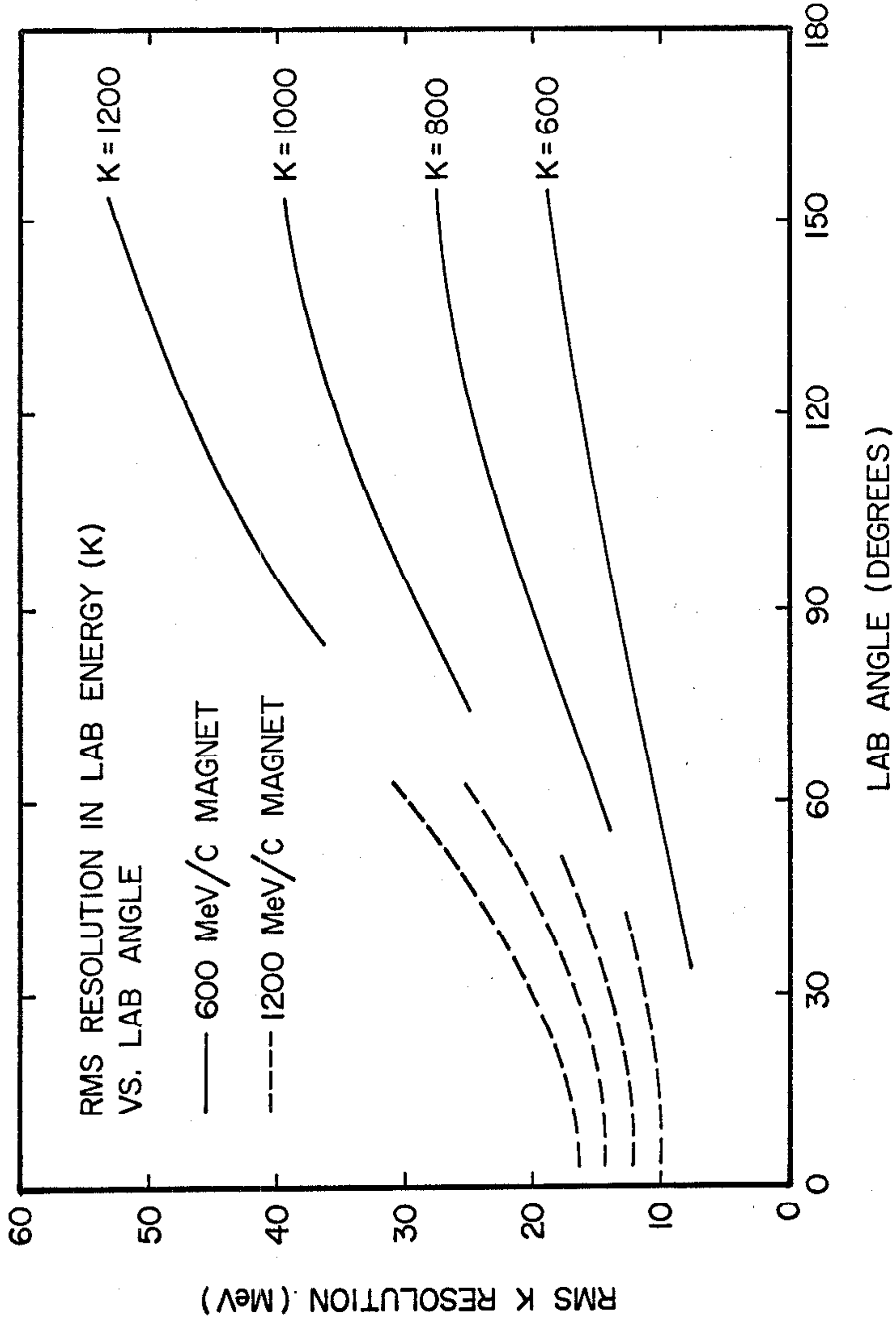
RMS RESOLUTION IN LAB ENERGY (K)
VS. LAB ANGLE
600 MeV/C MAGNET
1200 MeV/C MAGNET
K = 1200
K = 1000
K = 800
K = 600
RMS K RESOLUTION (MeV)
0
10
20
30
40
50
60
0
30
60
90
120
150
180
LAB ANGLE (DEGREES)
Figure 20

APPENDIX VI. PLEXIGLASS TARGET CALIBRATION RUNS

During the second period of data taking, a series of tests was made to determine the reproducibility of results obtained by this experiment. For these tests, the hydrogen target was replaced by a piece of "Plexiglass G" of the same dimensions as the hydrogen target appendix. The kinematic conditions were set up as follows:

E_o	850. MeV (meter)
P	573. MeV/c (magnetometer frequency 68.26 mc.)
θ_{lab}	51.0^o

These settings would yield the results for single pion photoproduction at a photon energy of 775 MeV and a center-of-mass pion angle of 76^o if the target were free protons. Except for the plexiglass target, the kinematic conditions were thus typical of those used during the experiment.

A plexiglass target calibration run was taken every few days during the second period of data taking. The runs were made with the same synchrotron operating conditions as any normal run. The quantameter calibration procedure used for the normal runs was also followed with one exception, namely, the beam catcher ion chamber was assumed to be stable for the entire period of the experiment and a value of Q/BC of 12.68 was used for all runs. The data obtained in 18 plexiglass target runs are presented in Table 15. These data are also plotted versus run number in Figure 21.

TABLE 15. Plexiglass Target Calibration Run Summary

Date	Run	π^+	QTC	Q40	QBC	QAVG	π/QTC	π/Q40	π/QBC	π/QAVG	R=(F+V) veto rate	$\frac{\pi^+(\bar{R}-R)}{QAVG}$*
26 Jan.	966	6424	103.3	104.4	101.0	102.9	62.21	61.55	63.62	62.45	0.090	-0.31
26 Jan.	973	6475	101.8	101.3	102.5	101.9	63.61	63.92	63.17	63.54	0.090	-0.31
27 Jan.	974	6488	102.7	101.7	102.8	102.4	63.17	63.80	63.11	63.36	0.090	-0.32
31 Jan.	1025	6416	103.9	104.6	104.2	104.2	61.75	61.34	61.57	61.57	0.099	-0.88
1 Feb.	1026	6275	103.0	104.8	102.4	103.4	60.92	59.88	61.28	60.59	0.096	-0.67
4 Feb.	1050	7073	113.3	112.2	114.2	113.2	62.43	63.04	61.94	62.48	0.089	-0.28
4 Feb.	1051	6257	102.8	101.7	103.7	102.7	60.87	61.52	60.34	60.93	0.089	-0.27
8 Feb.	1054	6859	105.8	106.9	106.0	106.2	64.83	64.16	64.71	64.58	0.085	0.00
9 Feb.	1065	6723	105.4	105.4	105.4	105.4	63.79	63.79	63.79	63.79	0.084	0.00
10 Feb.	1077	6892	105.9	106.4	106.0	106.1	65.08	64.77	65.02	64.96	0.082	+0.20
12 Feb.	1090	6769	107.1	106.1	106.2	106.5	63.20	63.80	63.74	63.56	0.092	-0.47
15 Feb.	1097	6721	104.8	103.3	105.3	104.5	64.13	65.06	63.83	64.32	0.091	-0.40
21 Feb.	1125	6523	104.6	105.4	105.2	105.1	62.36	61.89	62.01	62.06	0.086	-0.06
5 Mar.	1145	6746	106.4	106.7	106.6	106.6	63.40	63.22	63.28	63.28	0.076	+0.60
15 Mar.	1178	6542	106.1	108.3	107.0	107.1	61.66	60.41	61.14	61.08	0.085	0.00
19 Mar.	1195	6642	106.6	106.5	107.0	106.7	62.31	62.37	62.07	62.25	0.074	+0.73
19 Mar.	1199	6541	107.4	107.6	107.4	107.5	60.90	60.79	60.90	60.85	0.071	+0.91
20 Mar.	1200	6741	107.7	107.6	107.0	107.4	62.59	62.65	63.00	62.77	0.061	+1.34
						Mean	62.73	62.66	62.70	62.70	0.085	

* $\frac{\pi^+(\bar{R}-R)}{QAVG}$ is the expected variation in π^+/QAVG under the assumption that the F+V veto rate should be constant

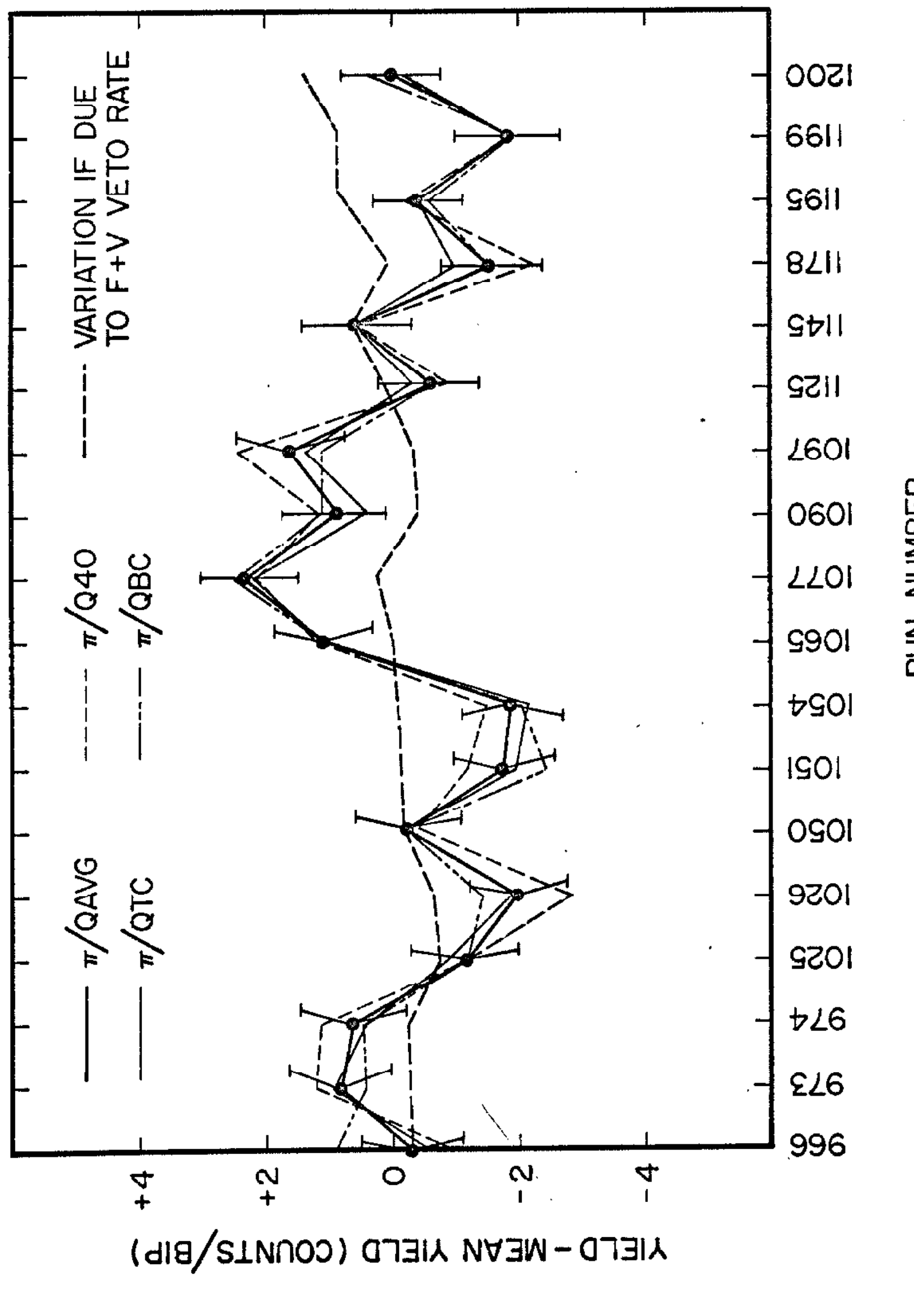

Figure 21. Plexiglass Target Calibration Run Data

It is immediately obvious that these runs are not consistent with the hypothesis that the only errors result from the counting statistics. Deviations of this magnitude should occur approximately one time in 10^4. Thus we must assume that there is some other effect which caused the inconsistencies. In the table below are presented the values of the variance of π/Q obtained using the various beam monitors as well as the "additional r. m. s. error" which is due to errors other than counting statistics.

	variance	counting statistics	additional rms error
π/QTC	1.98%	1.23%	1.55%
π/Q40	2.36%	1.23%	2.07%
π/QBC	2.07%	1.23%	1.66%
π/QAVG	2.06%	1.23%	1.65%

Figure 20 leads us to look for a slow variation which could take place with a period of several days. Because the singles rates from a lucite target are much higher than those obtained with hydrogen target, it is possible that accidentals or dead time effects could cause the observed discrepancies. However, a study showed that the variation in π^+/Q is not correlated with the average beam intensity. The efficiency of the fan counters might also have fluctuated since these were checked at only infrequent intervals. However, if we assume that the fraction of events which are vetoed by F + V should be a constant, we can compute the variations expected from the fact that the fractional F + V veto rate was not constant. The fractional F + V veto rate is given in Table 15, as well as the expected variation in π^+/QAVG due to this effect.

However, the plot of the expected variation vs. run number shown in Figure 20 clearly shows that this effect is not correlated with the observed fluctuations in π^+/QAVG. The pion and proton separation logic in the spectrometer was also shown to be constant to the order of 0.2%.

The beam monitoring was not completely consistent. However, the fact that the values at π/QTC and π/QBC are consistent to better than 0.5% r.m.s. indicates that the beam monitoring system was not responsible for the major part of the inconsistencies.

There remains the possibility that the plexiglass target was dimensionally unstable or absorbed water from the atmosphere. However, data from the manufacturer's catalog indicate that both these effects could contribute less than 0.3% variations in the π^+ rate.

The most likely reason for the discrepancy is that the cross section for π^+ photoproduction from free protons is changing rapidly with energy near the kinematic point chosen for the plexiglass runs. The slope of the yield vs. momentum curve can be obtained by looking at the observed yield in the various momentum channels. From this effect, we observe that an 0.25% r.m.s. momentum variation can cause the observed 1.65% r.m.s. variation in yield. The variation of momentum calibration is due to the motion of the beam centroid. An 0.11 inch r.m.s. motion of the beam centroid could cause the observed effect. Since the vertical position of the beam centroid is not under the control of the experimenter, this motion can exist. However, this much motion seems to be inconsistent with polaroid beam pictures taken each day.

Another possibility arising from the rapid variation of the cross section with kinematics is that the momentum of the spectrometer was constant but the synchrotron energy changed. A test run was made with $E_o = 890$ MeV, or 40 MeV higher than the normal runs. This test yielded the result of 88.0 ± 1.4 pions/QBIP. This amounts to an $8.5 \pm 2.0\%$ increase in the yield for a 40 MeV change in E_o. If the end point energy is responsible for all the fluctuations observed, then E_o must be drifting by 0.9% r.m.s.. This much drift is also unreasonable.

The conclusion drawn from the plexiglass target calibration runs is that there is a random error in the yields in addition to the counting statistics. This error can be the result of the compounding of a large number of smaller errors in many separate components including the beam monitoring, the momentum calibration, the synchrotron energy, and the operation of the electronics. On the basis of these runs, a random error of 1.65% was folded into the counting statistics of each run when the error bars on cross sections were computed.

REFERENCES

1. A. Bietti, Phys. Rev. 142, 1258 (1966).

2. A. Bietti, Phys. Rev. 144, 1289 (1966).

3. F. Gilman and H. Schnitzer, Phys. Rev., to be published.

4. P. Auvil, C. Lovelace, A. Donnachie, and A. T. Lea, Physics Letters 12, 76 (1964).

5. L. D. Roper, R. M. Wright, and B. T. Feld, Phys. Rev. 138, 190 (1965).

6. B. H. Bransden, P. J. O'Donnell, and R. G. Moorhouse, Phys. Rev. 139, B1566 (1965).

7. P. Bareyre, C. Brickman, A. V. Stirling, and G. Villet, Physics Letters 18, 342 (1965).

8. J. Cence, Physics Letters 20, 306 (1965).

9. S. D. Ecklund, Ph.D. Thesis, California Institute of Technology (1967).

10. C. Clinesmith, Private Communication.

11. M. G. Hauser, Private Communication.

12. F. Dixon, Ph.D. Thesis, California Institute of Technology (1960).

13. J. Kilner, Ph.D. Thesis, California Institute of Technology (1963).

14. M. Beneventano, R. Finzi, L. Mezzetti, L. Paoluzi, and S. Tazzari, Nuovo Cimento 28, 1464 (1963).

15. M. Heinberg, W. M. McClelland, F. Turkot, W. M. Woodward, R. R. Wilson, and D. M. Zipoy, Phys. Rev. 110, 1211 (1958).

16. L. Hand and C. Schaerf, Phys. Rev. Letters 6, 229 (1961).

17. C. Schaerf, Nuovo Cimento 44, 504 (1966).

18. J. Boyden, Ph. D. Thesis, California Institute of Technology (1961).

19. C. Peck, Ph. D. Thesis, California Institute of Technology (1964).

20. R. R. Wilson, Nuclear Instruments 1, 101 (1957).

21. H. A. Thiessen and J. Pine, "Calibration of the South Quantameter", CTSL Internal Report No. 22, Unpublished (1966).

22. H. A. Thiessen, Calibration of the 600 MeV/c Magnet CTSL Internal Report No. 26, Unpublished (1966).

23. C. Peck, SPECTROMETER Program Manual, in preparation.

24. A. Barna, J. H. Marshall, and D. Torzewski, Rev. Sci. Instr. 36, 1666 (1965).

25. A. Barna, J. H. Marshall, and M. Sands, Nucl. Instr. 12, 43 (1961).

26. J. H. Marshall, Ph. D. Thesis, California Institute of Technology (1965).

27. M. Hauser, "Description of Subroutine UNPACK", unpublished (1965). H. A. Thiessen, "Logic Subroutines for Translating the Output of the Scaling Adapter for the Nuclear Data Pulse Height Analyzer", unpublished (1965). Both these program writeups have been filed in the Synchrotron Library.

28. H. A. Thiessen, "A Scaling Adapter for the Nuclear Data 1024 Channel Pulse Height Analyzer", CTSL Internal Report No. 16, unpublished (1965).

29. H. A. Thiessen, "A Recalibration of the Beam Energy Meter", CTSL Internal Report No. 21, unpublished (1966).

30. F. Wolverton, "Thick Radiator Bremsstrahlung. Angular Dependence of the Spectrum for Electron Energies Greater Than 300 MeV", 1966 (to be published). An instruction manual for program BPAK I has been placed in the Synchrotron Library.

31. M. Hauser, "BR/Function to Obtain Synchrotron Beam Spectrum by Table Interpolation", unpublished (1966). This Program write up has been placed in the Synchrotron Library.

32. R. Gold, "An Iterative Unfolding Method for Response Matrices", ANL-6984, Argonne National Laboratory, Argonne, Illinois (1964).

33. S. Twomey, J. ACM 10, 97 (1963).

34. R. Diebold, Ph. D. Thesis, California Institute of Technology (1963).

35. R. L. Walker, J. G. Teasdale, V. Z. Peterson, and J. I. Vette, Phys. Rev. 99, 210 (1955).

36. A. V. Tollestrup, J. C. Keck, and R. M. Worlock, Phys. Rev. 99, 220 (1955).

37. J. Bizot, J. Perez y Jorba, and D. Trielle, Laboratory de l' Accelerateur Lineare, Orsay, France, preprint (1965).

38. D. Beder, Nuovo Cimento 33, 94 (1964).

39. J. J. Sakurai, Phys. Rev. Letters 7, 355 (1961).

40. F. Bulos et. al., Phys. Rev. Letters 13, 486 (1964).

41. W. Bruce Richards et. al., Phys. Rev. Letters 16, 1221 (1966).

42. E. P. Wigner, Phys. Rev. 73, 1002 (1948).

43. Robert K. Adair, Phys. Rev. 111, 632 (1958).

44. K. Prepost, D. Lundquist, and D. Quinn, Proceedings of the International Symposium on Electron and Photon Interactions at High Energies, Hamburg, 1965 (to be published).

45. F. Uchiyama-Campbell, Phys. Letters 18, 189 (1965).

46. Peter N. Dobson, Phys. Rev. 146, 146 (1966).

47. J. S. Ball, Private Communication.

48. A. W. Hendry and R. G. Moorhouse, Phys. Letters 18, 171 (1965).

49. I. P. Gyuk and S. F. Tuan, Phys. Rev. Letters 14, 121 (1965).

50. H. A. Thiessen, "Thermal Effects in a Wilson Quantameter", CTSL Internal Report No. 23, unpublished (1966).

51. Plastics Technical Evaluation Center, Picatinny Arsenal, Dover, N. J., "Properties of Plastics and Related Materials at Cryogenic Temperatures", PLASTEC Report 20 (1965).

52. Chelton and Mann, "Cryogenic Data Book", UCRL-3421 (1956).

53. Goodwin, Diller, and Roder, Cryogenics 2, 81 (1961). Note that some references give the hydrogen density in gram moles/cm^3. Chelton and Mann(52) seem to have confused grams for gram moles. In this respect, the UCRL Wallet Card value seems to be correct.

54. Petrov, Ivanor, and Rusakov, Soviet Physics JETP 10, 682 (1960).

55. Meshkouskii and Shalamov, Soviet Physics JETP 10, 697 (1960).

56. Balandin et. al., Soviet Physics JETP 19, 279 (1964).

57. R. L. Martin, Phys. Rev. 87, 1052 (1952).

58. J. W. Cronin, R. Cool, and A. Abashian, Phys. Rev. 107, 1121 (1957).

59. Jacob and Chew, Strong Interaction Physics, W. A. Benjamin, Inc. (1964).

60. B. Rossi, High Energy Particles, Prentice Hall, 1952.

61. H. A. Thiessen, "π-μ Decay Analysis Program", unpublished, (1964). A copy of this program writeup has been filed in the Synchrotron Library.